University of Alberta

Melting of Phlogopite-bearing Assemblages in the Earth's Mantle

by

Andreas Enggist

A thesis submitted to the Faculty of Graduate Studies and Research
in partial fulfillment of the requirements for the degree of

Doctor of Philosophy

Earth and Atmospheric Sciences

© Andreas Enggist
Fall 2012
Edmonton, Alberta

Permission is hereby granted to the University of Alberta Libraries to reproduce single copies of this thesis and to lend or sell such copies for private, scholarly or scientific research purposes only. Where the thesis is converted to, or otherwise made available in digital form, the University of Alberta will advise potential users of the thesis of these terms.

The author reserves all other publication and other rights in association with the copyright in the thesis and, except as herein before provided, neither the thesis nor any substantial portion thereof may be printed or otherwise reproduced in any material form whatsoever without the author's prior written permission.

To my parents, Agnes and Arthur

Abstract

Phlogopite, an alkali-rich and water-bearing mineral, is a common phase in the Earth's upper mantle. Its breakdown could generate melts or stabilize fluids that will metasomatize mantle rocks. To date, the effect of CO_2 on phlogopite stability remains unconstrained.

To evaluate the stability of phlogopite in the presence of carbonate, experiments were conducted in the KMAS-H_2O-CO_2, KCMAS-H_2O and KCMAS-H_2O-CO_2 systems at pressures from 4 to 8 GPa and temperatures from 1100 to 1600°C. The solidus of KMAS-H_2O-CO_2 was bracketed between 1200 and 1250°C at pressures of 4, 5 and 6 GPa, and between 1150 and 1200°C at a pressure of 7 GPa. Below the solidus, phlogopite coexists with magnesite, pyrope and a fluid. At the solidus magnesite reacts out, and enstatite and olivine appear.

The solidus of KCMAS-H_2O was bracketed between 1250-1300°C at 4 and 5 GPa, and between 1300-1350°C at 6, 7 and 8 GPa. The solidus of KCMAS-H_2O-CO_2 was bracketed between 1150-1200°C at 4, 5 and 6 GPa, and between 1100-1150°C at 7 and 8 GPa. Below the solidus in both systems, phlogopite is in equilibrium with enstatite, diopside, garnet, ±magnesite and a fluid. At 7 GPa phlogopite coexists with potassic richterite, enstatite, diopside, garnet, ±magnesite and a fluid. Potassic richterite is the stable K-bearing phase at 8 GPa and is in equilibrium with enstatite, diopside, garnet, ±magnesite and a fluid. Olivine forms at the solidus and coexists with enstatite, diopside, garnet and melt.

The solidus of CO_2-bearing systems is lowered such, that, in a very hot subduction environment, alkali-rich, CO_2-bearing melts can originate at a depth of ~240 km (~7.5 GPa). In a 40-mWm^{-2} subcontinental lithospheric mantle, phlogopite is stable to a depth of 200 km in the presence of carbonate and to 190 km in the presence of pyroxene with carbonate. Coexisting fluids become Si-rich with increasing pressure. Ascending alkali- and CO_2-rich melts from greater depths could react with peridotite at the base of the subcontinental lithospheric mantle, crystallizing phlogopite, carbonate and stabilizing a fluid at a depth of 170 to 200 km. Fluid and melt in KCMAS-H_2O-CO_2 remain immiscible phases to pressures >8 GPa.

Acknowledgements

I wish to thank my supervisor Bob Luth for all his advice and guidance over the past four years. Many thanks to Diane Caird, who trained me patiently to assemble experiments, to operate the multi-anvil apparatus, and who was in charge of XRD analyses. I am grateful to my colleagues and friends of the experimental petrology group at the University of Alberta (UofA), Linglin Chu and Sean Funk, for the numerous discussions about our projects. I would also like to acknowledge Sergei Matveev for his valuable help with the electron microprobe, Andrew Locock for discussions about mineralogy, Mark Labbe and Rob Stefaniuk for technical support. Furthermore, I would like to thank the members of the Committee, Stephen Foley, Thomas Stachel, Tom Chacko, Chris Herd and Arthur Mar, for the constructive comments and thoughtful reviews of the thesis draft.

Financial support for research costs was provided by a Discovery Grant from the National Science and Engineering Research Council of Canada to Bob Luth. I am grateful for the financial support from the Department of Earth and Atmospheric Sciences (UofA) through Teaching and Research Assistantships and the Christopher Scarfe Memorial Graduate Scholarship in Geology. I am grateful for receiving the Professional Development and Travel Grant by the Graduate Student Association (UofA), the J Gordin Kaplan Graduate Student Award by the Faculty of Graduate Studies and Research (UofA), the Postgraduate Student Bursary Award by The Mineralogical Society of Great Britain and Ireland, and a Goldschmidt 2010 Travel Grant administered by The Geochemical Society.

I would like to thank all my friends for the good times here in Edmonton, and for the unforgettable trips to the Canadian Rockies: Linglin Chu, Xianmin Hu, Hongwen Zhao, Isabel Lindner, Ali Imer, Guadalupe Moldonado Sanchez, Mary L. Borrero, Yi Zhao, Ji Lei, Rares Bistran, Miguel A. Cuba Espinoza, Ann Moore, Sean P. Funk, Nelson Bernal Cortes, Gideon Lambiv Dzemua, Osbaldo Zamora Vega, Praveen Veluthedathe Kuzhiyil, Qiang Wang, Giselle Norville, and more.

Last but not least, many thanks to my parents, Agnes and Arthur, to my sister Stefanie and brother-in-law Hane for endless support; and to Megan, who motivated me to work, and, in a constructive way, distracted me from it in stressful times. I couldn’t have done it without all of you.

Table of Contents

List of Tables

List of Figures

List of Symbols and Abbreviations

Al	Aluminum
apfu	Atoms per formula unit
b.d.	Below detection limit
BRIAN2	Modified natural lherzolite composition (Konzett and Ulmer 1999)
°C	Degree Celsius
Ca	Calcium
Cl	Chlorine
CO_2	Carbon dioxide
di	Diopside
emf	Electromotive force [V]
en	Enstatite
EPMA	Electron probe micro analysis
fl	Fluid
gr	Garnet (Ca-bearing)
GPa	Gigapascal
h	Hours
hydr sol	Hydrous solution
H_2O	Water
K	Potassium
K_2	Second critical end-point
K&U	Konzett and Ulmer (1999)
km	Kilometers
KCMAS-H_2O	Chemical 6-component system containing the following oxides: K_2O-CaO-MgO-Al_2O_3-SiO_2-H_2O
KCMAS-H_2O-CO_2	Chemical 7-component system containing the following oxides: K_2O-CaO-MgO-Al_2O_3-SiO_2-H_2O-CO_2
KMAS-H_2O-CO_2	Chemical 6-component system containing the following oxides: K_2O-MgO-Al_2O_3-SiO_2-H_2O-CO_2

KNCMASH	Chemical 7-component system containing the following oxides: K_2O-Na_2O-CaO-MgO-Al_2O_3-SiO_2-H_2O
kr	Potassic richterite
kV	Kilovolts
LILE	Large ion lithophile elements
M or m	Melt = liquid
mag	Magnesite
Maj comp	Majorite component
Mg	Magnesium
mg	Milligrams
mm	Millimeters
mV	Millivolts
mWm^{-2}	Milliwatts per meter-squared
µm	Micrometers
n	Number of analyses
nA	Nanoamperes
Na	Sodium
n/a	Not applicable
OD	Outer diameter
ol	Olivine
p	Primary phlogopite (also ‘p-phl’)
phl	Phlogopite
p-phl	Primary phlogopite (also ‘p’)
Pt	Platinum, the composition of the experimental capsules
py	Pyrope garnet
q	Quench phlogopite (also ‘q-phl’)
q-mag	Quench magnesite
q-phl	Quench phlogopite (also ‘q’)
s	Seconds
Si	Silicon
sp	Spinel

wt%	Weight percent
XRD	X-ray diffraction

Chapter 1: Introduction

Petrologic study of ultramafic xenoliths that were found in kimberlites or basalts (e.g. Dawson and Powell 1969; Boettcher and O'Neil 1980; Erlank et al. 1987; Nixon 1987) revealed textures showing the replacement of mineral phases by hydrous minerals, such as phlogopite or potassic richterite. Those textures were interpreted to be of a metasomatic origin (Harte 1983; Dawson 1984).

Erlank et al. (1987) reported that an average phlogopite-bearing garnet peridotite contains ~0.16 wt% K_2O, whereas the highly metasomatized phlogopite-potassic richterite peridotites contain ~1 wt% K_2O. A regular mantle peridotite contains only ~0.03 wt% K_2O (e.g. Frost 2006). To understand the enrichment of potassium in metasomatized mantle rocks, it is essential to constrain the stability of potassium-bearing minerals in the Earth's mantle. The breakdown of those water-bearing, alkali-rich minerals could induce partial melting, generating alkali-rich melts, or could release fluids. Both alkali-rich melts and fluids, will then infiltrate and metasomatize mantle rocks (cf. review by Thompson 1992). Hence, many experimental studies were carried out to understand the origin of such magmas and the role of the hydrous, alkali-rich minerals in their generation (cf. review by Frost 2006). It was demonstrated that phlogopite is the stable potassium-bearing mineral at lower pressures and will break down to potassic richterite at higher pressures (see below).

1.1 Previous work

Natural and synthetic phlogopite, and systems involving phlogopite were studied at pressures up to 0.3 GPa by e.g. Roy (1949), Schairer (1954), Yoder and Eugster (1954), Wones (1963), Crowley and Roy (1964), and others.

Luth (1967) reported results in the $KAlSiO_4$-Mg_2SiO_4-SiO_2-H_2O system at pressures up to 0.3 GPa. One of the reactions found was reaction (1.1) that he inferred could be of importance for the genesis of kimberlites:

$$\text{phlogopite + enstatite} = \text{forsterite + melt + vapor} \qquad (1.1)$$

Kushiro et al. (1967), who studied mantle assemblages, suggested that phlogopite could be an important K-bearing phase in the upper mantle to a depth of 150-200 km and about 1000°C, and proposed that alkali-rich magma, such as kimberlites, could result from low-degree partial melting of phlogopite-bearing peridotites. As starting material, they chose a natural and synthetic fluorine-bearing phlogopite. The phlogopite in their experiments started to break down above 4 GPa to garnet, an amphibole-like mineral and a fluid.

Modreski and Boettcher (1972) further investigated the stability of phlogopite in the K_2O-MgO-Al_2O_3-SiO_2-H_2O (KMASH) system using phlogopite (phl) and enstatite (en). The starting material consisted of a mixture of, by weight, $phl_{50}en_{50}$ and was run at pressures of 0.2-3.5 GPa under dry and wet conditions. The vapor-absent solidus they found has a positive slope extending from 1-3.5 GPa and 1050-1300°C, respectively, at which phlogopite and enstatite melt

incongruently to olivine plus melt (1.2) over a temperature range of about 50 and 80°C at 1 and 3.5 GPa, respectively (Figure 1-1):

phlogopite + enstatite =
olivine + melt (1.2)

The wet solidus extends from 1 to 3.5 GPa and 1050 to 1190°C, respectively. Starting mixtures of, by weight, $phl_{70}en_{30}$ and $phl_{40}en_{40}ol_{20}$ gave equivalent results. They found that, relative to a pure phlogopite system, adding enstatite reduces the stability of phlogopite at 1 GPa by 220 and 110°C in experiments with and without excess water, respectively.

In the K_2O-CaO-MgO-Al_2O_3-SiO_2-H_2O (KCMASH) system Modreski and Boettcher (1973) used a starting mix of, by weight, $phl_{50}diopside_{50}$. This mixture was run in experiments at pressures ranging from 1-3.5 GPa. The solidus of phlogopite in the presence of diopside (di) extends from 1-3 GPa and temperatures of 1150-1300°C, respectively, which is at higher temperatures (dry: +100°C at 1 GPa, +30°C at 3 GPa; wet: +50°C at 1 GPa, +20°C at 3 GPa) than in the phlogopite + enstatite system.

Excess water added to the system lowered the solidus temperatures at 1 and 3 GPa by 50 and 100°C, respectively. Experiments containing a starting material of, by weight, $phl_{40}en_{30}di_{30}$ yielded the same results as the phlogopite + diopside system, and they found the following melting relations (1.3, 1.4):

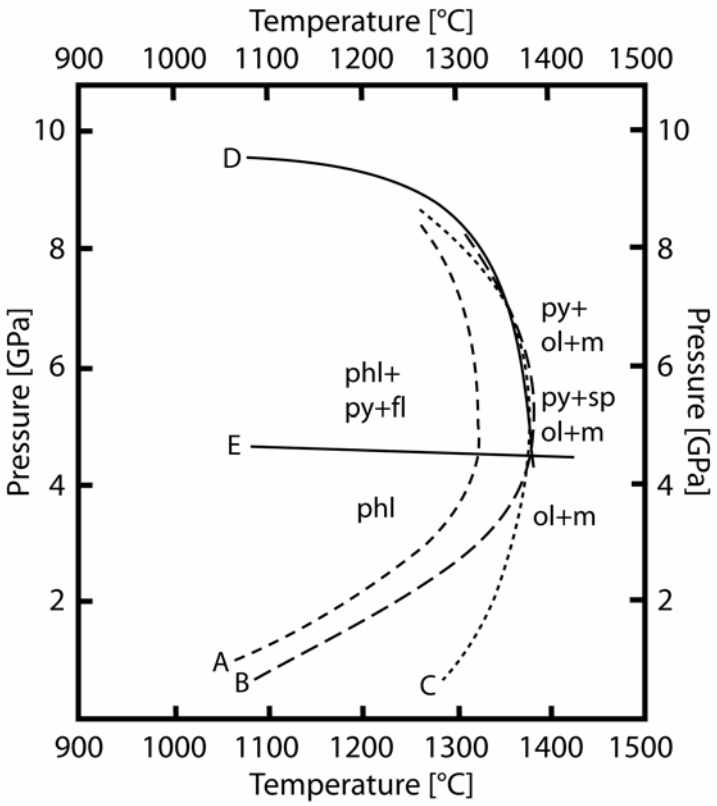

Figure 1-1 Solidi of phlogopite ± enstatite (modified from Frost 2006). **A** solidus of phlogopite + enstatite: Modreski and Boettcher (1972, wet solidus; <4 GPa), and Sato et al. (1997; >4 GPa). **B** phlogopite + enstatite (Modreski and Boettcher 1972, dry solidus; Sato et al. 1997). **C** natural, fluorine-bearing phlogopite (Sato et al. 1997, dry solidus). **D** synthetic phlogopite (Trønnes 2002). **E** Subsolidus breakdown reaction of phlogopite to pyrope and a fluid (Sato et al. 1997). See text for details. *phl* phlogopite, *en* enstatite, *py* pyrope, *ol* olivine, *fl* fluid, *sp* spinel, *m* melt

` phlogopite + diopside =

olivine + melt (1.3)

phlogopite + enstatite + diopside =

olivine + melt (1.4)

They reported that melts in equilibrium with phlogopite, enstatite and olivine become more alkalic and silica under-saturated with increasing pressure, and concluded that kimberlitic magmas would originate at higher pressures.

Wendlandt and Eggler (1980) used a natural lherzolite composition in their experiments and added 10 wt% of synthetic phlogopite. In their experiments with and without excess water, they found similar results as Modreski and Boettcher (1972), only, that the solidi they found were steeper: the dry solidus extends from 1-3 GPa and temperatures of 1100-1250°C, respectively. With excess water present, the solidus extends from 1-3 GPa and temperatures of 1050-1150°C, respectively.

Subsequently, the KCMASH system was explored to higher pressures. Sudo and Tatsumi (1990) used a starting material of, by weight, $phl_{50}di_{50}$ for most of their experiments. Two experiments were carried out containing a mix of, by weight, $phl_{33}en_{33}di_{33}$. They reported the following divariant subsolidus breakdown reaction (1.5) of phlogopite to potassic richterite, garnet, olivine and a fluid at pressures greater than 5 GPa (Figure 1-2). The melting relations, however, remained unconstrained.

$$2\ K_2Mg_6Al_2Si_6O_{20}(OH)_4\ \text{(phlogopite)} + 2\ CaMgSi_2O_6\ \text{(diopside)} = K_2CaMg_5Si_8O_{22}(OH)_2\ \text{(potassic richterite)} + CaMg_5Al_4Si_6O_{24}\ \text{(Ca-bearing garnet)} + 2\ Mg_2SiO_4\ \text{(olivine)} + (K_2O + 3\ H_2O)\ \text{(fluid)} \quad (1.5)$$

Luth (1997) synthesized phlogopite from an oxide-carbonate mixture crystallized using a piston cylinder, and diopside from an oxide-carbonate mixture fused to a glass, and used a starting composition of, by weight, $phl_{50}di_{50}$ in experiments run at pressures from 3-17 GPa (Figure 1-2). The phase relations found are similar to Modreski and Boettcher (1973) and Sudo and Tatsumi (1990) at higher pressures, only that olivine was present in some of the run products at

subsolidus conditions. Luth (1997) constrained the melting relations of phlogopite with diopside, which melts to olivine, diopside and melt at pressures of 3-5 GPa, and to olivine, diopside, garnet and melt at pressures of 7.5-11 GPa (reaction 1.6):

phlogopite + diopside = olivine + melt (3-5 GPa)
= olivine + garnet + melt (7.5-11 GPa) (1.6)

Experiments by Sato et al. (1997) using natural fluoro-phlogopite and synthetic enstatite from glass, mixed as even weight mixture $phl_{50}en_{50}$, yield very similar results to the F-free KMASH system by Trønnes (2002): the breakdown curve has a positive slope below 5 GPa, then turns into a negative slope to higher pressures. Phlogopite was stable to temperatures of ~1360°C at 5 GPa, and to pressures of ~9.5 GPa at a temperature of 1100°C (Figure 1-1). Trønnes (2002) reported a breakdown reaction (1.7) of phlogopite producing olivine, garnet and fluid at pressures from 7.5-10 GPa:

phlogopite =
olivine + garnet + fluid (1.7)

Konzett and Ulmer (1999) studied the stability of K-bearing phases in the synthetic K_2O-Na_2O-CaO-MgO-Al_2O_3-SiO_2-H_2O (KNCMASH) and natural lherzolite system from 4-9 GPa. The synthetic system contains an excess of phlogopite relative to orthopyroxene. Phlogopite breaks down above 8 GPa and 1150°C to potassic richterite, garnet, olivine and fluid.

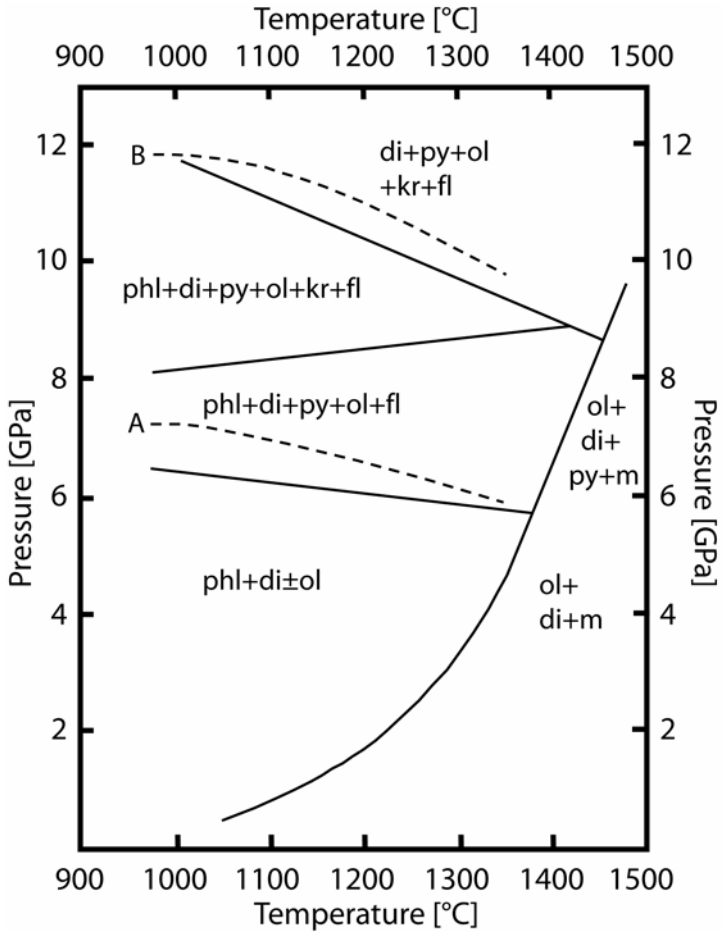

Figure 1-2 Melting relations of phlogopite in the KCMASH system (modified from Frost 2006). **A**, **B** Sudo and Tatsumi (1990). Solid lines refer to Luth (1997). The former did not report olivine below 6 GPa below the solidus, in contrast to the latter. See text for further details. *phl* phlogopite, *di* diopside, *py* pyrope, *ol* olivine, *kr* potassic richterite, *fl* fluid, *m* melt

In their experiments they used a natural spinel lherzolite composition from Mont Briançon (French Massif Central). Thirty wt% of olivine (Forsterite91) was subtracted to increase the amount of pyroxene relative to olivine. Furthermore, they added 5 wt% of synthetic phlogopite, and 0.4 wt% of Na_2O to avoid exhaustion of the jadeite component in clinopyroxenes, which could cause phlogopite to remain stable with K-richterite. The maximum stability of phlogopite in these experiments is shifted to lower pressures of ~6.5 GPa at

1000°C, and to pressures <6.5 GPa at 1100°C. Comparing K/OH ratios for phlogopite and potassic richterite in KNCMASH and KCMASH, they found that in the KNCMASH system, which is closer to a natural system, only small amounts of aqueous fluids will be released, as it more likely will be bound in the potassic richterite.

Melzer and Foley (2000) investigated the liquidus phase relations of fluorine- and potassium-bearing systems at 0.0001 and 1.8 GPa, and found fluorphlogopite to be stable as a liquidus phase to higher temperatures than in F-free systems.

The studies summarized above were carried out in CO_2-free systems. Carbonate inclusions found in mantle derived megacrysts, CO_2-rich fluid inclusions in mantle minerals and the occurrence of carbonatitic melt associated with kimberlites are evidence for CO_2 in the mantle (e.g. Irving and Wyllie 1973; Wyllie 1977). Carbonates and H_2O-CO_2-rich fluids in the mantle received considerable attention starting around the 1960s, as their role in the generation of kimberlitic and carbonatitic melts and fluids was recognized (Wyllie and Tuttle 1960; Holloway 1973; Brey and Green 1975; Wyllie and Huang 1975a, 1975b; Eggler 1978; Green and Wallace 1988; Canil and Scarfe 1990; Dasgupta and Hirschmann 2007; Dasgupta et al. 2007).

Wendlandt and Eggler (1980) constrained the stability of phlogopite in the $KAlSiO_4$-MSH-CO_2 system to 5 GPa using a starting material mixed from synthetic phlogopite, enstatite and magnesite. Based on their results at pressures

to 5 GPa, they suggested that phlogopite associated with enstatite and magnesite most likely will not be stable >5 GPa and ~1200°C. They formulated the following reaction (1.8) with melts produced ranging from carbonatite to silicate compositions.

$$\text{phlogopite} + \text{enstatite} + \text{magnesite} = \text{forsterite} + \text{pyrope} + \text{melt} \qquad (1.8)$$

Thibault et al. (1992) investigated the potential of near-solidus melts of a phlogopite-bearing lherzolite ± carbonate at 3 GPa as metasomatic agents. For the starting material they mixed a model lherzolite from oxides with natural minerals (phlogopite, olivine, ortho- and clinopyroxene) found in xenoliths in the West Eifel volcanic field, Germany. The carbonated phlogopite-bearing lherzolite at 1100°C yielded 4 wt% of alkaline dolomitic melt coexisting with a garnet-rich phlogopite lherzolite. At 1225°C the phlogopite-bearing lherzolite produced 7 wt% of a hydrous potassic and calcic silicate melt, which was in equilibrium with titaniferous phlogopite-bearing lherzolite. They concluded that these melts will infiltrate and metasomatise peridotites by enriching them modally in pyroxenes, carbonates and phlogopite.

Multiple saturation experiments with a synthetic carbonatite composition showed that Na- and K-dominant carbonatitic melt is in equilibrium with phlogopite lherzolite at ~2.5 GPa at 1170°C and at ~3.2 GPa at 1120°C, respectively (Sweeney 1994).

Previous experiments on kimberlites were mainly done on group I kimberlite compositions (e.g. Eggler and Wendlandt, 1979; Edgar et al., 1988;

Ringwood et al., 1992; Edgar and Charbonneau, 1993; Girnis et al., 1995). Ulmer and Sweeney (2002) chose an average group II kimberlite (orangeite) starting composition mixed from oxides. Liquidus phases are olivine, orthopyroxene and garnet from 4 to 10 GPa; at lower pressures only olivine is present. Phlogopite was found to break down at ~3-4 GPa and reactions proposed were the following; (1.9) and (1.10) at pressures ≤4 and >4 GPa, respectively:

2 phlogopite + CO_2 =

3 enstatite + garnet + (K_2CO_3 + 2 H_2O) (melt) (1.9)

2 phlogopite + magnesite =

olivine + 2 enstatite + garnet + (K_2CO_3 + 2 H_2O) (melt) (1.10)

1.2. Aim of this study

As outlined above, relatively few studies focus on the melting relations of phlogopite-bearing assemblages, and the phase relations of phlogopite in carbonated peridotite remain unconstrained. Different melting reactions (1.8) and (1.10) were proposed by Wendlandt and Eggler (1980), and by Ulmer and Sweeney (2002), respectively, that need to be constrained.

In a first step, I will locate the melting reaction proposed by Ulmer and Sweeney (2002) from 4-8 GPa in order to find the solidus in the simple phlogopite + magnesite system (see Chapter 2). The second stage then will be to extend the results of the simple system into the more complex pyroxene-bearing systems (see Chapter 3). To better understand the effect of CO_2 on the solidus, I

also will constrain the solidus of the CO_2-free, pyroxene-bearing system to complement the previous studies by Sudo and Tatsumi (1990) and Luth (1997).

The present study will, in a broad sense, contribute to the understanding of the recycling of potassium and water into the Earth's mantle, the sources of alkali-rich melts or fluids that are potential metasomatic agents, and the effect of CO_2 on the stability of alkali- and water-bearing minerals in the Earth's upper mantle.

References

Boettcher AL, O'Neil JR (1980) Stable isotope, chemical and petrographic studies of high-pressure amphiboles and micas: Evidence for metasomatism in the mantle source regions of alkali basalts and kimberlites. Amer J Sci 280A:594-621.

Brey G, Green DH (1975) Role of CO_2 in genesis of olivine melilite. Contrib Mineral Petrol 49:93-103.

Canil D, Scarfe CM (1990) Phase relations in peridotite + CO_2 systems to 12 GPa: Implications for the origin of kimberlite and carbonate stability in the Earth's upper mantle. J Geophys Res 95:15,805-15,816.

Crowley MS, Roy R (1964) Crystalline solubility in the muscovite and phlogopite groups. Am Miner 49:348-362.

Dasgupta R, Hirschmann MM (2007) Effect of variable carbonate concentration on the solidus of mantle peridotite. Am Mineral 92:370-379.

Dasgupta R, Hirschmann MM, Smith ND (2007) Partial melting experiments of peridotite + CO_2 at 3 GPa and genesis of alkalic ocean island basalts. J Petrol 48:2093-2124.

Dawson JB (1984) Contrasting types of upper-mantle metasomatism? In: Kornprobst J (ed) Kimberlites-II. The Mantle and Crust/Mantle Relationships. Elsevier, Developments in Petrology Series 11B, pp 290-294.

Dawson JB, Powell DG (1969) Mica in the upper mantle. Contrib Mineral Petrol 22:233-237.

Edgar AD, Arima M, Baldwin DK, Bell DR, Shee SR, Skinner MW, Walker EC (1988) High-pressure–high-temperature melting experiments on a SiO_2-poor aphanitic kimberlite from the Wesselton mine, Kimberley, South Africa. Am Mineral 73:524-533.

Edgar AD, Charbonneau HE (1993) Melting experiments on a SiO_2-poor aphanitic kimberlite from 5-10 GPa and their bearing on source of kimberlite magmas. Am Mineral 78:132-142.

Eggler DH (1978) The effect of CO_2 upon partial melting of peridotites in the system Na_2O-CaO-Al_2O_3-MgO-SiO_2-CO_2 to 35 kbar, with an analysis of melting in a peridotite-H_2O-CO_2 system. Am J Sci 278:305-343.

Eggler DH, Wendlandt RF (1979) Experimental studies on the relationship of kimberlite magmas

and partial melting of peridotite. In: Boyd FR, Meyer HO (eds) Extended Abstracts, 2nd International Kimberlite Conference. American Geophysical Union, p. 330-338.

Erlank AJ, Waters FG, Hawkesworth CJ, Haggerty SE, Allsopp HL, Rckard RS, Menzies M (1987) Evidence for mantle metasomatism in peridotite nodules from the Kimberley Pipes, South Africa. In: Menzies MA, Hawkesworth CJ (eds) Mantle Metasomatism. Academic Press Geology Series, pp 221-311.

Frost DJ (2006) The Stability of hydrous mantle phases. In: Keppler, H., and Smyth, J.R. (eds) Water in nominally anhydrous minerals. Mineral Soc Am 62:243-271.

Green DH, Wallace ME (1988) Mantle metasomatism by ephemeral carbonatite melts. Nature 336:459-462.

Girnis AV, Brey GP, Ryabchikov ID (1995) Origin of group IA kimberlites: Fluid-saturated melting experiments at 45–55 kbar. Earth Planet Sci Lett 134:283-296.

Harte B (1983) Mantle peridotites and processes-the kimberlite sample. In: Hawkesworth CJ, Norry MJ (eds) Continental Basalts and Mantle Xenoliths. Shiva Publishing Limited, pp 46-91.

Irving AJ, Wyllie PJ (1973) Melting relationships in CaO-CO_2 and MgO-CO_2 to 36 kilobars, with comments on CO_2 in the mantle: Earth Planet Sci Lett 20:220-225.

Konzett J, Ulmer P (1999) The Stability of hydrous potassic phases in lherzolitic mantle - an experimental study to 9.5 GPa in simplified and natural bulk compositions. J Petrol 40(4):629-652.

Kushiro I, Syono Y, Akimoto S (1967) Stability of phlogopite at high pressures and possible presence of phlogopite in the earth's upper mantle. Earth Planet Sci Lett 3:197-203.

Luth RW (1997) Experimental study of the system phlogopite-diopside from 3.5 to 17 GPa. Am Mineral 82:1198-1209.

Luth WC (1967) Studies in the system $KAlSiO_4$-Mg_2SiO_4-SiO_2-H_2O: I, inferred phase relations and petrologic applications. J Petrol 8(3):372-416.

Melzer S, Foley SF (2000) Phase relations and fractionation sequences in potassic magma series modelled in the system $CaMgSi_2O_6$-$KAlSiO_4$-Mg_2SiO_4-SiO_2-F_2O_{-1} at 1 bar to 18 kbar. Contrib Mineral Petrol 138:186-197.

Modreski PJ, Boettcher AL (1972) The stability of phlogopite + enstatite at high pressures: a model for micas in the interior of the earth. Am J Sci 272:852-869.

Modreski PJ, Boettcher AL (1973) Phase relationships of phlogopite in the system K_2O-MgO-CaO-Al_2O_3-SiO_2-H_2O to 35 kilobars: a better model for micas in the interior of the earth. Am J Sci 273:385-414.

Nixon PH (ed.) (1987) Mantle xenoliths. New York: John Wiley.

Ringwood AE, Kesson SE, Hibberson W, Ware N (1992) Origin of kimberlites and related magmas. Earth Planet Sci Lett 113:521-538.

Roy R (1949) Decomposition and synthesis of the micas. J Am Cer Soc 32:202-209.

Sato K, Katsura T, Ito E (1997) Phase relations of natural phlogopite with and without enstatite up to 8 GPa: implication for mantle metasomatism. Earth Planet Sci Lett 146:511-526.

Schairer JF (1954) The system K_2O-MgO-Al_2O_3-SiO_2: I Results of quenching experiments on

four joins in the tetrahedron cordierite-forsterite-leucite-silica and on the join cordierite-mullite-potash feldspar. J Am Cer Soc 37:501-533.

Sudo A, Tatsumi Y (1990) Phlogopite and K-amphibole in the upper mantle: Implication for magma genesis in subduction zones. Geophys Res Lett 17(1):29-32.

Sweeney RJ (1994) Carbonatite melt compositions in the Earth's mantle. Earth Planet Sci Lett 128:259-270.

Thibault Y, Edgar AD, Lloyd FE (1992) Experimental investigation of melts from a carbonated phlogopite lherzolite: Implications for metasomatism in the continental lithospheric mantle. Am Mineral 77:784-794.

Thompson AB (1992) Water in the earth's upper mantle. Nature 358:295-302.

Trønnes RG (2002) Stability range and decomposition of potassic richterite and phlogopite end members at 5-15 GPa. Mineral Petrol 74:129-148.

Ulmer P, Sweeney RJ (2002) Generation and differentiation of group II kimberlites: Constraints from a high-pressure experimental study to 10 GPa. Geochim Cosmochim Acta 66:2139-2153.

Wendlandt RF, Eggler DH (1980) The origins of potassic magmas: 2. stability of phlogopite in natural spinel lherzolite and in the system $KAlSiO_4$-MgO-SiO_2-H_2O-CO_2 at high pressures and high temperatures. Am J Sci 280:421-458.

Wones DR (1963) Physical properties of synthetic biotites on the join phlogopite-annite. Am Miner 48:1300-1321.

Wyllie (1977) Mantle fluid compositions buffered by carbonates in peridotite-CO_2-H_2O. J Geol 85:187-207.

Wyllie PJ, Huang WL (1975a) Influence of mantle CO_2 in the generation of carbonatites and kimberlites. Nature 257:297-299.

Wyllie PJ, Huang WL (1975b) Peridotite, kimberlite, and carbonatite explained in the system CaO-MgO-SiO_2-CO_2. Geology 3:621-624.

Wyllie PJ, Tuttle OF (1960) The system CaO-CO_2-H_2O and the origin of carbonatites. J Petrol 1:1-46.

Yoder HS Jr, Eugster HP (1954) Phlogopite synthesis and stability range. Geochim Cosmochim Acta 6:157-185.

Chapter 2: Phase Relations of Phlogopite with Magnesite from 4 to 8 GPa[1]

2.1. Introduction

Phlogopite is commonly found in mantle xenoliths in kimberlites (Erlank et al. 1987; van Achterbergh et al. 2001) or alkali basalts (Nixon 1987) and is a main constituent of mantle derived magmas such as group II kimberlites (orangeites) (Edwards et al. 1992; Mitchell 1995) and carbonatites (e.g. McCormick and Le Bas 1996). Inclusions of phlogopite in diamonds testify to its stability at depths where diamonds grow (Sobolev et al. 1997, 2009; Leost et al. 2003). The breakdown of this water-bearing, alkali-rich mineral will considerably affect mantle processes: Water released will lower the mantle solidus and induce partial melting or stabilize a fluid at subsolidus temperatures. Both alkali-rich melts and fluids will infiltrate and metasomatize mantle rocks (cf. review by Thompson 1992). Hence, many experimental studies have been carried out to constrain the stability of phlogopite in the Earth's mantle (cf. review by Frost 2006). Only a few studies focus on melting relations: pure phlogopite-bearing systems (Sato et al. 1997; Trønnes 2002), including phlogopite + enstatite (Modreski and Boettcher 1972; Sato et al. 1997) and phlogopite + diopside (Luth 1997). Phlogopite in a natural, carbonated spinel lherzolite was studied from 1 to 3 GPa (Wendlandt and Eggler 1980). More information on phlogopite stability

[1] A version of this chapter is published as Enggist A, Chu L, Luth RW (2012) Phase relations of phlogopite with magnesite from 4 to 8 GPa, *Contributions to Mineralogy and Petrology* 163:467-481. doi: 10.1007/s00410-011-0681-9

comes from multiple-saturation experiments on orangeites (Yamashita et al. 1995; Ulmer and Sweeney 2002). The former study reports the occurrence of phlogopite at a temperature of 1,450°C at 4 GPa and a high pressure limit of 6 GPa. Ulmer and Sweeney (2002) found phlogopite at temperatures <1,300°C at ~3 GPa, with pressures of 4-5 GPa as the pressure limit.

Two different melting reactions for phlogopite in carbonate-bearing peridotite have been proposed by (2.1) Wendlandt and Eggler (1980) and by (2.2) Ulmer and Sweeney (2002):

phlogopite + enstatite + magnesite =
forsterite + pyrope + melt at pressures >5 GPa, (2.1)

phlogopite + magnesite =
forsterite + enstatite + pyrope + melt at pressures >4GPa. (2.2)

As outlined above, no study focuses on melting relations of phlogopite in the presence of carbonates at pressures >3 GPa. The purpose of this study was to constrain phase relations of phlogopite in the presence of magnesite from 4 to 8 GPa by locating the proposed reaction (2.2), thereby contributing to the understanding of sources for alkali-rich melts and fluids that will be potential metasomatic agents in the mantle.

2.2. Experimental and analytical procedures

2.2.1. Starting material

Phlogopite was synthesized from high-purity oxides (MgO, Al_2O_3 and SiO_2 of 99.95, 99.99 and 99.5% purity, respectively) and carbonate (K_2CO_3 of

99.0% purity) from Alfa Chemicals. A stoichiometric mix was loaded into a 5-mm-outer diameter (OD) Pt capsule along with ~7 wt% distilled H_2O. The capsule containing the oxide-carbonate mix was sealed by arc-welding, assembled in a 19 mm talc-pyrex assembly (Kushiro 1976) and run in an end-loaded piston cylinder for 48 h at 1.5 GPa and a temperature of 1,000°C. Temperature was monitored using a $W_{95}Re_5$-$W_{74}Re_{26}$ thermocouple without correction for pressure effects on EMF. We did not decarbonate the mix beforehand, so that at run conditions, the CO_2 will be dissolved in the fluid, and the resulting H_2O-CO_2 fluid should contain less solute than a H_2O fluid (e.g. Eggler 1987). An aliquot of the synthesized phlogopite was checked by XRD to ensure that only phlogopite is present. Different batches of phlogopite were synthesized to test whether our results were reproducible with slightly changing compositions of the synthetic phlogopite. Chemical analysis by electron microprobe turned out to be problematic because of the extremely small grain size of the synthesized crystals (<1 μm). This required analysis with a focused beam, which resulted in the loss of potassium during the analysis and, consequently, relatively low K_2O contents (Table 2-1). Furthermore, the excited volume by the electron beam might exceed the size of the smallest crystals.

Fragments of natural magnesite from Mt. Brussilof, British Columbia, Canada, which were free of visible inclusions, were separated out under a binocular microscope, analyzed by electron microprobe (Table 2-1) and ground in an agate mortar. A mix of phl_{90} + mag_{10} (wt%), consistent with the stoichiometry

of the reaction proposed by Ulmer and Sweeney (2002), was used in the experiments.

Table 2-1 Composition of starting materials

[wt%]	Phlogopite (n = 19)	[wt%]	Magnesite (n =15)
SiO_2	43.7(4)	SiO_2	0.1(1)
Al_2O_3	12.3(2)	Al_2O_3	*b.d.*
MgO	27.8(4)	FeO_{tot}	0.2(1)
K_2O	10.3(2)	MnO	*b.d.*
Total	94.1(4)	MgO	47.3(2)
		CaO	0.02(1)
Cations per 22 O		Na_2O	*b.d.*
Si	6.11(4)	K_2O	*b.d.*
Al	2.02(3)	Total	47.6(2)
Mg	5.82(9)		
K	1.85(4)	[a]CO_2	52.4
Sum	15.80(6)		

[a] by difference, *b.d.* below detection limit, *n* number of analyses; 1 standard deviation in the last digit is given in parentheses

2.2.2 Experimental setup and analytical methods

Capsules were fabricated from 4 mm lengths of 1.5-mm-OD Pt tubing. One end was triple-crimped, sealed by arc welding and flattened. The starting material was loaded so that the capsule contains a thin layer of around 1-2 mm. After cleaning any powder from inside the top end of the capsule, it was triple-crimped, placed in an oven to dry overnight at 120°C and then sealed by arc-welding. A dampened tissue was wrapped around the lower part of the capsule during welding to keep the starting material cool. The sealed capsule was then compressed into cylindrical shape. At this point, the integrity of the capsule was tested by placing it into a water bath for several hours. If the capsule gained weight, it was not used.

All experiments were carried out using our standard 18/11 high-T assemblies (Walter et al. 1995). ZrO_2 sleeves with 7 mm outer and 3 mm inner diameter were inserted into semi-sintered, Cr_2O_3-doped (5%) MgO octahedra. MgO spacers were used to center the capsules, which were placed within a MgO sleeve. $W_{95}Re_5$-$W_{74}Re_{26}$ thermocouple wires (0.254 mm diameter) were inserted axially into the assembly, encased in a crushable Al_2O_3 four-bore sleeve. All experiments were heated by stepped graphite furnaces. Each sample assembly was dried at 120°C overnight and then fired without the sample capsule at 1,000°C for 1 h in a N_2-H_2 (2%) gas that prevents the thermocouple wires from oxidizing.

In experiments at pressures of up to 7 GPa, we did not need to protect the thermocouple wires with copper coils. At higher pressures, however, the thermocouple wires always were torn apart by the deformation of the pyrophyllite gaskets, resulting in failure of the experiment. Consequently, we were using Cu coils in experiments at pressures of 8 GPa, knowing that this may affect the EMF readings so that temperatures could be underestimated (Nishihara et al. 2006). Our EMF readings were not corrected for any pressure effects on the thermocouples.

All experiments were performed using the UHP-2000 uniaxial split-sphere multi-anvil apparatus at the University of Alberta. Samples were pressurized first and heated after at a rate of 60 mV per hour (~60°C min^{-1}) at pressures from 4 to 7 GPa. The heating rate was reduced to 30 mV per hour (~30°C min^{-1}) at 8 GPa, which helped to reduce thermocouple breaks. Experiments were quenched by cutting off the power to the furnaces, dropping the temperature below 300°C in 2-5 s, and then decompressed over 2.5-4 h. Experimental charges were mounted in

epoxy (Petropoxy 154), ground open, impregnated under vacuum and polished. Samples were polished using a rotating disk and Al_2O_3 powder of 5, 1 and 0.05 μm grain size suspended in oil, initially, to preserve potentially water-soluble phases. Precipitation of solute from a fluid phase (see below) made further impregnation with epoxy impossible leading to plucking. The polishing was improved by using the same corundum powder suspended in water instead. Samples were cleaned in an ultrasonic bath, dried overnight at 60°C and then carbon-coated for microprobe analysis.

Analyses were done using a JEOL 8900 microprobe (EPMA) at the University of Alberta with an acceleration voltage of 15 kV and a beam current of 15 nA measured in the Farraday cup. Standards were sanidine (K), Fo93 olivine (Mg), pyrope (Al, Si), diopside (Ca), albite (Na), willemite (Mn) and hematite (Fe). Counting time was set to 20 and 10 s on peak and background, respectively. A focused beam was used to analyze pyroxene, olivine, magnesite and garnet; beam diameters of up to 3 μm, depending on grain size, were chosen for phlogopite grains. Raw data were corrected using the Phi-Rho-Z (Armstrong 1988) program provided by JEOL. NORM was used to normalize and recalculate mineral compositions (P. Ulmer, personal communication, 2007).

Mineral modes of each charge were estimated using backscatter images taken with the EPMA. Generally, each experimental charge had to be polished several times, exposing different sections of the same charge, allowing better estimates of modal percentages.

2.3. Results

2.3.1. General observations

The synthetic phlogopite reacts to form phlogopite plus garnet and a fluid at subsolidus conditions and coexists with magnesite to 1,250, 1,200, 1,200 and 1,150°C at 4, 5, 6 and 7 GPa, respectively (Table 2-2; Fig. 2-1). A similar subsolidus reaction was observed by Sato et al. (1997) and Luth (1997). This phlogopite in equilibrium with garnet, magnesite and fluid is referred to as 'primary' in this paper.

Table 2-2 Experimental results KMAS-H_2O-CO_2

Run # ae-…	T [°C]	Pressure [GPa]	Duration [h]	Results
05	1150	4	8	p-phl + mag + py + fl
13		5	24	p-phl + mag + py + fl
22		5.5	48	p-phl + mag + py + fl
15		6	24	p-phl + mag + py + fl
94		7	24	p-phl + mag + py + fl
97		8	24	p/q-phl + py + ol + en + hydr sol
142	1200	4	24	p-phl + mag + py + fl
60		5	8	p-phl + mag + py + fl
40		6	8	p-phl + mag + py + fl
84		7	8	p/q-phl + py + ol + hydr sol
07	1250	4	24	p-phl + mag + py + fl
19		5	24	p/q-phl + py + ol + en + hydr sol
20		6	24	p/q-phl + py + ol + en + hydr sol
79	1300	4	24	p/q-phl + py + ol + en + hydr sol
83		5	8	p/q-phl + py + ol + en + hydr sol
78		6	8	p/q-phl + py + ol + hydr sol
14	1350	4	23	p/q-phl + py + ol + en + hydr sol
93		5	12	p/q-phl + py + ol + en + hydr sol
24		6	24	q-phl + py + ol + hydr sol
58		7	8	p/q-phl + py + ol + hydr sol
39	1400	5	10	q-phl + py + ol + hydr sol
23	1450	4	24	q-phl + py + ol + hydr sol
31		5	12	q-phl + py + ol + hydr sol
25		6	12	q-phl + py + ol + hydr sol
35	1500	4	10	q-phl + py + ol + sp + hydr sol
26	1550	4	12	q-phl + py + ol + sp + hydr sol
36		5	10	q-phl + py + ol + hydr sol
38		6	8	q-phl + py + ol + hydr sol

en enstatite, *fl* fluid, *hydr sol* hydrous solution, *mag* magnesite, *ol* olivine, *p-phl* primary phlogopite, *p/q-phl* primary and quench phlogopite present, *py* pyrope, *q-phl* quench phlogopite, *sp* spinel

To constrain the amount of fluid and vapor present at subsolidus conditions, we weighed several capsules, froze them at -20°C and cut them open with a razor blade. Fetid-smelling gas escaped, but the amount lost was too little to measurably change the weight of the frozen capsule. Capsules were then heated at 120°C for 20 min and lost ~0.03 mg of weight (~2-3 wt%), which reflects the amount of water present.

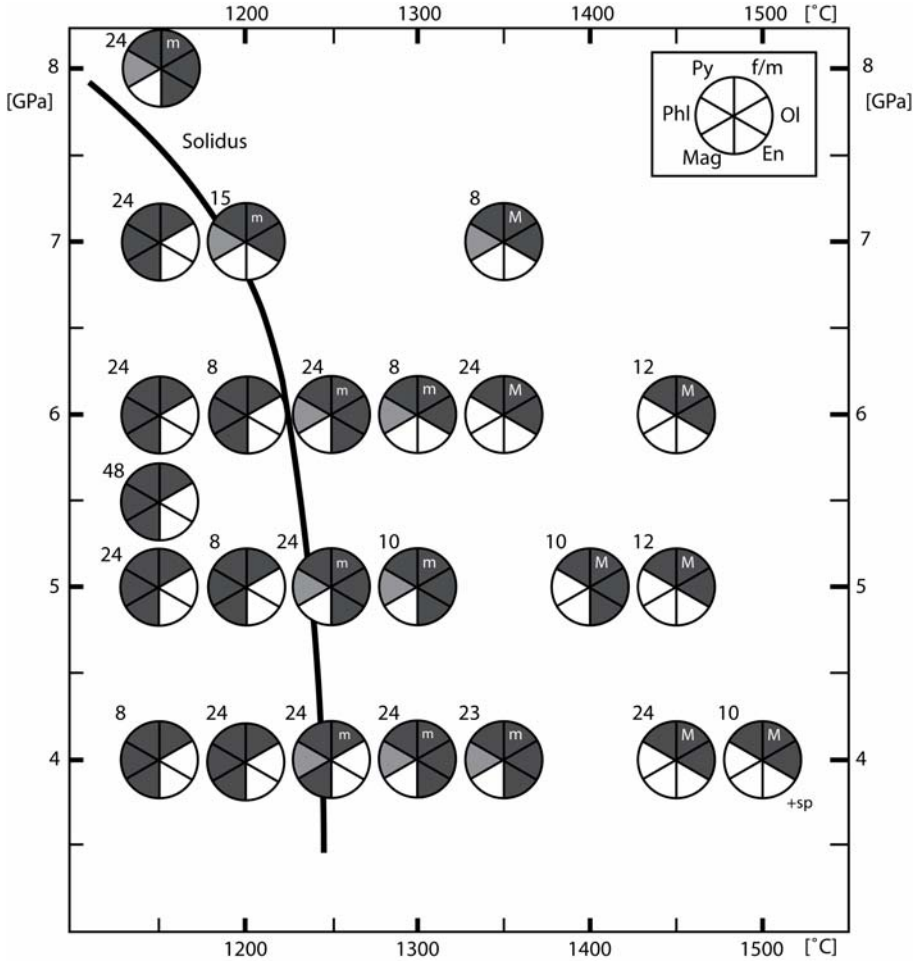

Figure 2-1 Phase relations of phlogopite with magnesite. Light grey quadrants indicate primary phlogopite that coexists with melt. Numbers indicate the duration of the experiment in hours. *En* enstatite, *f/m* fluid present if quadrant dark grey / dark grey quadrant with m to M for increasing melt portion, *Mag* magnesite, *Ol* olivine, *Phl* phlogopite, *Py* pyrope, *sp* spinel

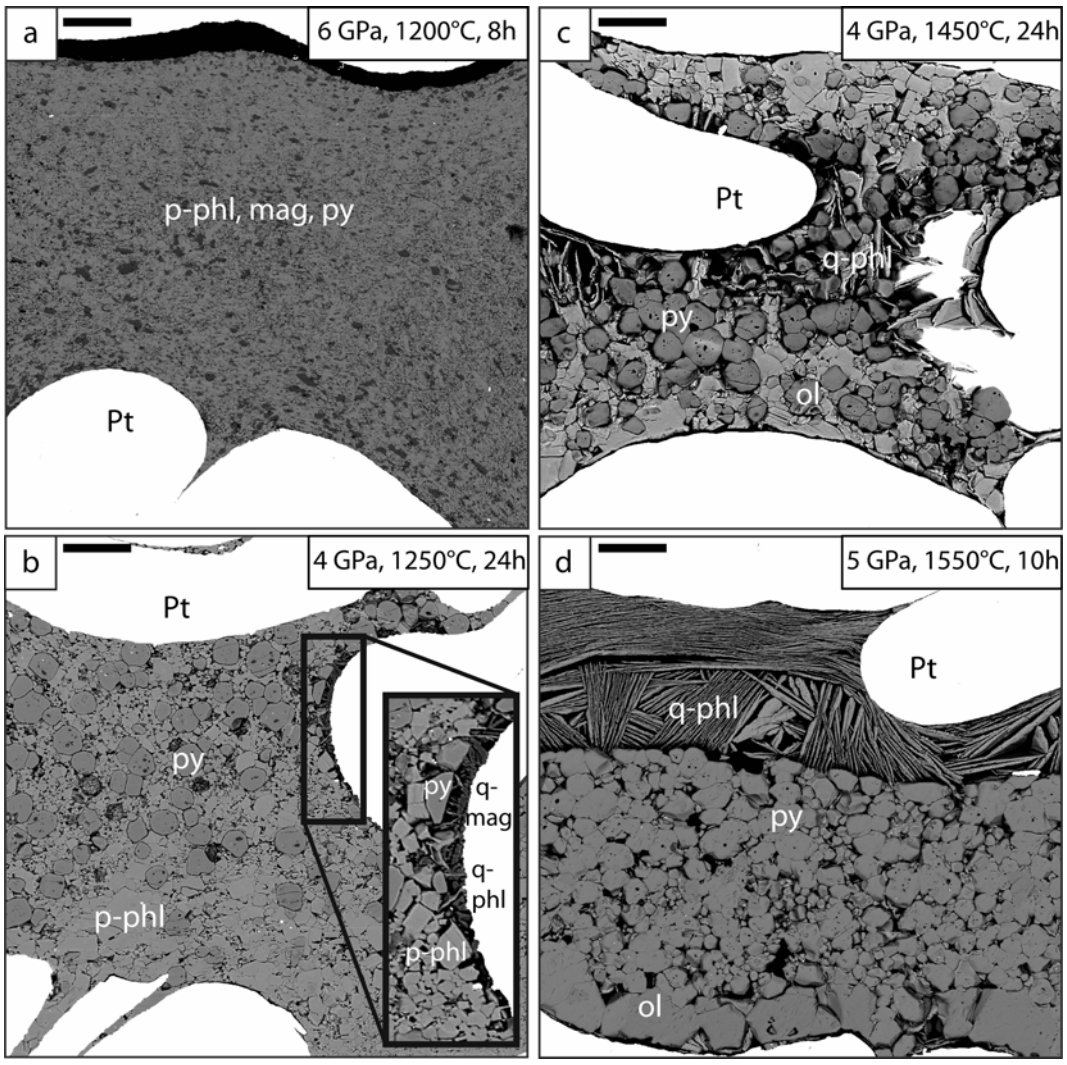

Figure 2-2 Textural changes from a) subsolidus, through b) solidus to c) and d) super-solidus. Scale bar in upper left of each image is 150 μm. Enstatite is absent in charges shown. a) Subsolidus assemblage: primary phlogopite (*p-phl*: light grey) in equilibrium with pyrope (*py*: grey, round grains) and magnesite (*mag*: dark grey). Magnesite is homogeneously distributed throughout the capsule. Grain size in general is small (1-50 μm) below solidus. b) Magnesite has reacted out, except for some relicts enclosed by garnet. Most phlogopite is still primary. Black box highlights the first small melt pocket along the capsule wall, identified by small quench phlogopite needles (*q-phl*: light grey) and quench magnesite patches (*q-mag*: black). Note the larger grain size compared to subsolidus conditions. c) Increasing the temperature further increases the melt fraction; quench phlogopite is present together with garnet and olivine. d) Q-phl (melt) accumulated in the upper half of the capsule as well as interstitially between garnet grains. Olivine grains are located at the bottom of the capsule.

A change in texture is obvious above 1,200, 1,200, 1,200 and 1,150°C at 4, 5, 6 and 7 GPa, respectively, and at 1,150°C at 8 GPa (Fig. 2-2): Over a temperature range of ~150°C the amount of primary phlogopite decreases and elongated, dendritic crystals become common, which were identified to be phlogopite by X-ray diffraction in combination with the EPMA data.

This dendritic phlogopite is interpreted to have grown upon quench of the experiment from a hydrous melt (e.g. Yoder and Kushiro 1969). In this ~150°C temperature interval, primary-textured phlogopite is also present and coexists with melt. Magnesite has reacted out at these conditions, and olivine and enstatite have formed and coexist with garnet.

Upon opening capsules that were run in the P/T zone of residual primary plus quench phlogopite, a hydrous solution and vapor, probably CO_2, bubble out. The solution precipitates a K-rich phase around the notch and within the capsule (Fig. 2-3).

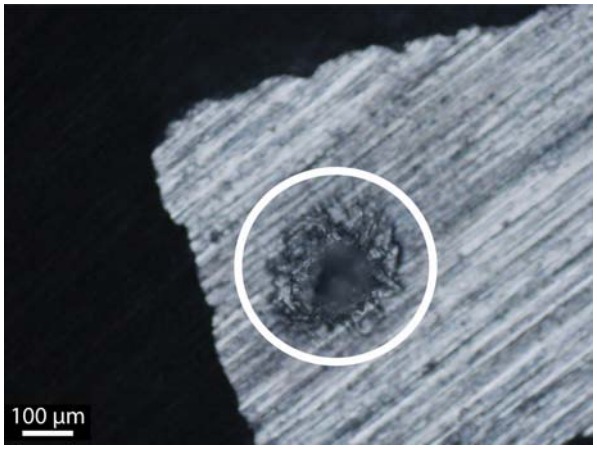

Figure 2-3 K-rich precipitates on the capsule surface viewed through a reflected light microscope. See text for details.

In experiments run above 1,300 and 1,350°C at 6 and 4 GPa, respectively, the only phlogopite is quench phlogopite, associated with olivine ± enstatite and garnet. At low pressure and high temperature, spinel occurs in some of the run products. In contrast to the above observations, the hydrous solution that escapes these capsules contains little or no solute.

The K-rich precipitates were identified qualitatively to be K-rich by EDS on the microprobe and are highly water soluble. Their small amount prohibited quantitative analysis, but we infer they are probably potassium carbonate.

2.3.2. Garnet

Pyrope grains are euhedral and generally up to 25 μm in diameter in subsolidus experiments, but up to 80 μm in diameter at and above the solidus (Fig. 2-2). Below the solidus, the modal abundance of garnet increases slightly to higher temperatures and pressures from ~10 to ~15%, whereas above the solidus, the modal abundance increases to ~30%.

As expected from earlier studies (e.g. Ringwood 1967; Kanzaki 1987; Luth 1997), the SiO_2 content of the garnet increases with increasing pressure, reflecting an increasing majoritic component. The number of Si cations is greater than 3 per 12 oxygen for some garnets at 4 GPa and for most garnets at pressures >5 GPa (Table 2-3). There seems to be a trend also of Si enrichment (by up to 0.13 cations per 12 oxygen) with increasing temperatures (cf. review by Frost 2006), which may reflect an increase in Si activity of the melt at higher

temperatures. In general, garnet grains were difficult to measure because of irregular surfaces, inclusions and potential overlap with coexisting phases.

Table 2-3 Average pyrope garnet compositions

P [GPa]	4	4	4	5	5	5	5
T [°C]	1150	1250	1500	1200	1250	1400	1550
Run # ae-…	05	07	35	60	19	39	36
N	7	27	11	10	8	10	11
SiO_2 [wt%]	44.6(7)	44.4(2)	45.3(8)	43.6(9)	45.0(6)	45.8(5)	45.2(6)
Al_2O_3	25.6(4)	25.4(2)	25.1(8)	25.9(8)	24.8(5)	24.5(6)	24.5(5)
MgO	29.4(5)	29.3(3)	29.7(8)	30.0(9)	28.9(9)	29.6(8)	29.4(3)
K_2O	0.0(0)	0.2(0)	0.0(1)	0.1(1)	0.0(0)	0.0(0)	0.0(0)
Total	99.7(9)	99.2(4)	100.1(5)	99.6(9)	98.8(5)	100.0(7)	99.1(7)
Cations per 12 O							
Si	3.00(3)	3.00(1)	3.04(4)	2.95(4)	3.05(3)	3.07(3)	3.06(3)
Al	2.03(1)	2.03(1)	1.97(5)	2.05(4)	1.98(4)	1.94(4)	1.95(3)
Mg	2.95(7)	2.95(3)	2.95(10)	3.02(11)	2.93(9)	2.96(8)	2.96(5)
K	0.0(0)	0.01(0)	0.0(0)	0.01(1)	0.00(0)	0.00(0)	0.00(0)
Sum	7.99(3)	7.99(1)	7.97(4)	8.03(5)	7.96(4)	7.96(3)	7.97(2)
Maj comp.	0.00(0)	0.00(0)	0.04(4)	0.00(1)	0.05(2)	0.07(3)	0.06(2)

Table 2-3 ***continued*** Average pyrope garnet compositions

P [GPa]	6	6	7	7	8
T [°C]	1250	1450	1150	1350	1150
Run # ae-…	20	25	94	58	97
n	6	18	4	10	2
SiO_2 [wt%]	46.0(5)	44.9(6)	43.6(6)	43.8(5)	46.7(6)
Al_2O_3	24.1(6)	24.4(8)	24.6(5)	24.8(5)	25.1(6)
MgO	29.0(7)	30.4(7)	31.5(7)	30.6(9)	27.8(6)
K_2O	0.0(0)	0.0(1)	0.1(0)	0.3(2)	0.3(0)
Total	99.0(7)	99.8(4)	99.9(9)	99.5(7)	99.9(18)
Cations per 12 O					
Si	3.11(4)	3.02(4)	2.94(3)	2.97(3)	3.13(2)
Al	1.92(4)	1.94(5)	1.96(2)	1.98(4)	2.98(1)
Mg	2.92(7)	3.05(7)	3.17(8)	3.08(6)	2.77(1)
K	0.00(0)	0.00(1)	0.01(0)	0.03(1)	0.03(0)
Sum	7.94(3)	8.02(3)	8.08(3)	8.06(3)	7.90(1)
Maj comp.	0.11(3)	0.02(3)	0.00(0)	0.00(1)	0.13(2)

Maj. comp. majorite component, *n* number of analyses, standard deviations in the last digit are given in parentheses

2.3.2. Magnesite

Magnesite grains are prismatic, subhedral to euhedral and up to 50 μm in length. Often, rounded grains are found as inclusions in garnet. Magnesite itself

does not contain mineral inclusions. It is non-stoichiometric with rather low MgO ranging from 39 to 44 wt%. Non-stoichiometry in carbonates was also reported in previous high-pressure studies; the data available from early research are limited, though, making it impossible to give a general explanation (Katsura and Ito 1990; Luth 2006; Keshav and Gudfinnsson 2010). The magnesite in our starting material is close to stoichiometric. Perhaps, the EPMA standard chosen for Mg (Forsterite93), possible overlap with other phases or poor polishing is responsible for the offset of the measurements from stoichiometric. At 4 and 5 GPa and 1,250°C, at the solidus, magnesite is intergrown with quench phlogopite (Fig. 2-2b).We interpret this magnesite to be a quench product from melt. No significant amount of potassium was detected, except for magnesite at 8 GPa (Table 2-4). With increasing pressure, the total MgO content measured increases from 39.4 to 44.9 wt% at 4 and 8 GPa, respectively.

Table 2-4 Magnesite compositions

P [GPa]	4	5	6	7	[b]8
T [°C]	1150	1200	1150	1150	1150
Run # ae-…	05	60	15	94	97
n	9	10	8	7	4
SiO_2 [wt%]	0.1(1)	0.1(0)	0.1(2)	0.2(1)	0.1(0)
Al_2O_3	0.1(0)	0.0(0)	0.0(0)	0.0(0)	0.0(0)
MgO	39.4(16)	38.7(7)	41.4(12)	43.2(13)	44.9(7)
K_2O	0.1(1)	0.1(1)	0.1(1)	0.1(1)	0.5(1)
Total	39.6(15)	38.9(8)	41.8(13)	43.6(14)	45.5(8)
Cations per 1 O					
Mg	1.00(0)	0.99(0)	0.99(0)	1.00(0)	0.99(0)
K	0.00(0)	0.00(0)	0.00(0)	0.00(0)	0.01(0)
[a]CO_2	60.4	61.1	58.2	56.4	54.5

[a] By difference, [b] quench magnesite, *n* number of analyses, standard deviations in the last digit are given in parentheses

2.3.3. Phlogopite

Primary phlogopite is elongated to equant and measures up to 100 μm in length. Quench phlogopite is of elongated, dendritic habit and is small (<1 μm) and interstitial or up to 500 μm in length, typically with a large length to width ratio. Primary phlogopite sometimes contains inclusions of small garnet grains, whereas quench phlogopite usually is free of mineral inclusions (Fig. 2-2).

At 1,150 and 1,250°C, primary phlogopite is slightly enriched in MgO and SiO_2 and depleted in Al_2O_3 to higher pressures (Table 2-5; Fig. 2-4). A similar trend was observed by Sato et al. (1997). Other studies report a slight enrichment in SiO_2 to higher pressures (Luth 1997; Konzett and Fei 2000; Trønnes 2002). Primary phlogopite melts over a temperature interval of ~150°C. One super-solidus experiment (ae-58, 1,350°C, 7 GPa) contains, besides residual primary phlogopite, a few grains of a nearly anhydrous phase with a water content of ~1 wt% (46.55, 12.68, 28.73 and 11.05 wt% for SiO_2, Al_2O_3, MgO and K_2O, respectively, and a total of 99.01 wt%). For quench phlogopite, see 'Melt' section below.

2.3.4. Pyroxene

Enstatite occurs only above the solidus, is limited to lower temperatures and is prismatic, euhedral, up to 50 μm in length and free of mineral inclusions. Enstatite is rare or absent above 1,400°C or at pressures >6 GPa, and olivine is more common or the only phase coexisting with garnet and melt. All orthopyroxenes incorporate Al. At the solidus, at 5 GPa and 1,250°C, the

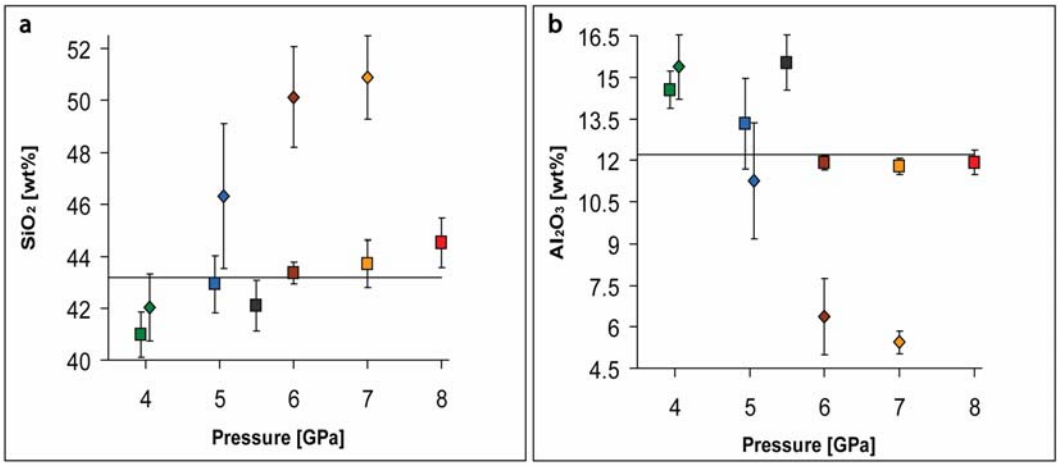

Figure 2-4 Variation of SiO_2 and Al_2O_3 in phlogopite as a function of pressure. Squares (*p-phl* primary phlogopite) and diamonds (*q-phl* quench phlogopite) give the average composition at the given pressure over the whole temperature range phlogopite is present. Horizontal lines mark stoichiometric SiO_2 and Al_2O_3 content. Error bars give the standard deviation. a) With increasing pressure SiO_2 increases and increases dramatically in p-phl and q-phl, respectively. Q-phl at 4 GPa is similar in composition to p-phl. The large standard deviation for q-phl at 5 GPa is due to the presence of residual p-phl coexisting with melt at 1400°C. With increasing temperature p-phl disappeared and SiO_2 in q-phl decreases. b) Al_2O_3 decreases and decreases dramatically in p-phl and q-phl, respectively. Compositions at 5.5 GPa (ae-22) break the trend, which could be due to variations in the starting material. See text for further details.

Table 2-5 Average phlogopite compositions

[a]p or q	p	p	p	p	[b]p	p	[c]p
P [GPa]	4	5.5	6	7	8	5	4
T [°C]	1150	1150	1150	1150	1150	1200	1250
Run # ae-…	05	22	15	94	97	60	07
n	13	9	12	12	14	12	11
SiO_2 [wt%]	42.1(2)	42.6(9)	43.4(4)	43.7(9)	44.5(9)	41.3(6)	41.5(4)
Al_2O_3	15.4(3)	15.6(9)	11.9(3)	11.8(3)	11.9(4)	15.3(7)	14.7(3)
MgO	26.2(4)	26.0(10)	27.9(5)	28.7(7)	28.3(5)	27.1(8)	26.3(3)
K_2O	11.3(1)	11.3(1)	11.3(3)	10.8(2)	10.8(2)	11.0(2)	11.4(1)
Total	94.9(4)	95.4(8)	94.5(7)	95.1(9)	95.5(11)	94.6(6)	94.0(3)
Cations per 22 O							
Si	5.88(2)	5.91(8)	6.10(4)	6.09(8)	6.15(7)	5.79(6)	5.87(5)
Al	2.53(5)	2.55(15)	1.97(5)	1.93(3)	1.94(6)	2.52(10)	2.45(4)
Mg	5.45(8)	5.37(22)	5.83(10)	5.96(18)	5.83(14)	5.67(19)	5.55(6)
K	2.01(3)	1.99(3)	2.03(5)	1.93(3)	1.91(4)	1.96(4)	2.06(2)
Sum	15.86(4)	15.82(10)	15.93(6)	15.91(10)	15.83(8)	15.93(10)	15.93(4)

[a] *p* primary phlogopite and *q* quench phlogopite distinguished by texture, [b] minor olivine, enstatite, quench magnesite present and quench phlogopite not abundant, [c] primary magnesite out and minor quench phlogopite, quench magnesite present, *n* number of analyses; standard deviations in the last digit are given in parentheses

pyroxenes contain ~0.9 wt% of Al_2O_3, whereas at 1,400°C and the same pressure, they contain 1.5 wt% Al_2O_3. We interpret this change to result from the dissolution of phlogopite into the melt, increasing the activity of Al_2O_3 in the melt, thereby increasing the Al content of the orthopyroxene, as observed at lower pressures by Modreski and Boettcher (1972).

Table 2-5 *continued* Average phlogopite compositions

[a]p or q	[c]p	[c]p	q	[d]q	[d]q	q	q
P [GPa]	5	6	6	7	5	4	6
T [°C]	1250	1250	1350	1350	1400	1450	1450
Run # ae-…	19	20	24	58	39	23	25
n	14	15	4	12	9	9	8
SiO_2 [wt%]	43.1(8)	43.6(5)	51.7(18)	50.7(17)	48.9(20)	41.2(15)	49.1(20)
Al_2O_3	12.9(2)	12.0(3)	5.1(13)	5.4(4)	9.0(3)	15.0(5)	6.7(13)
MgO	27.4(5)	27.8(7)	26.9(3)	27.4(6)	24.8(18)	26.4(8)	28.3(17)
K_2O	11.0(1)	11.0(2)	11.3(3)	10.6(7)	10.7(4)	11.6(2)	10.7(3)
Total	94.4(11)	94.3(6)	95.0(4)	94.1(9)	93.3(9)	94.2(10)	94.7(9)
Cations per 22 O							
Si	6.04(5)	6.12(8)	7.12(20)	7.03(14)	6.81(26)	5.79(7)	6.79(22)
Al	2.14(2)	1.98(4)	0.82(22)	0.89(7)	1.50(8)	2.53(3)	1.09(23)
Mg	5.73(11)	5.82(12)	5.53(10)	5.66(17)	5.20(46)	5.58(14)	5.84(35)
K	1.96(4)	1.97(3)	1.98(7)	1.89(14)	1.88(9)	2.10(4)	1.88(7)
Sum	15.89(6)	15.88(7)	15.45(12)	15.47(17)	15.38(29)	16.00(9)	15.60(19)

[a] *p* primary phlogopite and *q* quench phlogopite distinguished by texture, [c] primary magnesite out and minor quench phlogopite, quench magnesite present, [d] primary phlogopite present still, *n* number of analyses; standard deviations in the last digit are given in parentheses

Table 2-5 *continued* Average phlogopite compositions

[a]p or q	q	q	q	q
P [GPa]	4	4	5	6
T [°C]	1500	1550	1550	1550
Run # ae-…	35	26	36	38
n	8	8	9	8
SiO_2 [wt%]	42.3(11)	42.7(8)	44.6(16)	49.4(20)
Al_2O_3	16.6(6)	15.1(10)	13.3(5)	7.0(12)
MgO	25.4(10)	25.4(13)	25.5(10)	26.4(16)
K_2O	11.0(2)	11.3(2)	10.5(8)	10.8(2)
Total	95.2(9)	94.5(8)	93.9(8)	93.6(4)
Cations per 22 O				
Si	5.86(9)	5.98(9)	6.23(16)	6.90(24)
Al	2.72(11)	2.48(17)	2.19(7)	1.15(20)
Mg	5.24(19)	5.30(31)	5.32(25)	5.51(37)
K	1.94(6)	2.02(4)	1.88(15)	1.93(5)
Sum	15.75(9)	15.79(15)	15.62(22)	15.49(22)

[a] *p* primary phlogopite and *q* quench phlogopite distinguished by texture, *n* number of analyses, standard deviations in the last digit are given in parentheses

2.3.5. Olivine

Olivine only occurs above the solidus and exhibits a prismatic to equant habit, is subhedral to rarely euhedral and grows to up to 200 μm in size (Fig. 2-2). Olivine contains no mineral inclusions and often is present at the bottom of the capsules. Olivine is stoichiometric and does not significantly substitute Al or K, which is consistent with the observations of Luth (1997) and Trønnes (2002).

2.3.6. Melt

Sato et al. (1997) approximate their melt composition by analyzing quench phlogopite. In our experiments, however, it is obvious that the hydrous quench solution carries solute, especially over the temperature range where primary phlogopite melts out (Fig. 2-3). But this approach becomes more realistic as a valid approximation at higher temperatures, where less or no solute is precipitating from that solution and where less solution seems to be occurring in the presence of more abundant quench phlogopite (Fig. 2-2d).

Intergrowth of only minor Si-rich quench phlogopite with magnesite along the capsule walls at 4 and 5 GPa at 1,250°C, together with the observation of K-rich precipitates, is taken as evidence that the first melt is K-CO_2-H_2O-Mg-rich and relatively Si-poor. More Si-rich quench phlogopite present at 5 GPa could reflect an increase in Si activity in the melt at higher pressures.

Within the temperature range where primary phlogopite remains in the capsule, the associated quench phlogopite is rich in SiO_2 (~45-48 wt%) and low in

Al_2O_3 (~5-9 wt%). At higher temperatures and 4 GPa, without primary phlogopite present, the average composition of quench phlogopite is close to that of primary phlogopite, but showing a wider standard deviation with respect to Si, Mg and Al content. This variation may be either caused by poor measurements on the small dendritic crystals or by heterogeneity of the melt itself. Potassium remains close to stoichiometric.

There is a clear trend in the quench phlogopite compositions at conditions without residual primary phlogopite and increasing pressure: from 4 GPa with SiO_2 ~42 wt%, Al_2O_3 ~15 wt%, which is similar to primary phlogopite, to 5 GPa with SiO_2 ~46 wt%, Al_2O_3 ~11 wt%, to 6 GPa with SiO_2 ~50 wt%, Al_2O_3 ~6 wt%, to 7 GPa with SiO_2 ~51 wt% and Al_2O_3 ~5 wt% (Table 2-5; Fig. 2-4). In our experiments, this trend becomes apparent at temperatures of 1,350, 1,450-1,550°C.

2.4. Discussion

2.4.1. Phase relations

The observed phase relations are controlled by two main reactions: reaction (2.3) and (2.4):

original synthetic phlogopite breaks down at subsolidus conditions to primary phlogopite + garnet + K-bearing fluid. (2.3)

A similar subsolidus breakdown of phlogopite has been observed at a pressure of ~4.5 and ~6 GPa by Sato et al. (1997) and Luth (1997), respectively. The former formulated the following reaction to explain the occurrence of pyrope

and the enrichment of SiO_2 and MgO in primary phlogopite to higher pressures (modified by Trønnes 2002):

$$K_2Mg_6Al_2Si_6O_{20}(OH)_4 \text{ (phlogopite)} = Mg_3Al_2Si_3O_{12} \text{ (pyrope)} + \frac{3}{7} K_2Mg_7Si_7O_{20}(OH)_4 \text{ (hypothetical phlogopite)} + \frac{4}{7} (K_2O + 2H_2O) \text{ (fluid)} \quad (2.3a)$$

The hypothetical phlogopite in reaction (2.3a) requires Mg to occupy tetrahedral sites. Alternatively, a magnesian montdiorite ($KMg_{2.5}Si_4O_{10}(OH)_2$) component with $2Si^{IV}+\square^{VI}=2Al^{IV}+Mg^{VI}$ (Seifert and Schreyer 1971) could explain the observed compositional trend in the phlogopite with Al>2 cations per 22 oxygen. Primary and quench phlogopite below 6 GPa have Al<2 cations per 22 O, which points to an eastonite component $Si^{IV}+ Mg^{VI}=Al^{IV}+Al^{VI}$ (Arai 1984).

In our experiments, the occurrence of pyrope can be explained by formulating a simplified reaction such as (2.3b) with stoichiometric synthetic phlogopite and with stoichiometric K, (OH), vacancies (□) in the octahedral site, all Al in tetrahedral coordination and $(Al,Si)^{IV}_{\Sigma=4}$ on the product side:

$$2\ KMg_3AlSi_3O_{10}(OH)_2 \text{ (synthetic phlogopite)} = KMg_{2.75}\square_{0.25}Al_{0.5}Si_{3.5}O_{10}(OH)_2 \text{ (Si-rich phlogopite)} + \frac{3}{4} Mg_3Al_2Si_3O_{12} \text{ (pyrope)} + (\frac{2}{4} K_2O + MgO + \frac{1}{4} SiO_2 + H_2O) \text{ (fluid)} \quad (2.3b)$$

The fluid phase contains K_2O, MgO and SiO_2. A higher Si activity of the fluid at higher pressures probably is reflected by the increasing SiO_2 in primary phlogopite with increasing pressure. The Mg and CO_2 content of the fluid may be buffered by the magnesite, which has higher MgO contents with increasing pressure (see 'Magnesite' section above). Pyrope abundance at subsolidus conditions is not increasing much from 4 to 8 GPa, from ~10 to ~15 modal%, respectively. The water of the fluid is mainly produced by the breakdown reaction of phlogopite (2.3b). A smaller amount of water probably comes from dehydroxylation (e.g. Vedder and Wilkins 1969) of the primary phlogopite itself, which is reflected by a tendency in the primary phlogopite data to have higher totals (>95 wt%) at higher pressures. Reaction (2.3b), however, does not explain why the synthetic phlogopite is unstable.

Sato et al. (1997) use natural, Fe-bearing phlogopite in their starting material and perform experiments using Pt capsules. In their study, phlogopite breakdown could result from Fe loss to the platinum capsule, since Pt is known to alloy with iron (Isaacs and Tamman 1907; Bowen and Schairer 1932). Phlogopite in their starting material contains 1.83 wt% FeO, whereas in the run products, it only contains 0.01-0.31 wt% FeO. Why this breakdown is observed ≥4.5 GPa is unclear, though, and implies that another mechanism is involved as well, since Fe is also lost to the capsule at 4 GPa without phlogopite being destabilized. To illustrate the Fe loss, a simplified reaction (2.3c) can be formulated. Phlogopite compositions chosen ($(K)^{XII}_{\Sigma=1}(Mg,Fe^{2+})^{VI}_{\Sigma=3}(Al,Si)^{IV}_{\Sigma=4}$) are similar to Sato et al. (1997) with respect to Mg and Fe cations:

$$2\ KMg_{2.9}Fe_{0.1}AlSi_3O_{10}(OH)_2\ \text{(Fe-bearing phlogopite)} + Pt_{100}\ \text{(Pt capsule)} =$$
$$KMg_{2.9}\square_{0.1}Al_{0.9}Si_{3.1}O_{10}(OH)_2\ \text{(Fe-free phlogopite)} +$$
$$\frac{22}{40}Mg_3Al_2Si_3O_{12}\ \text{(pyrope)} +$$
$$\left(\frac{20}{40}K_2O + \frac{50}{40}MgO + \frac{50}{40}SiO_2 + \frac{3}{40}O_2 + H_2O\right)\ \text{(fluid)} +$$
$$Pt_{99.8}Fe_{0.2}\ \text{(Pt-Fe capsule)} \qquad (2.3c)$$

The breakdown in our experiments is not caused by Fe loss, and pure synthetic phlogopite experiments we performed rule out the presence of carbonate as the trigger as well. Trønnes (2002) did not observe this breakdown of synthetic phlogopite in his experiments. Unfortunately, grains were too small for a chemical analysis of his starting material. More likely, a non-stoichiometric nature of the synthetic phlogopite causes this breakdown. As mentioned above, it was difficult to get a chemical analysis of the synthesized, <1 μm-sized phlogopite crystals. K is low (1.85 cations per 22 O) because we had to probe with a focused beam, and Si is higher (6.11 cations per 22 O), possibly a result of homogenizing the starting material in an agate mortar. Si/Al is close to the ideal 3/1 with Al being 2.02 cations per 22 O. Mg is low with 5.82 cations per 22 oxygen. Luth's (1997) synthetic phlogopite has 6.04, 2.02, 5.90 and 2.00 for Si, Al, Mg and K cations per 22 O, respectively. Luth (1997) has some vacancy (~0.1) in the octahedral site, whereas the other sites are full and stoichiometric. Sato et al. (1997) have vacancies of 0.117 in their octahedral site. In our case, the vacancy is 0.11, and we might have vacancies of <0.15 per 22 O in the interlayer site. Perhaps, vacancies in the crystal structure are the trigger for such a breakdown.

The reaction primary phlogopite + magnesite + fluid =
olivine + enstatite + garnet + K-CO_2-H_2O-rich melt marks
the location of the first occurrence of melt and thus
the location of the solidus. (2.4)

More garnet, relative to the amount resulting from (2.3b), is produced in this reaction; thus, we assume reaction (2.4) to be univariant in the six-component

system and think that the divariant appearance is caused by thermal gradients within the Pt capsule. We show in this study that reaction (2.4) is sensitive to temperature rather than pressure and find that phlogopite, in the presence of carbonate, is stable to pressures up to 8 GPa and temperatures <1,150°C. This is in contrast to reaction (2.2) that was proposed by Ulmer and Sweeney (2002), which predicts that phlogopite melts at >4 GPa in the presence of carbonate. They, however, use a different experimental approach (multiple saturation), which can be problematic in the presence of K-H_2O phases that exhibit incongruent melting (Yoder and Kushiro 1969). In addition, they use a more complex starting mix (synthetic kimberlite), which would reduce the phlogopite stability compared to simple or end-member systems.

An increase in the amount of garnet is observed to higher temperatures and pressures (Sato et al. 1997; Trønnes 2002; this study) and is coupled with the composition of primary and quench phlogopite, which get enriched in Si and depleted in Al. Sato et al. (1997) did not find exactly the same trend in their quench phlogopite compositions of the phlogopite–enstatite system. Al_2O_3 in phlogopite decreases to high pressures with 12.03, 12.23, 9.24 and 6.25 wt% at 4, 5, 6 and 8 GPa, respectively. In agreement with our study, Al_2O_3 decreases more rapidly at pressures >5 GPa. SiO_2 in their study, on the other hand, is high already at 4 GPa (~50 wt%) and varies from 45 to 48 wt% to higher pressures.

In our study, quench phlogopite, identified by texture at 4 GPa, shows compositions similar to primary phlogopite to temperatures as high as 1,550°C. Probably, residual primary phlogopite was still present at low pressures in Sato et

al. (1997) (see 'Melt' section above). This similarity in the composition of quench to primary phlogopite could lead to misinterpretations in studies that only use chemical arguments to distinguish between them. Other studies within the same pressure range either do not observe quench phlogopite or do not report its composition.

Enrichment of Si in phlogopite compositions was also observed in the previous studies. Trønnes (2002) did experiments in a pure synthetic phlogopite system and reports compositions containing 42.8-43.4 wt% SiO_2 at pressures of 4.5-7.4 GPa, respectively. Luth (1997) ran synthetic phlogopite with diopside and measured phlogopite with 42.2-42.5 wt% SiO_2 at pressures of 3-5 GPa, respectively. Fluid was absent at the above conditions, and phlogopite compositions remain constant. The following studies contain a fluid below the solidus: Above 6 GPa, Luth's (1997) phlogopite breaks down releasing a fluid, and the remaining phlogopite compositions are enriched in SiO_2, ranging from 43.6 to 43.7 wt% at a pressure of 7.5 GPa. Sato et al. (1997) performed experiments in the pure natural phlogopite system and report SiO_2 contents of 41.04, 40.73 and 41.69 wt% at pressures of 4, 6 and 8 GPa, respectively. Further experiments using natural phlogopite with synthetic enstatite result in SiO_2 contents of 41.71, 45.95 and 44.71 wt% at pressures of 4, 6 and 8 GPa, respectively. Experiments using synthetic phlogopite with natural magnesite (this study) result in SiO_2 contents of 42.1-44.5 wt% at pressures of 4-8 GPa, respectively. Konzett and Ulmer (1999) did experiments in KNCMASH with 1.22 wt% of H_2O resulting in SiO_2 contents in phlogopite varying from 42.1 to 45.2 at

pressures of 4-8 GPa, respectively. In the modified lherzolite system (BRIAN2), 0.21 wt% H_2O is present and SiO_2 ranges from 41.7 to 43.5 wt% at pressures of 6-6.5 GPa, respectively (Fig. 2-5). Konzett and Fei (2000) have 4.76 wt% water in KNCMASH, and their phlogopite contains 43.3-43.9 wt% SiO_2 at a pressure of 10 GPa.

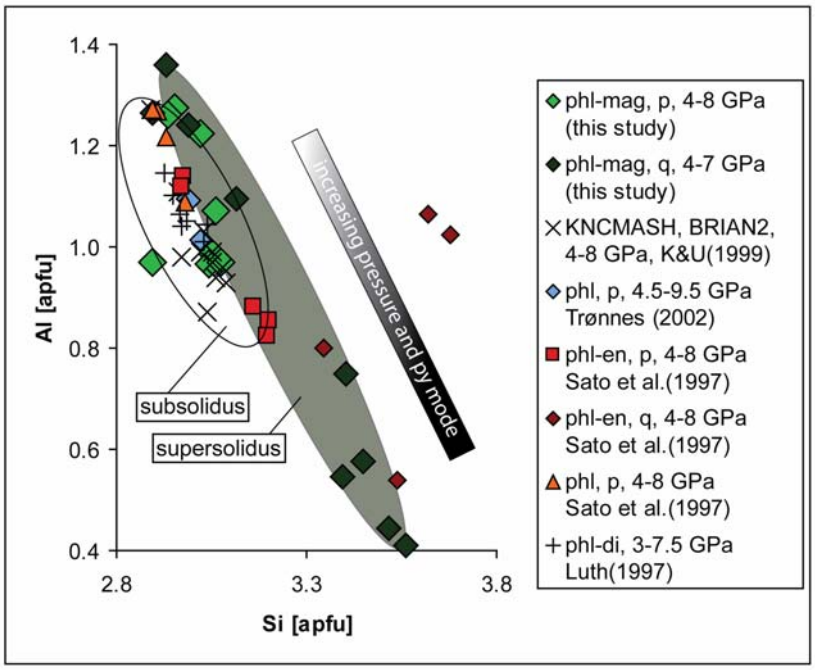

Figure 2-5 Comparison of phlogopite data. Systems with fluid at subsolidus conditions show a wider spread in Al and Si apfu. Modal abundance of garnet increases to higher pressures from ~10-15 % and ~10-30 % at sub- and super-solidus conditions, respectively. See text for discussion. *BRIAN2* modified natural lherzolite, *di* diopside, *en* enstatite, *K&U* Konzett and Ulmer, *KNCMASH* K_2O-Na_2O-CaO-MgO-Al_2O_3-SiO_2-H_2O, *p* primary phlogopite, *phl* phlogopite, *py* pyrope, *q* quench phlogopite

Quench phlogopite compositions (this study) show a dramatic increase in SiO_2 above the solidus of 41.2, 44.6, 49.1 and 50.7 wt% at pressures of 4, 5, 6 and 7 GPa, respectively. Although this quenched phlogopite does not represent an exact melt composition, the increase in silicon may reflect a higher Si activity in the melt at pressures ≥5 GPa.

Generally, a hydrous fluid or melt at subsolidus or supersolidus conditions, respectively, coupled with and maybe controlled by garnet-forming reactions such as (2.3b), enhances a montdioritic substitution in phlogopite with increasing pressure, leading to hypersilicic phlogopite compositions.

2.4.2. Implications for subduction environments

Phlogopite can be produced above a subducting slab by reactions of hydrous K- rich fluid with peridotite (Sato et al. 1997; Konzett and Ulmer 1999) or with metasediments (Massonne 1992; ii in Fig. 2-7a). K-rich melts and fluids originate from the melting of phengite (Vielzeuf and Schmidt 2001) and successive dehydration of phengite, respectively (Schmidt 1996; Hermann and Spandler 2008). Furthermore, reactions of hydrous silicate melt from the slab with peridotite in the mantle wedge will result in the precipitation of phlogopite and enstatite (Wyllie and Sekine 1982). Assuming common subduction zone geometries with geotherms parallel to a subducting slab (Davies and Stevenson 1992; Schmidt and Poli 1998), with an ambient mantle temperature of 1,250°C at ~160 km depth, resulting in slab surface temperatures of <1,000°C below the arc (Kincaid and Sacks 1997; van Keken et al. 2002), and considering solidi of previous studies (see 'Introduction' for references; Fig. 2-6), phlogopite remains stable above the slab. In this case, phlogopite is dragged to greater depths, until it breaks down at subsolidus conditions to K-richterite over the pressure range of 7-11 GPa (Sudo and Tatsumi 1990), 9-11 GPa (Luth 1997) and 6.5-8.5 GPa (Konzett and Ulmer 1999).

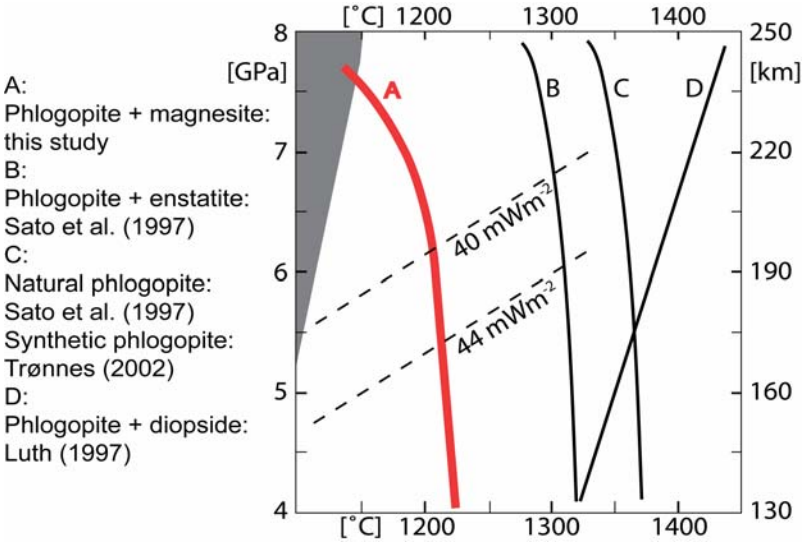

Figure 2-6 Compilation of phlogopite breakdown curves with continental geotherms (dashed) and Cascadia type subduction geotherm (shaded region). Addition of CO_2 shifts the solidus significantly to lower temperatures. D: note positive sloping solidus in phlogopite + diopside with amphibole becoming stable from 6 GPa. See text for discussion.

It is unclear how far above the slab phlogopite would form. In the following discussion, slab surface temperatures, thus, are taken to be the minimum temperature at which phlogopite could occur. The further away from the surface, the hotter will be temperatures in the phlogopite-bearing peridotite. Conder (2005) shows that older subduction models use parameters that will underestimate a slab surface temperature by 200-300°C. Furthermore, slab surface temperatures may vary locally within a slab, depending on subduction style and slab-mantle wedge interaction, by up to 200°C (Kincaid and Griffiths 2003). Syracuse et al. (2010) compare different models, and hottest slab surface temperatures calculated at a depth of 240 km are ~1,150°C. Solidi of previous phlogopite studies are located at too high temperatures (≥1,250°C), and phlogopite remains stable above the slab.

In contrast, LaTourrette et al. (1995) conclude that phlogopite should be involved in the melting process to produce the common geochemical arc magma signature with respect to LILE. K-rich lamprophyric rocks found in arcs of young subduction zones (e.g. Esperança and Holloway 1987; Hochstaedter et al. 1996; Maria and Luhr 2008; Owen 2008; Vigouroux et al. 2008) support the presence and melting of phlogopite within the mantle wedge. Previous CO_2-free studies cannot support this idea, because phlogopite is stable to too high temperatures (Fig. 2-6). CO_2, however, should be considered because carbonates are present in most subduction environments and are subducted into the mantle (Rea and Ruff 1996; Plank and Langmuir 1998). Modeling shows that more than 70% of carbonates in a slab will be stable in the typical volcanic arc region and will be transported to greater depths (Thomsen and Schmidt 2008). Metamorphic devolatilization of carbonates is promoted by hydrous fluids infiltrating carbonate sediments (Kerrick and Connolly 2001), and resulting CO_2-bearing fluids will react with peridotite to form carbonates (i in Fig. 2-7a). The stability of carbonates has been studied extensively to date (cf. review by Luth 1999), and different peridotite carbonation reactions have been proposed: e.g. olivine + diopside + CO_2 = dolomite + enstatite (Wyllie et al. 1983); magnesite + diopside = dolomite + enstatite (Brey et al. 1983), with magnesite being the stable carbonate at higher pressures, in the diamond stability field.

If carbonation reactions and phlogopite metasomatism take place within the mantle wedge, our study shows that the presence of carbonate will lower the temperature stability of phlogopite considerably. If not broken down to K-

richterite yet, phlogopite will melt at pressures of ~7.5 GPa (this study) in the presence of carbonate in a Cascadia-type subduction zone (shaded region in Fig. 2-6; star in Fig. 2-7a).

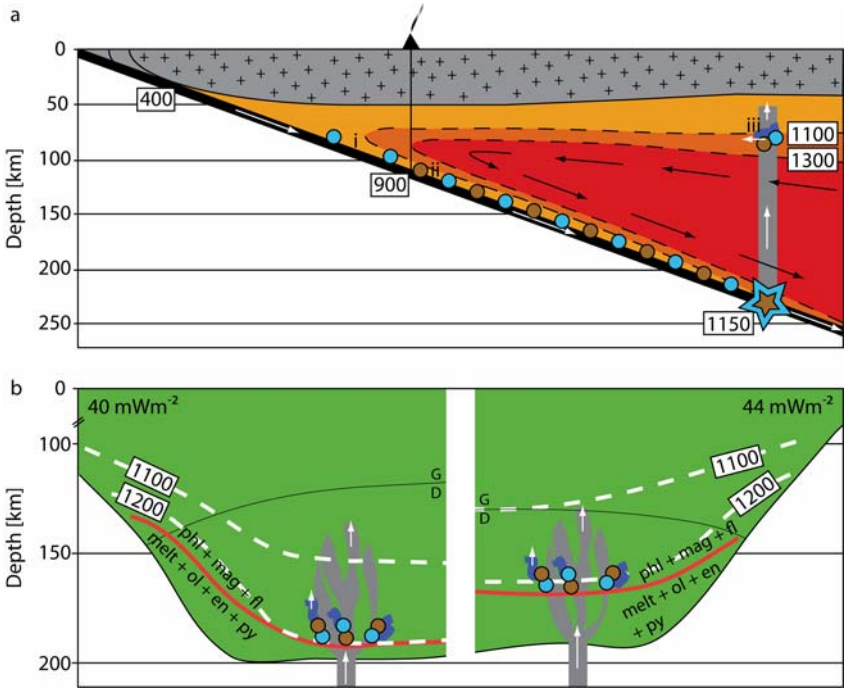

Figure 2-7 Sketch of a) Cascadia type subduction zone (numbers from Syracuse et al. 2010). Slab temperatures and mantle isotherms in °C. Blue and brown denotes presence of carbonate and phlogopite, respectively. Phlogopite with carbonate melts at a depth of ~240 km (star). Resulting melts rise and enrich the mantle wedge in K and CO_2. Melt could react with cooler mantle underneath the continent (iii), possibly crystallizing phlogopite and carbonate, which could be transported back into the mantle wedge. See text for i-ii. b) Melt from below infiltrates the sub-continental lithospheric mantle and reacts with enstatite, olivine and pyrope to phlogopite, magnesite and a fluid. *en* enstatite, *fl* fluid (dark blue), *G/D* graphite/diamond transition, *mag* magnesite (light blue), melt (grey), *ol* olivine, *phl* phlogopite (brown), *py* pyrope

Alternatively, assuming phlogopite forms away from the slab surface, or, considering a tendency to underestimate slab surface temperatures and local variations in temperatures on the slab surface, the solidus may be reached in the hotter region above a slab in a very hot young and slow subduction environment

at lower pressures already. In this case, phlogopite melting above the slab may happen locally, on a smaller scale, whereas phlogopite in cooler regions would be subducted to greater depths.

2.4.3. Implication for the subcontinental lithospheric mantle

The addition of CO_2 to the system shifts the solidus significantly to lower temperatures (Fig. 2-6), whereas the pressure stability is not dramatically reduced in this simple system. A cool 40-mWm^{-2} geotherm intersects the carbonated solidus above 6 GPa, implying that phlogopite will be stable to a depth of ~200 km in the presence of carbonate. Unlike the suggestion of Ulmer and Sweeney (2002), the presence of a C-O-H fluid does not destabilize the phase assembly present at subsolidus conditions at pressures >4 GPa. In a colder lithospheric mantle (<40 mWm^{-2}), the stability would extend to even higher pressures. The hotter geotherm (44 mWm^{-2}) intersects the solidus at a depth of ~180 km. To this depth, a fluid that, with increasing pressure becomes enriched in Si (see 'Phase relations' section above), is coexisting with phlogopite, magnesite and pyrope. This is in agreement with the data of Mibe et al. (2002) who found an increasing amount on Mg and Si being dissolved in a fluid in the MgO-SiO_2-H_2O system with increasing pressure. Beyond 180 km depth, at the base of a subcontinental lithospheric mantle, a hydrous, Si-, K- and CO_2-bearing silicate melt will be present and could be a potential metasomatic agent. Consequently, potassium- and CO_2-rich magmas, such as kimberlites, originate at pressures beyond 5 GPa, which is in agreement with early studies (Wyllie 1980; Canil and Scarfe 1990;

Dalton and Presnall 1998). Ascending melts, on the other hand, that were produced deeper could freeze within the subcontinental lithospheric mantle by reacting with garnet, olivine and pyroxene to form phlogopite plus carbonate and thus could be trapped (Fig. 2-7b). This freezing of the melt will happen at ~200 km or at ~180 km depth in a cold (40 mWm^{-2}) or in a warmer lithospheric mantle (44 mWm^{-2}), respectively. Resulting fluids will further percolate upwards in that lithospheric mantle. Reactivation of the lithosphere (Foley 2008) then might melt this low temperature assemblage and possibly will produce K-rich magmas. Given that phlogopite and carbonate need to occur in the same potential source region for group II kimberlites, and that carbonate and phlogopite can coexist to a considerable depth (i.e. to 180-200 km depth) in a continental lithospheric mantle, might be responsible for the scarcity of group II kimberlites reaching the surface.

2.5. Conclusions

Phlogopite, garnet and a C-O-H-fluid are in equilibrium with magnesite at 4, 5, 6 and 7 GPa to temperatures of 1,250, 1,200, 1,200, and 1,150°C, respectively. At higher temperatures, phlogopite and magnesite react to form enstatite, forsterite, pyrope and a hydrous Si-, K- and CO_2-bearing melt. The modal amount of garnet above solidus further increases to higher pressures and temperatures from ~10 to ~30%. Melt quenches to dendritic phlogopite crystals and a hydrous solution. There is a dramatic change in quench phlogopite compositions along isotherms with increasing pressure from close to primary at 4 GPa, to hypersilicic at pressures ≥5 GPa.

In a subduction zone, the simple infiltration of a K-rich fluid and C-O-H fluid will not necessarily induce melting by destabilizing carbonate and phlogopite, respectively, as temperature rather than pressure is the limiting factor of such a phase assembly. A Cascadia-type subduction geotherm intersects the solidus found in the present study at a pressure of ~7.5 GPa, where phlogopite in the presence of carbonate will melt.

In a cold (40 mWm^{-2}) subcontinental lithospheric mantle, phlogopite will be stable to 200 km depth in the presence of carbonate, and to a depth of 180 km assuming a 44-mWm^{-2} geotherm. Kimberlitic melts could be trapped at the base of a subcontinental lithospheric mantle by reactions with peridotite at ~180-200 km depth to form phlogopite and carbonate. Fluids in phlogopite-bearing peridotite become richer in Si at pressures ≥5 GPa. The same holds for a carbonated phlogopite-bearing lherzolite as long the CO_2 is buffered by the stable carbonate phase.

References

Arai S (1984) Pressure-temperature dependent compositional variation of phlogopitic micas in upper mantle peridotites. Contrib Mineral Petrol 87:260-264.

Armstrong JT (1988) Quantitative analysis of silicate and oxide materials: comparison of Monte Carlo, ZAF, and phi(rho Z) procedures, In: Newbury DE (ed) Microbeam Analysis, pp 239-246.

Bowen NL, Schairer JF (1932) The system FeO-SiO_2. Am J Sci 224(24):177-213.

Brey G, Brice WR, Ellis DR, Green DH, Harris KL, Ryabchikov ID (1983) Pyroxene-carbonate reactions in the upper mantle. Earth Planet Sci Lett 62:63-74.

Canil D, Scarfe CM (1990) Phase Relations in Peridotite + CO_2 Systems to 12 GPa: Implications for the Origin of Kimberlite and Carbonate Stability in the Earth's Upper Mantle. J Geophys Res 95:15,805-15,816.

Conder JA (2005) A case for hot slab surface temperatures in numerical viscous flow models of

subduction zones with an improved fault zone parameterization. Phys Earth Planet In 149:155-164.

Dalton JA, Presnall DC (1998) The Continuum of Primary Carbonatitic-Kimberlitic Melt Compositions in Equilibrium with Lherzolite: Data from the System CaO-MgO-Al_2O_3-SiO_2-CO_2 at 6 GPa. J Petrol 39:1953-1964.

Davies JH, Stevenson DJ (1992) Physical model for the source region of subduction zone volcanics. J Geophys Res 97:2037-2070.

Edwards D, Rock NMS, Taylor WR, Griffin BJ, Ramsay RR (1992) Mineralogy and Petrology of the Aries Diamondiferous Kimberlite Pipe, Central Kimberley Block, Western Australia. J Petrol 33:1157-1191.

Eggler DH (1987) Solubility of Major and Trace Elements in the Mantle Metasomatic Fluids: Experimental Constraints. In: Menzies MA, Hawkesworth CJ (eds) Mantle Metasomatism. Academic Press Geology Series, pp 21-41.

Erlank AJ, Waters FG, Hawkesworth CJ, Haggerty SE, Allsopp HL, Rckard RS, Menzies M (1987) Evidence for Mantle Metasomatism in Peridotite Nodules from the Kimberley Pipes, South Africa. In: Menzies MA, Hawkesworth CJ (eds) Mantle Metasomatism. Academic Press Geology Series, pp 221-311.

Esperança S, Holloway JR (1987) On the origin of some mica-lamprophyres: experimental evidence from a mafic minette. Contrib Mineral Petrol 95:207-216.

Foley SF (2008) Rejuvenation and erosion of the cratonic lithosphere. Nature Geosci 1:503-510.

Frost DJ (2006) The Stability of Hydrous Mantle Phases. In: Keppler, H., and Smyth, J.R. (eds) Water in nominally anhydrous minerals. Mineral Soc Am 62:243-271.

Hermann J, Spandler CJ (2008) Sediment Melts at Sub-arc Depths: an Experimental Study. J Petrol 49(4):717-740.

Hochstaedter AG, Ryan JG, Luhr JF, Hasenaka T (1996) On B/Be ratios in the Mexican Volcanic Belt. Geochim Cosmochim Acta 60(4):613:628.

Isaacs E, Tamman G (1907) Über die Legierungen des Eisens mit Platin. Z Anorg Chem 55:63-71.

Kanzaki M (1987) Ultrahigh-pressure phase relations in the system $Mg_4Si_4O_{12}$-$Mg_3Al_2Si_3O_{12}$. Phys Earth Planet In 49:168-175.

Katsura T, Ito E (1990) Melting and subsolidus phase relations in the $MgSiO_3$-$MgCO_3$ system at high pressures: implications to evolution of the Earth's atmosphere. Earth Planet Sci Lett 99:110-117.

Kerrick DM, Connolly JAD (2001) Metamorphic devolatilization of subducted marine sediments and the transport of volatiles into the Earth's mantle. Nature 411:293-296.

Keshav S, Gudfinnsson G (2010) Experimentally dictated stability of carbonated oceanic crust to moderately great depths in the Earth: Results from the solidus determination in the system CaO-MgO-Al_2O_3-SiO_2-CO_2. J Geophys Res 115:20pp.

Kincaid C, Griffiths RW (2003) Laboratory models of the thermal evolution of the mantle during rollback subduction. Nature 425:58-62.

Kincaid C, Sacks IS (1997) Thermal and dynamical evolution of the upper mantle in subduction zones. J Geophys Res 102:12295-12315.

Konzett J, Fei Y (2000) Transport and Storage of Potassium in the Earth's Upper Mantle and Transition Zone: an Experimental Study to 23 GPa in Simplified and Natural Bulk Compositions. J Petrol 41(4):583-603.

Konzett J, Ulmer P (1999) The Stability of Hydrous Potassic Phases in Lherzolitic Mantle-an Experimental Study to 9.5 GPa in Simplified and Natural Bulk Compositions. J Petrol 40(4):629-652.

Kushiro I (1976) Changes in viscosity and structure of melt of $NaAlSi_2O_6$ composition at high pressures. J Geophys Res 81:6347-6350.

LaTourrette T, Hervig RL, Holloway JR (1995). Trace element partitioning between amphibole, phlogopite, and basanite melt. Earth Planet Sci Lett 135:13–30.

Leost I, Stachel T, Brey GP, Harris JW, Ryabchikov ID (2003) Diamond formation and source carbonation: mineral associations in diamonds from Namibia. Contrib Mineral Petrol 145:15-24.

Luth RW (1997) Experimental study of the system phlogopite-diopside from 3.5 to 17 GPa. Am Mineral 82:1198-1209.

Luth RW (1999) Carbon and Carbonates in the mantle. In: Fey Y, Bertka CM, Mysen BO (eds) Mantle Petrology: Field Observations and High Pressure Experimentation: A Tribute to Francis R (Joe) Boyd. The Geochemical Society, Special Publication 6, pp 297-316.

Luth RW (2006) Experimental study of the $CaMgSi_2O_6$-CO_2 system at 3-8 GPa. Contrib Mineral Petrol 151:141-157.

Maria AH, Luhr JF (2008) Lamprophyres, Basanites, and Basalts of the Western Mexican Volcanic Belt: Volatile Contents and a Vein–Wallrock Melting Relationship. J Petrol 49:2123-2156.

Massonne HJ (1992) Evidence for low-temperature ultrapotassic siliceous fluids in subduction zone environments from experiments in the system K_2O-MgO-Al_2O_3-SiO_2-H_2O (KMASH). Lithos 28:421-434.

McCormick GR, Le Bas MJ (1996) Phlogopite crystallization in carbonatitic magmas from Uganda: Can Mineral 34:469-478.

Mibe K, Fujii T, Yasuda A (2002) Composition of aqueous fluid coexisting with mantle minerals at high pressure and its bearing on the differentiation of the Earth's mantle. Geochim Cosmochim Acta 66:2273-2285.

Mitchell RH (ed.) (1995) Kimberlites, orangeites, and related rocks. New York : Plenum Press 410 p.

Modreski PJ, Boettcher AL (1972) The stability of phlogopite + enstatite at high pressures: a model for micas in the interior of the earth. Am J Sci 272:852-869.

Nishihara Y, Matsukage KN, Karato SI (2006) Effects of metal protection coils on thermocouple EMF in multi-anvil high-pressure experiments. Am Mineral 91:111-114.

Nixon PH (ed.) (1987) Mantle Xenoliths. New York: John Wiley.

Owen JP (2008) Geochemistry of lamprophyres from the Western Alps, Italy: implications for the origin of an enriched isotopic component in the Italian mantle. Contrib Mineral Petrol 155:341-362.

Plank T, Langmuir CH (1998) The chemical composition of subducting sediment and its consequences for the crust and mantle. Chem Geol 145:325-94.

Rea DK, Ruff LJ (1996) Composition and mass flux of sediment entering the world's subduction zones: implications for global sediment budgets, great earthquakes, and volcanism Earth Planet Sci Lett 140:1-12.

Ringwood AE (1967) Pyroxene-garnet transformations in the Earth's mantle. Earth Planet Sci Lett 2:255-263.

Sato K, Katsura T, Ito E (1997) Phase relations of natural phlogopite with and without enstatite up to 8 GPa: implication for mantle metasomatism. Earth Planet Sci Lett 146:511-526.

Schmidt MW (1996) Experimental Constraints on Recycling of Potassium from Subducted Oceanic Crust. Science 272:1927-1930.

Schmidt MW, Poli S (1998) Experimentally based water budgets for dehydrating slabs and consequences for arc magma generation. Earth Planet Sci Lett 163:361-379.

Seifert F, Schreyer W (1971) Synthesis and stability of micas in the system K_2O-MgO-SiO_2-H_2O and their relations to phlogopite. Contrib Mineral Petrol 30:196-215.

Sobolev NV, Kaminsky FV, Griffin WL,Yefimova ES, Win TT, Ryan CG, Botkunov AI (1997) Mineral inclusions in diamonds from the Sputnik kimberlite pipe, Yakutia. Lithos 39:135-157.

Sobolev NV, Logvinova AM, Efimova ES (2009) Syngenetic phlogopite inclusions in kimberlite-hosted diamonds: implications for role of volatiles in diamond formation. Russ Geol Geophys 50(12):1234-1248.

Sudo A, Tatsumi Y (1990) Phlogopite and K-amphibole in the upper mantle: Implication for magma genesis in subduction zones. Geophys Res Lett 17(1):29-32.

Syracuse EM, van Keken PE, Abers GA (2010) The global range of subduction zone thermal models. Phys Earth Planet In 183:73-90.

Thompson AB (1992) Water in the earth's upper mantle. Nature 358:295-302.

Thomsen TB, Schmidt MW (2008) Melting of carbonated pelites at 2.5-5.0 GPa, silicate-carbonatite liquid immiscibility, and potassium-carbon metasomatism of the mantle. Earth Planet Sci Lett 267:17-31.

Trønnes RG (2002) Stability range and decomposition of potassic richterite and phlogopite end members at 5-15 GPa. Mineral Petrol 74:129-148.

Ulmer P, Sweeney RJ (2002) Generation and differentiation of group II kimberlites: Constraints from a high-pressure experimental study to 10 GPa. Geochim Cosmochim Acta 66:2139-2153.

van Achterbergh E, Griffin WL, Stiefenhofer J (2001) Metasomatism in mantle xenoliths from the Letlhakane kimberlites: estimation of element fluxes. Contrib Mineral Petrol 141:397-414.

van Keken PE, Kiefer B, Peacock SM (2002) High-resolution models of subduction zones: implications for mineral dehydration reactions and the transport of water into the deep mantle. Geochem Geophys Geosyst 3:1056-1076.

Vedder W, Wilkins RWT (1969) Dehydroxylation and Rehydroxylation, Oxidation and Reduction of Micas. Am Mineral 54:482-509.

Vigouroux N, Wallace PJ, Kent AJR (2008) Volatiles in High-K Magmas from the Western Trans-

MexicanVolcanic Belt: Evidence for Fluid Fluxing and Extreme Enrichment of the Mantle Wedge by Subduction Processes. J Petrol 49(9):1589-1618.

Vielzeuf D, Schmidt MW (2001) Melting relations in hydrous systems revisited: application to metapelites, metagreywackes and metabasalts. Contrib Mineral Petrol 141:251-67.

Walter MJ, Thibault Y, Wei K, Luth RW (1995) Characterizing experimental pressure and temperature conditions in multianvil apparatus. Can J Phys 73:273-286.

Wendlandt RF, Eggler DH (1980) The origins of potassic magmas: 2. stability of phlogopite in natural spinel lherzolite and in the system $KAlSiO_4$-MgO-SiO_2-H_2O-CO_2 at high pressures and high temperatures. Am J Sci 280:421-458.

Wyllie PJ (1980) The Origin of Kimberlite. J Geophys Res 85:6902-6910.

Wyllie PJ, Sekine T (1982) The formation of mantle phlogopite in subduction zone hybridization. Contrib Mineral Petrol 4:375-380.

Wyllie PJ, Huang W-L, Otto J, Byrnes AP (1983) Carbonation of peridotites and decarbonation of siliceous dolomites represented in the system CaO-MgO-SiO_2-CO_2 to 30 kbar. Tectonophys 100:359-388.

Yamashita H, Arima M, Ohtani E (1995) High pressure melting experiments on group II kimberlite up to 8 GPa; implications for mantle metasomatism. Proc Int Kimberlite Conf 6:669-671.

Yoder HS, Kushiro I (1969) Melting of a hydrous phase: phlogopite. Am J Sci 267(A):558-582.

Chapter 3: Phase Relations of Phlogopite and Pyroxene with Magnesite from 4 to 8 GPa: KCMAS-H_2O and KCMAS-H_2O-CO_2[1]

3.1. Introduction

In the Earth's interior, volatiles play a fundamental role in processes in, such as metasomatism, which is widespread in the Earth's mantle and probably is one of the most complex processes. Hydrous minerals and carbonates play a key role in melting processes that depend on the stability of these OH- and CO_2-bearing phases (cf. reviews by Luth 2004; Frost 2006; Dasgupta and Hirschmann 2010). Previous experimental studies involving phlogopite mainly focus on subsolidus breakdown reactions (cf. review by Frost 2006) and only a few studies constrain the melting relations: pure phlogopite systems (Sato et al. 1997; Trønnes 2002), phlogopite with enstatite (Modreski and Boettcher 1972; Sato et al. 1997), phlogopite with diopside (Luth 1997), phlogopite with magnesite (Enggist et al. 2012), and phlogopite with enstatite and diopside (Modreski and Boettcher 1973). Natural, carbonated spinel lherzolite was studied from 1 to 3 GPa (Wendlandt and Eggler 1980), and more information on phlogopite stability comes from multiple saturation experiments on orangeites (Yamashita et al. 1995; Ulmer and Sweeney 2002). The work of Modreski and Boettcher (1973) was extended to higher pressures by Sudo and Tatsumi (1990) by constraining subsolidus reactions involving phlogopite with enstatite and diopside.

[1] A version of this chapter was submitted for publication in *Contributions to Mineralogy and Petrology*.

Melting relations of the phlogopite with enstatite and diopside assemblage remain unconstrained, as does the effect of CO_2. Previous authors suggested that the infiltration of a C-O-H fluid into metasomatized peridotite will trigger the breakdown of phlogopite, or that a K-OH fluid will destabilize carbonates, and will result in K-C-OH-rich melts at pressures >4 GPa (Wendlandt and Eggler 1980; Ulmer and Sweeney 2002). Enggist et al. (2012) show that phlogopite can be stable in the presence of carbonate to pressures greater than 7 GPa. The results of that simple system need to be extended into more complex systems.

In the present study we constrain the melting relations of phlogopite and pyroxene with and without magnesite from 4 to 8 GPa. This study contributes to the understanding of potassium and water recycling into the Earth's mantle, sources of alkali-rich melts or fluids that are potential metasomatic agents, and the effect of CO_2 on the stability of K-OH-phases.

3.2. Experimental procedures

3.2.1. Starting materials

High purity oxides (Al_2O_3, MgO and SiO2 of 99.99%, 99.95% and 99.5% purity, respectively) and carbonate (K_2CO_3 of 99.0% purity) from Alfa Chemicals were used to prepare an anhydrous phlogopite mixture. Phlogopite was synthesized using an end-loaded piston-cylinder at the University of Alberta (for details see Enggist et al. 2012). The products of the synthesis were checked by XRD to ensure that only phlogopite (phl) is present. Phlogopite crystals were small (≤1 μm) and chemical analysis by electron microprobe, therefore, was

problematic. Fragments of natural magnesite (mag) from Mt. Brussilof, British Columbia, Canada, that were free of visible inclusions, were separated out under a microscope and were ground in an agate mortar before added to the starting material mixture. A synthetic enstatite-diopside (en-di) glass ($en_{50}di_{50}$; wt%) was prepared from high purity oxides (MgO and SiO_2; purity as above) and $CaCO_3$ powder of 99.95% purity from Alfa Chemicals. The mix, contained in a Pt-crucible, was fused in a one atmosphere furnace at 1600°C for 8 h. The melt was quenched to a glass by dipping the Pt-crucible into distilled water. The resulting glass disc was wrapped into a plastic bag and crushed into small fragments using a hammer. The fragments then were ground in an agate mortar. The resulting glass powder was, again, melted at 1600°C for 8 h and quenched as before. This crushing, melting and quenching cycle was repeated 3 times for each en-di glass batch in order to obtain a homogeneous glass composition. For the KCMAS-H_2O and KCMAS-H_2O-CO_2 system, starting materials of, by weight, $phl_{33}en_{33}di_{33}$ and $phl_{32}en_{32}di_{32}mag_4$ were prepared, respectively, and used in the experiments (Table 3-1). The composition of the synthetic phlogopite and natural magnesite, and their relative molar proportion in the starting material (2:1), is the same as in Enggist et al. (2012).

3.2.2. Experimental setup

Approximately 1-3 mg of starting material was loaded into 1.5 mm outer diameter Pt capsules. The tops of the capsules were triple-crimped and capsules then were placed in an oven to dry at 120°C overnight. No water was added to the

samples. They were welded shut with a dampened tissue wrapped around the lower part of the capsule to keep the starting material cool. Sealed capsules were gently compressed into a cylindrical shape in a brass die.

The capsules were run in 18/11 assemblies (Walter et al. 1995) that were prepared as described in Enggist et al. (2012). Frequent shorting of the thermocouple wires to the anvils, which can lead to erroneous emf readings, was reduced by replacing the solid graphite ring in the top part of the assembly by a split ring.

Table 3-1 Composition of starting materials

[wt%]	Phlogopite (n = 19)	[wt%]	Magnesite (n =15)	[a]En-Di (n = 14)
SiO_2	43.7(4)	SiO_2	0.1(1)	57.9(1)
Al_2O_3	12.3(2)	Al_2O_3	*b.d.*	-
MgO	27.8(4)	FeO_{tot}	0.2(1)	-
K_2O	10.3(2)	MnO	*b.d.*	-
Total	94.1(4)	MgO	47.3(2)	29.1(1)
		CaO	0.02(1)	12.7(1)
Cations per 22 O		Na_2O	*b.d.*	-
Si	6.11(4)	K_2O	*b.d.*	-
Al	2.02(3)	Total	47.6(2)	99.7(1)
Mg	5.82(9)			
K	1.85(4)	[b]CO_2	52.4	
Sum	15.80(6)			

[a] enstatite-diopside glass (50/50 wt%), [b] by difference, *b.d.* below detection limit, *n* number of analyses; 1 standard deviation in the last digit is given in parentheses

All experiments were performed using the UHP-2000 uniaxial split-sphere multi-anvil apparatus at the University of Alberta. Samples were pressurized first and then heated at a rate of 60 mVh^{-1} (~60°C min^{-1}) at pressures from 4-7 GPa. At 8 GPa the heating rate above 800°C was reduced to ≤30 mVh^{-1} (≤30°C min^{-1}), which decreased the number of thermocouple breaks. Experiments were quenched by cutting off the power to the furnaces, causing the temperature to drop below 300°C in 2-5 s, and then decompressed over 2.5-4 h. Experimental charges were

mounted in epoxy (Petropoxy 154), ground open and impregnated under vacuum. Samples were polished using a rotating disc and Al_2O_3-powder of 5, 1 and 0.05 μm grain size with oil, ethanol or acetone to preserve water soluble phases. Polished samples were cleaned in an ultrasonic bath, dried at 60°C and then carbon-coated for microprobe analysis.

3.2.3. Analytical methods

A JEOL 8900 electron microprobe at the University of Alberta was used for the analysis of the experimental products. The acceleration voltage was set to 15 kV and the cup beam current to 15 nA. Standards were albite (Na), diopside (Ca), forsterite93 (Mg), hematite (Fe), pyrope (Al, Si), orthoclase (K) and willemite (Mn). Counting times were 20 and 10 s on peak and background, respectively. A focused beam was used to analyze diopside, enstatite, garnet, magnesite and olivine, and beam diameters of up to 3 μm, depending on grain size, were chosen for phlogopite and potassic richterite grains. The Phi-Rho-Z (Armstrong 1988) correction provided by JEOL was applied to the raw data, and Norm spread sheets by P. Ulmer (personal communication, 2007) were used to calculate mineral compositions.

Mineral modes of each charge were estimated using backscatter images taken with the EPMA. Generally, each experimental charge had to be polished several times, exposing different sections of the same charge, allowing better estimates of modal percentages.

3.3. Results

3.3.1. General observations

Kinetics for both systems are slow, and run times from 8-144 h at high and low temperatures, respectively, were required to achieve equilibrium (Table 3-2).

Table 3-2 Experimental results KCMAS-H_2O

Run # ae-…	T [°C]	Pressure [GPa]	Duration [h]	Results
157	1250	4	72	p-phl + en + di + gr + fl
147		5	72	p-phl + en + di + gr + fl
163	1300	4	72	p/q-phl + en + di + gr + melt
118		5	24	p/q-phl + en + di + gr + melt
129		5.5	48	p/q-phl + en + di + gr + melt
132		5.5	72	p/q-phl + en + di + gr + melt
158		6	48	p-phl + en + di + gr + fl
152		7	48	kr + p-phl + en + di + gr + fl
117		8	24	kr + en + di + gr + ol + fl
140	1350	4	48	p/q-phl + en + di + gr + ol + melt
33		6	10	p/q-phl + en + di + gr + ol + melt
112		7	24	en + di + gr + melt
161		8	48	kr + en + di + gr + melt
32	1400	5	10	p/q-phl + en + di + gr + ol + melt
30		6	10	p/q-phl + en + di + gr + ol + melt
111		7	24	kr + en + di + gr + ol + melt
139		7	24	kr + en + di + gr + ol + melt
120		8	24	en + di + gr + ol + melt
65	1450	5	8	p/q-phl + en + di + gr + ol + melt
146		6	72	p/q-phl + en + di + gr + ol + melt
50	1500	5	8	q-phl + en + di + gr + ol + melt
131		7	24	en + di + gr + ol + melt

di diopside, *en* enstatite, *fl* fluid, *gr* garnet, *hydr sol* hydrous solution, *kr* potassic richterite, *ol* olivine, *p-phl* primary phlogopite, *p/q-phl* primary and quench phlogopite present, *q-phl* quench phlogopite

Below the solidus, the grain size can be extremely small (<1-5 µm). In the carbonate-free system (KCMAS-H_2O), the solidus is characterized by a change in texture with the occurrence of interstitial quench phlogopite and melt in the hot spot of the capsules. In the CO_2-bearing system (KCMAS-H_2O-CO_2), the disappearance of magnesite together with the occurrence of quench phlogopite

and melt marks the solidus. A fluid (~2 wt%) is present below the solidus, resulting from a breakdown reaction of the synthetic phlogopite to phlogopite, garnet and a fluid (Sato et al. 1997; Luth 1997; Enggist et al. 2012).

Table 3-2 *continued* Experimental results KCMAS-H_2O-CO_2

Run # ae-…	T [°C]	Pressure [GPa]	Duration [h]	Results
155	1100	7	144	p-phl + kr + mag + en + di + gr + fl
156		8	120	kr + mag + en + di + gr + fl
151	1150	4	72	p-phl + mag + en + di + gr + fl
159		5	72	p-phl + mag + en + di + gr + fl
149		6	48	p-phl + mag + en + di + gr + fl
148		7	48	kr + en + di + gr + melt
162		8	48	kr + en + di + gr + melt
143	1200	4	72	p-phl + en + di + gr + melt
110		5	96	p/q-phl + en + di + gr + ol + melt
160		6	48	p/q-phl + en + di + gr + ol + melt
59	1300	5	8	p/q-phl + en + di + gr + ol + melt
69		6	8	en + di + gr + ol + melt
145		7	72	en + di + gr + ol + melt
71		8	8	en + di + gr + ol + melt
52	1400	5	8	q-phl + en + di + gr + ol + melt
55	1500	4	8	q-phl + en + di + gr + ol + melt
70	1600	4	8	q-phl + en + di + gr + ol + melt
144	~1600[a]	7	72	melt + ol
153	~1500[a]	8	72	melt + en + di+ ol

[a] estimated temperature (see text), *di* diopside, *en* enstatite, *fl* fluid, *gr* garnet, *hydr sol* hydrous solution, *kr* potassic richterite, *mag* magnesite, *ol* olivine, *p-phl* primary phlogopite, *p/q-phl* primary and quench phlogopite present, *q-phl* quench phlogopite

The phlogopite that coexists with garnet, diopside, enstatite, ± magnesite and a fluid below the solidus is referred to as "primary phlogopite" in this article. Amphibole found as a breakdown product of phlogopite below the solidus was described in Sudo and Tatsumi (1990), Sato et al. (1997), Luth (1997), Konzett and Ulmer 1999 and Konzett and Fei (2000). In Na-bearing systems, this amphibole was called K-richterite, with K in the A-site and Na in the M2-site. In Na-free systems K is found in A- and M2 sites and the amphibole was called KK-

richterite (Konzett and Ulmer 1999; Yang et al. 1999). The amphibole found in the present study will be referred to as 'potassic richterite'.

The solidus in KCMAS-H_2O was bracketed between 1250 and 1300°C at 4 and 5 GPa, 1300 and 1350°C at 6, 7 and 8 GPa (Fig. 3-1).

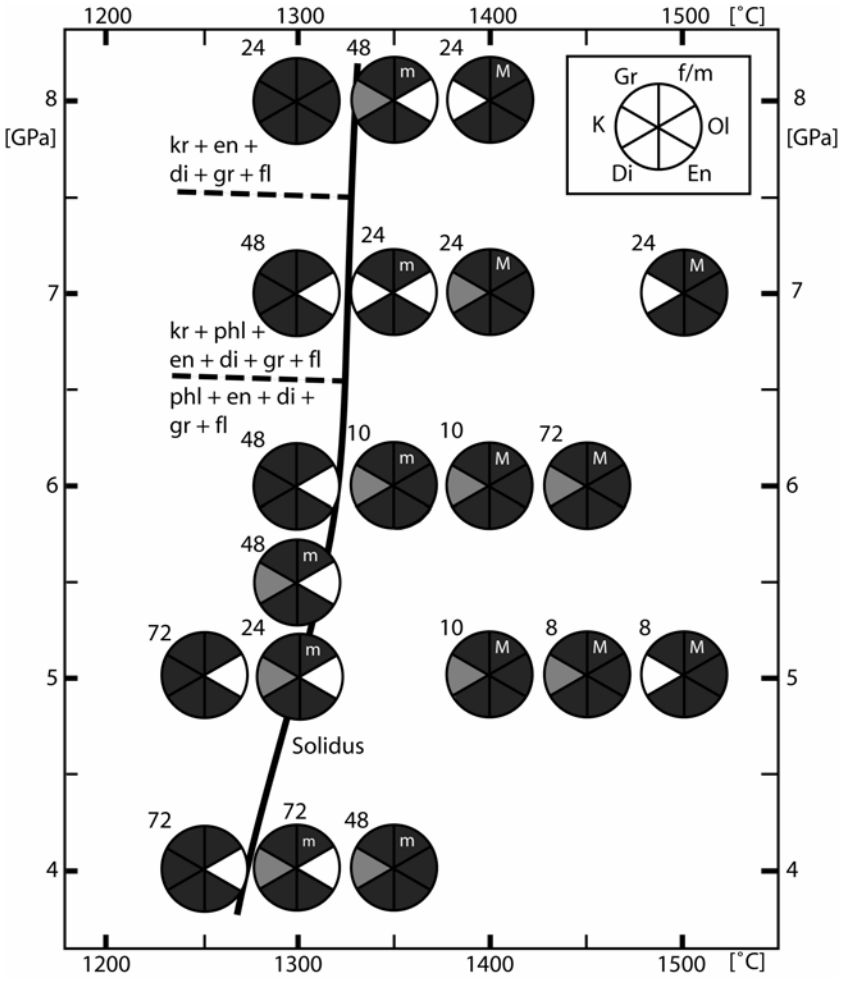

Figure 3-1 Phase relations of phlogopite with pyroxene in the KCMAS-H_2O system. Light gray quadrants indicate primary phlogopite that coexists with melt. Numbers indicate the duration of the experiment in hours. *Di* diopside, *En* enstatite, *f/m* fluid present if quadrant dark gray / dark gray quadrant with m to M for increasing melt portion, *Gr* garnet, *K* primary potassium-bearing phase (phlogopite or potassic richterite), *Kr* potassic richterite, *Ol* olivine; *Phl* phlogopite

In KCMAS-H_2O-CO_2, the solidus is located between 1150 and 1200°C at 4, 5 and 6 GPa, and between 1100 and 1150°C at 7 and 8 GPa (Fig. 3-2). Below the solidus at 4 to 6 GPa, primary phlogopite is in equilibrium with garnet, enstatite, diopside, ± magnesite and a fluid. At 7 GPa, primary phlogopite coexists with potassic richterite, garnet, enstatite, diopside, ± magnesite and a fluid.

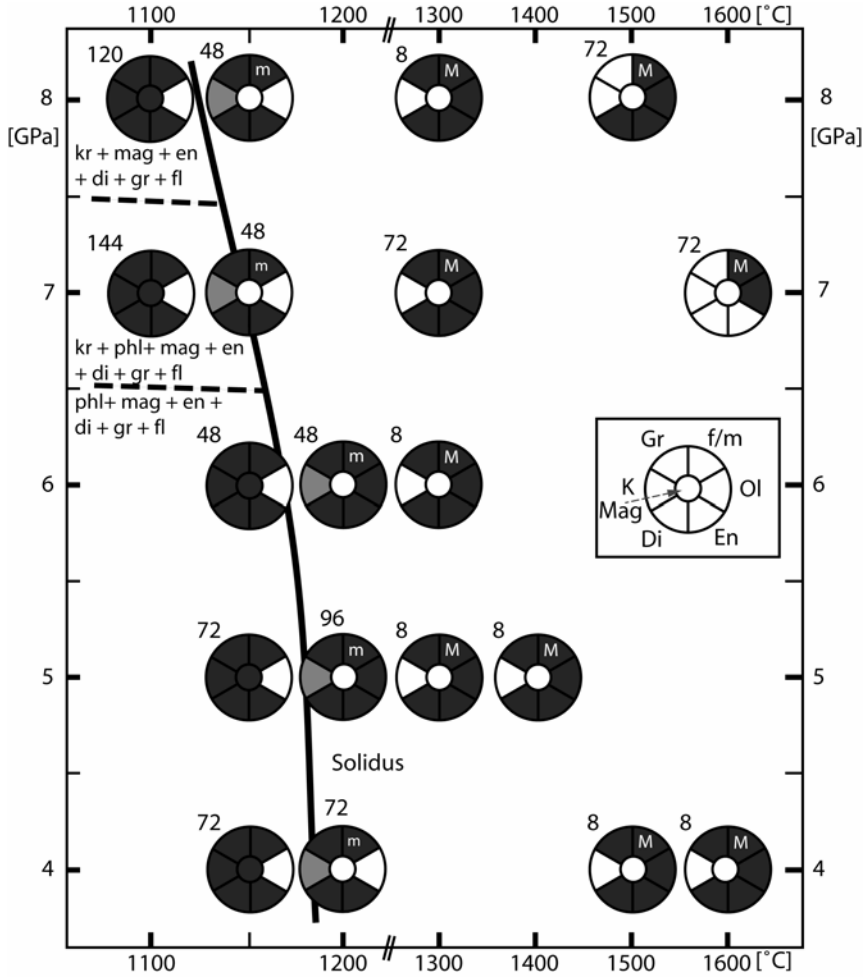

Figure 3-2 Phase relations of phlogopite and pyroxene with magnesite in the KCMAS-H_2O-CO_2 system. Light gray quadrants indicate primary phlogopite that coexists with melt. Numbers indicate the duration of the experiment in hours. *Di* diopside, *En* enstatite, *f/m* fluid present if quadrant dark gray / dark gray quadrant with m to M for increasing melt portion, *Gr* garnet, *K* primary potassium-bearing phase (phlogopite or potassic richterite), *Kr* potassic richterite; *Mag* magnesite, *Ol* olivine, *Phl* phlogopite

At 8 GPa, the stable assemblage is potassic richterite, garnet, enstatite, diopside, ± magnesite and a fluid. Primary phlogopite and potassic richterite was found coexisting with melt in capsules run at temperatures ~100°C above the solidus.

After quench, a hydrous solution is present in experiments at the solidus, which was observed to exit the capsule after breach. The amount is very little and no precipitates on the capsule surface were observed, in contrast to the simple phlogopite + magnesite system described in Enggist et al. (2012). Above the solidus no hydrous solution was seen to escape the charge upon breach.

3.3.2. Diopside

The grain size below the solidus is ≤5 μm. At and above the solidus, diopside grains are up to 25 μm in size, sub- to euhedral and of equant habit. Diopside is free of mineral inclusions, and the grain size gets smaller (1-10 μm) with increasing pressure. With increasing temperature, the Mg content increases by up to ~2 wt% and the Ca content decreases by up to ~5 wt%. The measured K_2O and Al_2O_3 contents range from 0.1-1.4 wt% and 0.4-2.4 wt%, respectively, with higher values at higher temperatures (Table 3-3). This trend probably results from the dissolution of phlogopite or potassic richterite into the melt, which increases the activity of K_2O and Al_2O_3 in the melt, thereby increasing the K and Al content of the pyroxene (Modreski and Boettcher 1972; Enggist et al. 2012). K contents increase to higher pressures and supersolidus from 0.01-0.06 cations per

formula unit (apfu). SiO_2 contents are close to stoichiometric with 2 Si apfu, and vary from ~53-56 wt%.

Table 3-3 Diopside compositions (KCMAS-H_2O)

P [GPa]	4	5	5	5	6	6	6
T [°C]	1350	1400	1450	1500	1350	1400	1450
Run # ae-…	140	32	65	50	33	30	146
n	4	10	14	18	14	13	2
SiO_2 [wt%]	55.5(2)	54.9(8)	55.9(9)	55.4(6)	55.0(11)	55.6(6)	55.1(25)
Al_2O_3	1.5(1)	1.4(1)	1.4(2)	1.6(1)	1.2(9)	1.3(9)	1.1(2)
MgO	20.7(5)	22.1(5)	22.4(9)	23.5(7)	21.1(8)	20.8(10)	22.8(14)
CaO	20.4(1)	20.2(4)	18.9(7)	18.3(4)	21.3(6)	21.5(7)	19.4(0)
K_2O	1.0(2)	1.0(3)	0.8(3)	0.5(1)	0.6(2)	0.5(1)	1.3(2)
Total	99.1(3)	99.5(5)	99.4(7)	99.3(6)	99.2(7)	99.7(7)	99.8(11)
Cations per 6 O							
Si	1.99(1)	1.97(2)	1.99(2)	1.97(1)	1.98(3)	1.99(2)	1.97(5)
Al	0.06(0)	0.06(0)	0.06(1)	0.07(1)	0.05(4)	0.05(4)	0.05(1)
Mg	1.14(7)	1.18(3)	1.19(4)	1.25(3)	1.13(4)	1.11(5)	1.22(10)
Ca	0.76(5)	0.78(2)	0.72(3)	0.70(2)	0.82(3)	0.82(3)	0.74(1)
K	0.04(1)	0.05(2)	0.04(1)	0.2(1)	0.03(1)	0.02(1)	0.06(1)
Sum	4.00(1)	4.03(2)	4.00(2)	4.01(1)	4.01(2)	4.00(2)	4.04(6)

n number of analyses; standard deviations in the last digit are given in parentheses

Table 3-3 ***continued*** Diopside compositions (KCMAS-H_2O)

P [GPa]	7	7	8	8
T [°C]	1400	1500	1300	1400
Run # ae-…	111	131	117	120
n	10	10	15	10
SiO_2 [wt%]	55.3(5)	56.0(8)	56.0(4)	55.4(7)
Al_2O_3	1.6(3)	1.5(2)	0.9(1)	1.3(1)
MgO	21.3(7)	22.2(8)	20.9(6)	21.9(6)
CaO	20.5(4)	18.4(11)	21.2(5)	19.2(5)
K_2O	1.1(3)	1.4(2)	0.7(1)	1.4(1)
Total	99.8(7)	99.5(7)	99.8(7)	99.3(7)
Cations per 6 O				
Si	1.98(1)	2.00(2)	2.00(1)	1.99(2)
Al	0.07(1)	0.06(1)	0.04(0)	0.06(0)
Mg	1.13(3)	1.18(4)	1.11(3)	1.17(3)
Ca	0.78(1)	0.70(4)	0.81(2)	0.74(2)
K	0.05(1)	0.06(1)	0.03(0)	0.06(1)
Sum	4.01(1)	4.00(2)	4.00(1)	4.02(2)

n number of analyses; standard deviations in the last digit are given in parentheses

Table 3-3 *continued* Diopside compositions (KCMAS-H_2O-CO_2)

P [GPa]	4	4	4	4	5	5	5
T [°C]	1150	1200	1500	1600	1200	1300	1400
Run # ae-…	151	143	55	70	110	59	52
N	10	18	1	6	7	10	12
SiO_2 [wt%]	53.6(7)	56.8(8)	53.7	55.6(5)	55.8(9)	54.9(12)	55.3(7)
Al_2O_3	0.9(3)	1.0(2)	2.0	2.4(2)	0.4(0)	1.4(3)	1.4(6)
MgO	22.5(7)	20.1(8)	24.8	25.9(9)	20.0(6)	22.7(7)	22.5(6)
CaO	22.6(7)	21.8(6)	17.6	15.6(9)	22.6(7)	19.6(6)	19.8(9)
K_2O	0.5(3)	0.3(1)	0.6	0.4(1)	0.1(0)	0.6(1)	0.3(1)
Total	100.2(8)	100.1(5)	98.7	99.9(6)	98.9(3)	99.3(8)	99.4(8)
Cations per 6 O							
Si	1.93(2)	2.02(2)	1.93	1.95(1)	2.01(3)	1.97(3)	1.97(1)
Al	0.04(1)	0.04(1)	0.08	0.10(1)	0.02(0)	0.06(1)	0.06(3)
Mg	1.20(3)	1.06(4)	1.33	1.36(5)	1.07(4)	1.21(4)	1.20(3)
Ca	0.87(3)	0.83(3)	0.68	0.58(4)	0.87(3)	0.75(3)	0.76(4)
K	0.02(1)	0.01(0)	0.03	0.02(0)	0.01(0)	0.03(1)	0.01(1)
Sum	4.06(2)	3.97(2)	4.05	4.01(2)	3.98(3)	4.02(3)	4.00(1)

n number of analyses; standard deviations in the last digit are given in parentheses

Table 3-3 *continued* Diopside compositions (KCMAS-H_2O-CO_2)

P [GPa]	6	6	7	7	7	8	8
T [°C]	1150	1300	1100	1150	1300	1100	1300
Run # ae-…	149	69	155	148	145	156	71
n	9	13	8	7	7	3	14
SiO_2 [wt%]	55.2(9)	55.9(8)	55.7(7)	55.7(7)	56.2(8)	55.1(1)	56.2(7)
Al_2O_3	0.7(2)	0.9(1)	1.1(2)	0.7(1)	1.4(2)	0.9(2)	1.0(2)
MgO	21.5(10)	21.5(7)	20.1(5)	21.7(10)	20.5(11)	20.3(10)	22.5(8)
CaO	22.0(5)	21.1(5)	22.5(5)	21.2(10)	21.1(7)	22.2(7)	19.3(4)
K_2O	0.5(2)	0.6(1)	0.8(2)	0.6(1)	1.0(3)	0.5(1)	0.9(1)
Total	100.0(6)	100.0(8)	100.2(9)	100.0(7)	100.2(6)	99.0(6)	100.0(7)
Cations per 6 O							
Si	1.97(3)	1.99(2)	1.99(1)	1.99(1)	2.00(2)	1.99(1)	2.00(1)
Al	0.03(1)	0.04(0)	0.05(1)	0.03(0)	0.06(1)	0.04(1)	0.04(1)
Mg	1.15(5)	1.14(4)	1.07(2)	1.16(5)	1.09(6)	1.09(5)	1.19(4)
Ca	0.84(2)	0.81(2)	0.86(2)	0.81(4)	0.80(3)	0.86(3)	0.73(2)
K	0.02(1)	0.03(0)	0.03(1)	0.03(1)	0.04(1)	0.02(0)	0.04(0)
Sum	4.02(3)	4.00(2)	4.00(1)	4.01(1)	3.99(2)	4.00(1)	4.00(1)

n number of analyses; standard deviations in the last digit are given in parentheses

3.3.3. Enstatite

At pressures of 4 to 6 GPa, the grains measure 5-20 μm below and up to 30 μm above the solidus. Enstatite is sub- to euhedral and prismatic, and often contains inclusions of euhedral garnet and anhedral diopside grains. At pressures

>6 GPa, grains measure 100 to 200 μm in length below and above solidus, and contain numerous small (1-10 μm) inclusions (Fig. 3-3b). Al_2O_3 (0.3-2.4 wt%) and CaO (0.4-2.4 wt%) contents increase with increasing temperature, displaying a sudden increase from sub- to supersolidus conditions. SiO_2 contents (~57-60 wt%) are close to stoichiometric with 2 Si apfu, and tend to decrease with increasing temperature (Table 3-4). As in the case of diopside (see above), the increase in Al can be attributed to the melting of phlogopite or potassic richterite. The increasing Ca content above the solidus reflects the increasing temperature and the associated incorporation of Ca in the orthopyroxene. MgO contents range from ~37-40 wt% and decrease to higher temperatures.

3.3.4. Garnet

Garnet grains are 1-10 μm in diameter below the solidus, up to 20 μm at the solidus and ~1-3μm above the solidus. Grains are sub- to euhedral, and are free of mineral inclusions. SiO_2 increases to higher pressures and temperatures with contents measured ranging from ~43-46 wt% (Table 3-5). Al_2O_3 varies from ~20-25 wt%, showing a trend to lower Al contents at higher pressures. MgO contents vary from ~24-28 and increase to higher pressures from ~2.5 to 2.7 Mg apfu at 4 and 8 GPa, respectively. All garnets contain CaO, which is similar to previous studies (Brey et al. 1990; Sudo and Tatsumi 1990; Luth 1997; Konzett and Ulmer 1999). Si increases with increasing pressures from 2.94 at 4 GPa to 3.18 apfu at 8 GPa. No clear trend of enrichment of Si to higher temperature was

observed. The modal abundance increases from ~8 below to ~15 modal% above the solidus.

Table 3-4 Enstatite compositions (KCMAS-H_2O)

P [GPa]	4	5	5	5	6	6	7
T [°C]	1350	1400	1450	1500	1350	1400	1400
Run # ae-…	140	32	65	50	33	30	111
n	6	8	11	13	8	9	15
SiO_2 [wt%]	59.3(9)	59.1(8)	58.9(6)	58.2(5)	58.7(7)	58.9(9)	59.5(6)
Al_2O_3	1.2(2)	1.1(2)	1.2(2)	1.4(0)	0.8(3)	0.7(1)	0.5(2)
MgO	37.6(9)	37.7(4)	38.4(6)	38.0(6)	38.1(13)	38.5(6)	38.6(7)
CaO	1.3(1)	1.3(2)	1.6(1)	1.8(1)	1.1(3)	1.0(4)	1.1(1)
K_2O	0.2(2)	0.2(3)	0.1(1)	0.1(1)	0.4(2)	0.1(1)	0.0(0)
Total	99.7(13)	99.5(8)	100.1(9)	99.5(8)	99.1(6)	99.4(8)	99.7(7)
Cations per 6 O							
Si	1.99(2)	1.99(1)	1.98(2)	1.97(1)	1.99(2)	1.99(1)	2.00(2)
Al	0.05(1)	0.04(1)	0.05(1)	0.06(0)	0.03(1)	0.03(0)	0.02(1)
Mg	1.89(4)	1.89(3)	1.92(3)	1.91(2)	1.93(6)	1.94(3)	1.93(3)
Ca	0.05(1)	0.05(1)	0.06(0)	0.06(0)	0.04(1)	0.04(1)	0.04(0)
K	0.01(1)	0.01(1)	0.00(0)	0.00(0)	0.02(1)	0.01(0)	0.00(0)
Sum	3.99(2)	3.99(1)	4.00(1)	4.01(1)	4.00(2)	4.00(1)	3.99(2)

Table 3-4 ***continued*** Enstatite compositions (KCMAS-H_2O)

P [GPa]	7	8	8
T [°C]	1500	1300	1400
Run # ae-…	131	117	120
n	17	12	10
SiO_2 [wt%]	59.0(9)	59.9(7)	58.8(10)
Al_2O_3	0.7(3)	0.6(3)	0.8(4)
MgO	38.1(5)	38.4(7)	38.0(6)
CaO	1.4(2)	0.9(3)	1.0(3)
K_2O	0.3(2)	0.0(0)	0.4(1)
Total	99.5(9)	99.9(7)	99.0(4)
Cations per 6 O			
Si	1.99(1)	2.01(2)	1.99(3)
Al	0.03(1)	0.02(1)	0.03(2)
Mg	1.92(4)	1.92(3)	1.92(4)
Ca	0.05(1)	0.03(1)	0.04(1)
K	0.01(1)	0.00(0)	0.02(1)
Sum	4.00(2)	3.98(2)	4.00(2)

n number of analyses; standard deviations in the last digit are given in parentheses

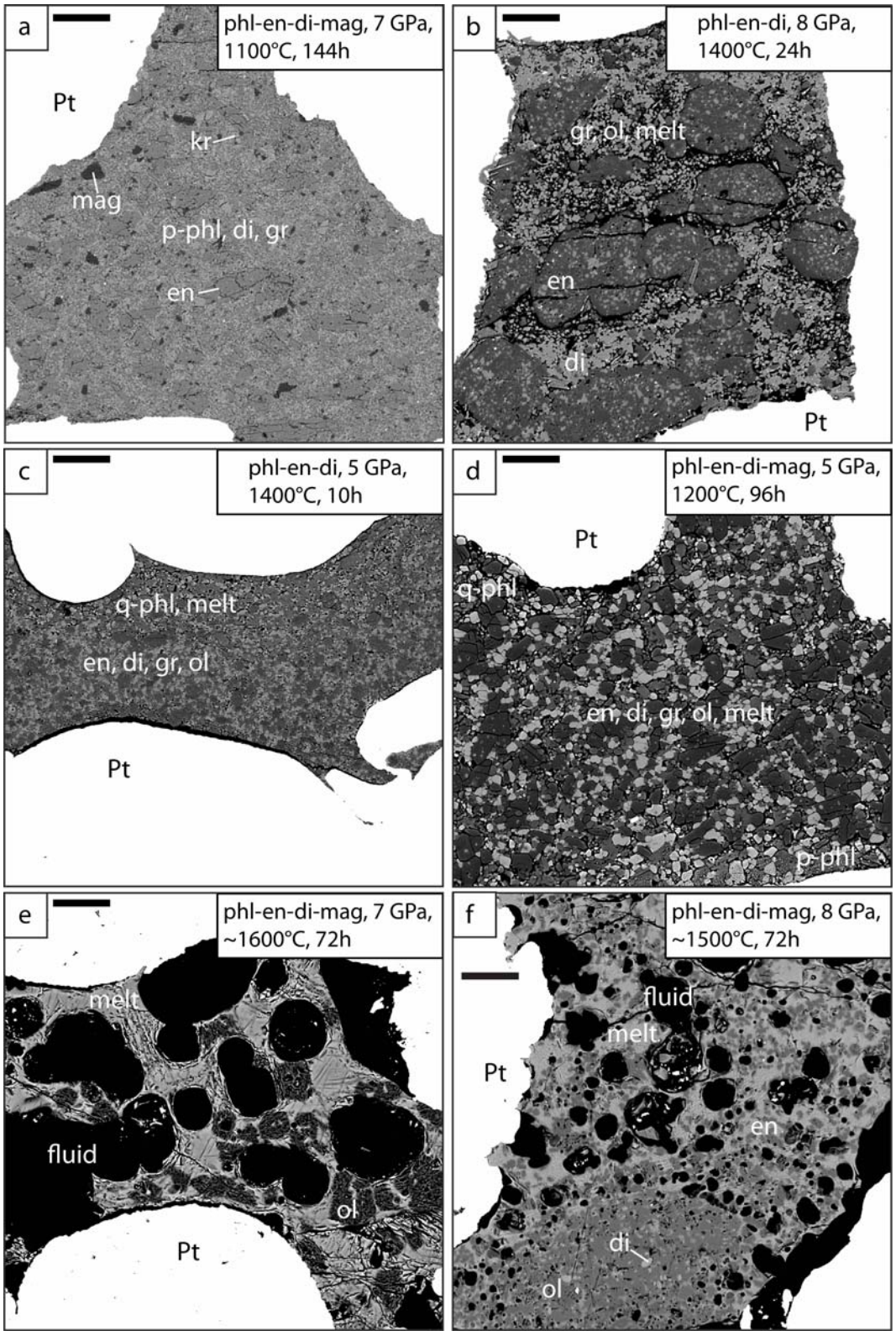

Figure 3-3 Scale bar in upper left of each image is 100 µm. a) Subsolidus assemblage: p-phl in equilibrium with gr, mag, en, di and kr. Mag is homogeneously distributed throughout the

capsule. b) Supersolidus: p-phl reacted out, and a melt phase is present with q-phl needles, di, en, gr and ol grains. c) Supersolidus: at high pressures en grows to ≤200 µm and encloses di and gr. Phases present are en, di, gr, ol and melt. d) Supersolidus: closer to solidus, p-phl is coexisting with melt, en, di, gr, ol. Q-phl present besides melt. e) Temperature on sample too high (thermocouple shorting) and is estimated to be ~1600°C. Ol coexists with melt. Spherical voids indicate the presence of a fluid phase. f) Temperature on sample too high (thermocouple shorting) and is estimated by using 2-pyroxene thermometers to be ~1500°C. Ol, en and di coexist with melt. Spherical voids (fluid phase) are present in the melt. *di* diopside, *en* enstatite, *gr* garnet, *kr* potassic richterite, *mag* magnesite, *p-phl* primary phlogopite, *q-phl* quench phlogopite

Table 3-4 *continued* Enstatite compositions (KCMAS-H_2O-CO_2)

P [GPa]	4	4	4	4	5	5	5
T [°C]	1150	1200	1500	1600	1200	1300	1400
Run # ae-…	151	143	55	70	110	59	52
N	13	4	5	14	11	20	13
SiO_2 [wt%]	58.4(7)	58.8(6)	57.4(5)	57.1(5)	59.3(5)	59.5(7)	57.8(6)
Al_2O_3	0.6(0)	0.8(0)	1.8(1)	2.4(1)	0.5(0)	0.9(2)	1.1(2)
MgO	39.6(5)	39.7(6)	37.7(6)	37.7(5)	39.0(5)	38.1(7)	39.0(6)
CaO	0.7(1)	1.0(2)	2.0(1)	2.4(1)	0.6(0)	1.3(2)	1.3(2)
K_2O	0.1(1)	0.0(0)	0.2(2)	0.2(1)	0.1(0)	0.0(0)	0.1(1)
Total	99.4(7)	100.4(10)	99.1(5)	99.8(8)	99.4(5)	99.9(5)	99.3(6)
Cations per 6 O							
Si	1.97(1)	1.97(1)	1.95(2)	1.93(1)	1.99(1)	2.00(2)	1.96(2)
Al	0.03(0)	0.03(0)	0.07(0)	0.10(0)	0.02(0)	0.03(1)	0.05(1)
Mg	1.99(3)	1.98(2)	1.91(3)	1.90(2)	1.95(3)	1.91(4)	1.97(3)
Ca	0.02(0)	0.04(1)	0.07(0)	0.09(0)	0.02(0)	0.05(1)	0.05(1)
K	0.00(0)	0.00(0)	0.01(1)	0.01(1)	0.00(0)	0.00(0)	0.00(0)
Sum	4.02(1)	4.02(1)	4.02(2)	4.03(1)	4.00(1)	3.99(2)	4.02(2)

Table 3-4 *continued* Enstatite compositions (KCMAS-H_2O-CO_2)

P [GPa]	6	6	7	7	7	8	8
T [°C]	1150	1300	1100	1150	1300	1100	1300
Run # ae-…	149	69	155	148	145	156	71
n	9	7	7	11	4	6	4
SiO_2 [wt%]	59.4(6)	58.0(7)	59.3(4)	59.3(5)	58.9(7)	59.0(8)	57.5(6)
Al_2O_3	0.4(1)	0.6(2)	0.5(5)	0.4(2)	0.5(1)	0.3(1)	1.0(3)
MgO	39.2(8)	40.3(7)	39.1(7)	38.6(3)	38.8(5)	39.5(4)	37.6(7)
CaO	0.7(1)	1.0(1)	0.7(2)	0.7(1)	1.1(3)	0.4(2)	2.2(5)
K_2O	0.1(0)	0.1(1)	0.0(0)	0.2(2)	0.0(0)	0.0(0)	0.3(1)
Total	99.7(8)	100.0(6)	99.7(9)	99.2(5)	99.3(5)	99.2(4)	98.7(2)
Cations per 6 O							
Si	1.99(2)	1.95(2)	1.99(2)	2.00(1)	1.99(1)	1.99(2)	1.97(2)
Al	0.01(0)	0.02(1)	0.02(2)	0.02(1)	0.02(0)	0.01(1)	0.04(1)
Mg	1.97(3)	2.02(3)	1.96(3)	1.94(1)	1.95(2)	1.99(3)	1.92(3)
Ca	0.02(0)	0.04(0)	0.03(1)	0.03(0)	0.04(1)	0.01(1)	0.08(2)
K	0.00(0)	0.00(1)	0.00(0)	0.01(1)	0.00(0)	0.00(0)	0.01(1)
Sum	4.00(2)	4.04(2)	4.00(2)	3.99(1)	4.00(1)	4.00(2)	4.02(1)

n number of analyses; standard deviations in the last digit are given in parentheses

3.3.5. Potassic richterite

Grains are 10-80 μm long, are sub- to euhedral, and larger grains often enclose garnet (Fig. 3-3a). Potassic richterite occurs at 7 GPa, where it coexists with primary phlogopite, and at 8 GPa as the only K-bearing phase below the solidus (Table 3-6). Potassic richterite melts over a ~100°C temperature interval. Residual potassic richterite above the solidus contains up to 2.7 wt% Al_2O_3, compared to the 1.3-1.9 wt% at subsolidus conditions. Relative to the ideal composition ($K_2CaMg_5Si_8O_{22}(OH)_2$), the present richterite is deficient in Si (7.80-7.85 apfu), as the site is shared with Al. Richterite, furthermore, is deficient in K (1.77-1.84 apfu) and Mg (4.72-4.93 apfu), contains extra Ca (1.09-1.22 apfu), and contains 0.21-0.45 Al apfu, similar to the compositions reported by Sudo and Tatsumi (1990), Konzett and Ulmer (1999) and Konzett and Fei (2000).

3.3.6. Magnesite

Magnesite is sub- to euhedral, prismatic and only occurs below the solidus. Grains are up to 20 μm in size and are free of mineral inclusions. Magnesite is the first phase to disappear at the solidus. All magnesite grains contain Ca, and CaO decreases with increasing pressure from 1.9 to 0.4 wt% at 4 to 8 GPa, respectively. MgO content measured at 4 GPa is low with 44.4 wt%, is higher with 47.4, 46.9 and 46.8 wt% at 5, 6 and 7 GPa, respectively, and is 47.9 wt% at 8 GPa (Table 3-7). Magnesite is non-stoichiometric as reported in previous studies (Luth 2006; Keshav and Gudfinnsson 2010; Enggist et al. 2012). In this study, Mg was standardized using forsterite93 for the electron microprobe analysis, and the

reported non-stoichiometry may be a result of this standardization and/or the Phi-Rho-Z correction scheme.

Table 3-5 Garnet compositions (KCMAS-H_2O)

P [GPa]	4	5	5	5	5	6	6
T [°C]	1350	1250	1400	1450	1500	1350	1400
Run # ae-…	140	147	32	65	50	33	30
n	5	1	10	11	15	10	11
SiO_2 [wt%]	44.4(7)	43.0	44.3(4)	43.6(5)	43.9(7)	44.5(8)	44.7(4)
Al_2O_3	25.4(8)	26.7	24.6(4)	24.1(4)	24.0(8)	24.6(6)	24.0(5)
MgO	24.7(11)	24.7	25.1(8)	26.7(7)	26.0(5)	25.2(6)	25.8(6)
CaO	4.8(2)	4.8	5.3(4)	5.1(3)	5.2(5)	5.3(4)	5.3(5)
K_2O	0.3(2)	0.1	0.6(2)	0.1(2)	0.1(2)	0.3(1)	0.2(1)
Total	99.5(10)	99.3	99.9(7)	99.7(7)	99.2(5)	99.9(8)	100.0(6)
Cations per 12 O							
Si	3.03(2)	2.94	3.03(2)	2.99(3)	3.02(5)	3.03(4)	3.05(2)
Al	2.04(7)	2.16	1.98(2)	1.95(3)	1.95(7)	1.98(5)	1.92(4)
Mg	2.51(11)	2.52	2.55(8)	2.72(8)	2.66(4)	2.58(7)	2.63(6)
Ca	0.35(2)	0.35	0.39(3)	0.38(2)	0.38(4)	0.38(2)	0.39(3)
K	0.02(2)	0.01	0.06(2)	0.01(2)	0.01(2)	0.03(1)	0.02(1)
Sum	7.96(4)	7.98	8.01(3)	8.04(3)	8.02(2)	7.99(3)	8.00(3)
Maj comp	0.03(4)	0.00	0.03(3)	0.00(1)	0.02(4)	0.03(2)	0.05(2)

n number of analyses; standard deviations in the last digit are given in parentheses

Table 3-5 ***continued*** Garnet compositions (KCMAS-H_2O)

P [GPa]	7	7	8	8
T [°C]	1400	1500	1300	1400
Run # ae-…	111	131	117	120
n	14	4	10	10
SiO_2 [wt%]	44.4(4)	45.1(3)	45.3(4)	45.2(6)
Al_2O_3	23.6(3)	22.9(3)	23.7(5)	23.4(6)
MgO	27.5(2)	26.6(5)	26.2(8)	27.1(9)
CaO	4.4(3)	4.7(8)	4.4(4)	4.3(5)
K_2O	0.0(0)	0.5(4)	0.1(0)	0.3(1)
Total	99.8(8)	99.7(10)	99.7(6)	100.3(7)
Cations per 12 O				
Si	3.02(1)	3.08(3)	3.08(2)	3.07(3)
Al	1.89(2)	1.84(3)	1.90(4)	1.87(4)
Mg	2.79(3)	2.71(4)	2.66(7)	2.73(9)
Ca	0.32(2)	0.34(5)	0.32(3)	0.31(4)
K	0.00(0)	0.04(3)	0.00(0)	0.02(1)
Sum	8.03(1)	8.02(4)	7.97(4)	8.01(4)
Maj comp	0.02(1)	0.08(2)	0.08(2)	0.07(2)

n number of analyses; standard deviations in the last digit are given in parentheses

Table 3-5 *continued* Garnet compositions (KCMAS-H_2O-CO_2)

P [GPa]	4	4	4	5	5	5	6
T [°C]	1150	1200	1500	1200	1300	1400	1150
Run # ae-…	151	143	55	110	59	52	149
n	11	5	3	9	10	16	3
SiO_2 [wt%]	43.9(7)	43.0(7)	44.1(6)	44.8(5)	44.1(8)	44.6(5)	44.7(2)
Al_2O_3	24.7(6)	25.3(5)	23.9(12)	24.5(4)	24.6(6)	24.2(6)	23.9(6)
MgO	26.0(6)	25.6(8)	26.7(8)	25.1(7)	25.7(7)	26.0(5)	26.4(4)
CaO	5.5(5)	6.1(6)	5.1(3)	4.9(4)	5.4(5)	5.3(4)	5.4(10)
K_2O	0.0(0)	0.0(0)	0.2(3)	0.1(1)	0.1(1)	0.1(1)	0.1(0)
Total	100.1(9)	100.1(10)	100.1(6)	99.3(8)	99.9(9)	100.2(8)	100.5(12)
Cations per 12 O							
Si	2.99(4)	2.94(3)	3.01(2)	3.06(3)	3.01(4)	3.04(3)	3.03(1)
Al	1.98(5)	2.04(5)	1.92(8)	1.98(2)	1.98(4)	1.94(5)	1.91(5)
Mg	2.64(5)	2.61(7)	2.71(10)	2.56(7)	2.61(9)	2.63(5)	2.67(1)
Ca	0.40(4)	0.45(5)	0.37(3)	0.36(3)	0.40(3)	0.39(3)	0.39(7)
K	0.00(0)	0.00(0)	0.02(2)	0.00(0)	0.01(1)	0.01(1)	0.01(0)
Sum	8.02(2)	8.04(2)	8.04(6)	7.96(3)	8.00(4)	8.00(3)	8.01(3)
Maj comp	0.00(0)	0.00(0)	0.01(2)	0.06(3)	0.01(4)	0.04(3)	0.03(2)

n number of analyses; standard deviations in the last digit are given in parentheses

Table 3-5 *continued* Garnet compositions (KCMAS-H_2O-CO_2)

P [GPa]	6	7	7	7	8	8
T [°C]	1300	1100	1150	1300	1100	1300
Run # ae-…	69	155	148	145	156	71
n	8	2	8	4	4	3
SiO_2 [wt%]	45.1(8)	46.2(3)	43.8(6)	45.2(6)	43.6(3)	46.7(10)
Al_2O_3	23.0(6)	24.2(1)	23.3(8)	23.8(10)	23.4(5)	19.6(5)
MgO	26.7(8)	24.1(2)	27.6(6)	26.3(8)	27.9(2)	27.2(4)
CaO	5.5(4)	3.7(0)	4.9(3)	5.2(6)	4.5(4)	6.1(4)
K_2O	0.1(1)	1.3(1)	0.4(3)	0.2(2)	0.6(2)	0.5(2)
Total	100.3(9)	99.4(7)	99.9(10)	100.7(5)	100.0(12)	100.1(7)
Cations per 12 O						
Si	3.06(4)	3.15(0)	3.00(1)	3.06(3)	2.98(1)	3.19(5)
Al	1.84(5)	1.95(0)	1.88(6)	1.90(8)	1.89(2)	1.58(5)
Mg	2.71(7)	2.45(1)	2.82(8)	2.66(9)	2.85(2)	2.77(5)
Ca	0.40(3)	0.27(0)	0.36(2)	0.38(4)	0.33(2)	0.45(3)
K	0.01(0)	0.11(1)	0.04(3)	0.02(1)	0.05(2)	0.04(1)
Sum	8.02(3)	7.93(0)	8.08(5)	8.00(4)	8.10(1)	8.04(2)
Maj comp	0.06(4)	0.15(0)	0.00(0)	0.06(4)	0.00(0)	0.19(4)

n number of analyses; standard deviations in the last digit are given in parentheses

Table 3-6 Potassic richterite compositions (KCMAS-H_2O and KCMAS-H_2O-CO_2)

			c	c
P [GPa]	[a]7	8	[b]7	8
T [°C]	1400	1300	1100	1100
Run # ae-…	139	117	155	156
n	12	18	12	16
SiO_2 [wt%]	55.4(11)	54.6(9)	54.7(9)	54.5(6)
Al_2O_3	2.7(5)	1.9(1)	1.5(2)	1.3(1)
MgO	22.5(16)	22.7(6)	22.8(5)	23.0(5)
CaO	7.2(5)	7.9(4)	7.5(1)	7.6(1)
K_2O	10.2(5)	9.4(3)	9.7(3)	9.7(2)
Total	98.1(9)	96.5(10)	96.1(14)	96.0(5)
Cations per 23 O				
Si	7.80(14)	7.81(7)	7.84(4)	7.85(7)
Al	0.45(8)	0.32(2)	0.25(3)	0.21(2)
Mg	4.72(33)	4.83(13)	4.87(8)	4.93(11)
Ca	1.09(8)	1.22(7)	1.14(2)	1.17(2)
K	1.84(9)	1.71(6)	1.87(9)	1.77(4)
Sum	15.89(16)	15.89(7)	15.97(5)	15.93(6)

[a] supersolidus, [b] coexisting with primary phlogopite, *c* KCMAS-H_2O-CO_2, *n* number of analyses; standard deviations in the last digit are given in parentheses

Table 3-7 Magnesite compositions (KCMAS-H_2O-CO_2)

P [GPa]	4	5	6	7	8
T [°C]	1150	1150	1150	1100	1100
Run # ae-…	151	159	149	155	156
n	13	7	12	15	10
SiO_2 [wt%]	0.2(1)	0.2(1)	0.3(1)	0.1(1)	0.2(2)
Al_2O_3	0.1(1)	0.1(0)	0.0(0)	0.0(0)	0.1(1)
MgO	44.4(8)	47.4(9)	46.9(7)	46.8(5)	47.9(7)
CaO	1.9(1)	1.1(2)	0.8(3)	0.4(1)	0.4(1)
K_2O	0.1(0)	0.0(0)	0.1(1)	0.0(0)	0.0(0)
Total	46.8(8)	48.9(8)	48.1(7)	47.4(6)	48.6(5)
Cations per 1 O					
Mg	0.96(1)	0.98(1)	0.98(1)	0.99(0)	0.99(0)
Ca	0.03(0)	0.02(0)	0.01(0)	0.01(0)	0.01(0)
Sum	1.00(0)	1.00(0)	1.00(0)	1.00(0)	1.00(0)
[a]CO_2	53.2	51.1	51.9	52.6	51.4

[a] by difference, *n* number of analyses; standard deviations in the last digit are given in parentheses

3.3.7. Olivine

Olivine was found above the solidus but also in one experiment below the solidus. Grains exhibit a prismatic to equant habit, are subhedral, grow to up to 30 μm in size, contain no mineral inclusions and are stoichiometric, features that are consistent with previous studies (Luth 1997; Trønnes 2002; Enggist et al. 2012).

3.3.8. Phlogopite

Primary phlogopite grains are 5-30 μm in length, are sub- to euhedral, of prismatic habit and inclusion free. Quench phlogopite grains are 5-50 μm in length and exhibit a dendritic habit. In KCMAS-H_2O, SiO_2 of primary phlogopite compositions varies from 43.2 to 40.6 and 45.6 wt% at 4, 5 and 7 GPa, respectively, and suggests enrichment of Si to higher pressures. Although the standard deviation at 7 GPa is large, higher Si contents were measured at the higher pressure (Table 3-8). Al_2O_3 shows a trend of depletion to higher pressures with 13.7, 12.3 and 12.3 wt% at 4, 5 and 7 GPa, respectively, which is similar to the results of Enggist et al. (2012). MgO is similar (25.9 and 26.0 wt%) at 4 and 7 GPa, but is higher (28.0 wt%) at 5 GPa. K_2O is lower at the higher pressure (10.0 wt%). In KCMAS-H_2O-CO_2, SiO_2 of primary phlogopite is 44.0, 44.3 and 43.9 wt% at 4, 6 and 7 GPa. Al_2O_3 follows the above trend of depletion to higher pressures with 13.3 to 11.5 and 10.9 wt% at a pressure of 4, 6 and 7 GPa, respectively. MgO is 26.5, 26.3 and 27.1 wt% at 4, 6 and 7 GPa, respectively, and K_2O, as above, is higher (10.7 wt%) at 4 GPa and lower (10.1 and 10.2 wt%) at 6 and 7 GPa. For quench phlogopite see “Melt” section below.

Table 3-8 Phlogopite compositions (KCMAS-H_2O)

[a]p or q	p	p	q	q
P [GPa]	4	5	5	5
T [°C]	1250	1250	1400	1450
Run # ae-…	157	147	32	65
n	7	4	12	9
SiO_2 [wt%]	43.2(4)	40.6(8)	40.1(10)	42.9(9)
Al_2O_3	13.7(4)	12.3(4)	12.7(3)	13.1(3)
MgO	25.9(7)	28.0(9)	28.7(7)	27.3(5)
CaO	0.1(0)	0.4(2)	0.1(1)	0.1(0)
K_2O	11.3(3)	10.9(5)	10.8(3)	11.3(1)
Total	94.2(12)	92.3(9)	92.4(9)	94.6(10)
Cations per 22 O				
Si	6.07(5)	5.87(9)	5.79(9)	6.02(6)
Al	2.27(5)	2.10(5)	2.17(4)	2.16(2)
Mg	5.42(10)	6.04(22)	6.17(18)	5.71(13)
CaO	0.01(1)	0.05(4)	0.02(2)	0.01(1)
K	2.02(7)	2.02(7)	1.98(5)	2.03(4)
Sum	15.80(5)	16.08(13)	16.12(8)	15.92(8)

[a] *p* primary phlogopite and *q* quench phlogopite distinguished by texture, *n* number of analyses; standard deviations in the last digit are given in parentheses

Table 3-8 ***continued*** Phlogopite compositions (KCMAS-H_2O)

[a]p or q	q	q	q	p
P [GPa]	5	6	6	[b]7
T [°C]	1500	1350	1400	1300
Run # ae-…	50	33	30	152
n	4	16	10	2
SiO_2 [wt%]	49.9(10)	43.9(6)	43.9(4)	45.6(20)
Al_2O_3	12.4(1)	11.9(3)	12.1(6)	12.3(13)
MgO	22.9(10)	27.0(8)	27.0(7)	26.0(6)
CaO	0.4(2)	0.1(1)	0.5(2)	0.6(2)
K_2O	7.9(12)	10.9(2)	10.5(5)	10.0(1)
Total	93.4(5)	93.7(5)	94.0(13)	94.7(27)
Cations per 22 O				
Si	6.81(11)	6.19(7)	6.16(7)	6.31(7)
Al	1.99(5)	1.98(4)	2.01(7)	2.01(15)
Mg	4.66(20)	5.67(17)	5.66(10)	5.38(31)
CaO	0.06(2)	0.01(1)	0.07(3)	0.10(3)
K	1.38(22)	1.97(5)	1.88(9)	1.77(3)
Sum	14.89(21)	15.81(9)	15.77(7)	15.57(16)

[a] *p* primary phlogopite and *q* quench phlogopite distinguished by texture, [b] coexisting with potassic richterite, *n* number of analyses; standard deviations in the last digit are given in parentheses

Table 3-8 *continued* Phlogopite compositions (KCMAS-H_2O-CO_2)

[a]p or q	p	Q	q	q
P [GPa]	4	4	4	5
T [°C]	1150	1500	1600	1200
Run # ae-…	151	55	70	110
n	10	4	5	13
SiO_2 [wt%]	44.3(12)	42.4(10)	43.1(6)	43.3(9)
Al_2O_3	13.4(4)	10.1(10)	15.3(5)	12.5(7)
MgO	26.5(8)	27.8(13)	24.5(13)	26.1(6)
CaO	0.2(2)	0.5(0)	0.5(3)	0.2(3)
K_2O	10.8(2)	10.5(10)	10.9(4)	10.1(4)
Total	95.2(13)	91.4(13)	94.2(18)	92.1(12)
Cations per 22 O				
Si	6.15(10)	6.16(8)	6.04(12)	6.17(9)
Al	2.20(3)	1.74(19)	2.52(7)	2.10(10)
Mg	5.43(23)	6.01(21)	5.11(21)	5.56(14)
CaO	0.02(1)	0.08(1)	0.07(4)	0.02(4)
K	1.90(3)	1.95(20)	1.94(4)	1.84(9)
Sum	15.70(12)	15.94(11)	15.67(13)	15.69(9)

[a] *p* primary phlogopite and *q* quench phlogopite distinguished by texture; standard deviations in the last digit are given in parentheses

Table 3-8 *continued* Phlogopite compositions (KCMAS-H_2O-CO_2)

[a]p or q	q	Q	p	P
P [GPa]	5	5	6	[b]7
T [°C]	1300	1400	1150	1100
Run # ae-…	59	52	149	155
n	4	8	14	8
SiO_2 [wt%]	40.8(19)	45.4(10)	44.3(9)	43.9(10)
Al_2O_3	12.9(17)	10.5(7)	11.5(4)	10.9(3)
MgO	28.3(13)	27.3(7)	26.3(6)	27.1(4)
CaO	0.2(1)	0.3(2)	0.2(1)	0.3(2)
K_2O	10.3(4)	10.7(4)	10.1(8)	10.2(4)
Total	92.6(19)	94.1(9)	92.4(7)	92.3(12)
Cations per 22 O				
Si	5.85(24)	6.35(11)	6.30(8)	6.26(6)
Al	2.18(26)	1.74(10)	1.92(6)	1.83(5)
Mg	6.05(34)	5.69(16)	5.58(13)	5.76(9)
CaO	0.04(1)	0.05(4)	0.03(2)	0.04(2)
K	1.89(5)	1.90(6)	1.84(15)	1.86(9)
Sum	16.01(15)	15.73(8)	15.66(14)	15.75(9)

[a] *p* primary phlogopite and *q* quench phlogopite distinguished by texture, [b] coexisting with potassic richterite, *n* number of analyses; standard deviations in the last digit are given in parentheses

3.3.9. Melt

Melt compositions were difficult to determine for two main reasons. Firstly, the amount of melt close to the solidus is very small and the melt is interstitial, making quantitative analysis difficult. Secondly, in near-solidus experiments, the quenched melt consists of a hydrous solution, quench phlogopite, plus an unidentifiable, non-phlogopite quench phase, which will be referred to as "quench phase" in this paper. The melt only quenched to glass at high melt fractions, exsolved a fluid phase upon quench, and was not observed to occur together with quench phlogopite in the same capsule. Consequently, the term "melt" in this paper refers to the sum of hydrous solution + quench phlogopite + quench phase at low melt fractions (<40 %), or to glass + fluid at high melt fractions (>50 %).

The low-melt-fraction assemblage can coexist with residual primary phlogopite, which is similar to the findings in Enggist et al. (2012). Just above the solidus and to higher temperatures, no hydrous solution was observed, but quenched phlogopite needles were found along with the quench phase.

In KCMAS-H_2O, SiO_2 of quench phlogopite increases with increasing temperature from 40.1 to 42.9 and 49.9 wt% at 5 GPa and 1400, 1450 and 1500°C, respectively (Table 3-8). At 6 GPa SiO_2 remains 43.9 wt% at 1350 and 1400°C. Furthermore, SiO_2 increases with increasing pressure at a similar temperature from 40.1 to 43.9 wt% at 5 GPa (1400°C) and 6 GPa (1350°C), respectively. As is the case with primary phlogopite, the Al_2O_3 content of quench phlogopite decreases from ~13-12 wt% at 5 and 6 GPa, respectively. K_2O content

decreases with increasing temperature from 10.8 to 7.9 wt% measured at 5 GPa and 1400 to 1500°C, respectively. In KCMAS-H_2O-CO_2, SiO_2 content of quench phlogopite crystals follows a similar trend as described above and increases with increasing temperature ranging from 42.4 to 43.1 wt% at 4 GPa,1500 and 1600°C, respectively. At 5 GPa SiO_2 varies from 43.3 to 40.8 and 45.4 wt% at 1200, 1300 and 1400°C, respectively. Al_2O_3 and K_2O varies from ~10-15 and ~10-11 wt%, respectively. No significant trends to extreme quench phlogopite compositions with respect to Si or Al were observed, in contrast to the results of Enggist et al. (2012). In both systems MgO decreases with increasing temperature.

The compositions of the quench phase and the glass are given in Table 3-9 and Figure 3-4. The modal abundance of quench phlogopite is about half the abundance of the quench phase in the experimental results, and the total amount of melt was estimated using mass balance calculations using the program Igpet04. Possible melt compositions are illustrated in Figure 3-4.

Table 3-9 Quench phase and glass compositions (KCMAS-H_2O and KCMAS-H_2O-CO_2)

				c	c	c
P [GPa]	[a]5	[a]5	[a]8	[a]5	[b]7	[b]8
T [°C]	1400	1500	1400	1400	~1600	~1500
Run # ae-…	32	50	120	52	144	153
n	2	2	3	4	10	10
SiO2 [wt%]	40.9(1)	50.3(8)	48.9(18)	42.3(27)	54.4(16)	55.7(8)
Al2O3	10.1(1)	7.6(17)	13.3(23)	7.9(3)	7.9(6)	11.3(13)
MgO	23.4(4)	15.5(13)	15.2(15)	24.2(5)	16.9(18)	7.9(12)
CaO	7.5(7)	7.5(7)	4.7(21)	4.3(3)	13.7(14)	14.3(11)
K2O	7.6(10)	6.5(22)	8.9(16)	6.6(14)	4.1(2)	6.7(10)
Total	88.2(4)	87.4(11)	91.0(3)	85.5(41)	97.2(10)	95.9(9)

[a] interstitial quench phase in addition to quench phlogopite, [b]quenched glass without quench phlogopite present, *c* KCMAS-H_2O-CO_2, *n* number of analyses; standard deviations in the last digit are given in parentheses

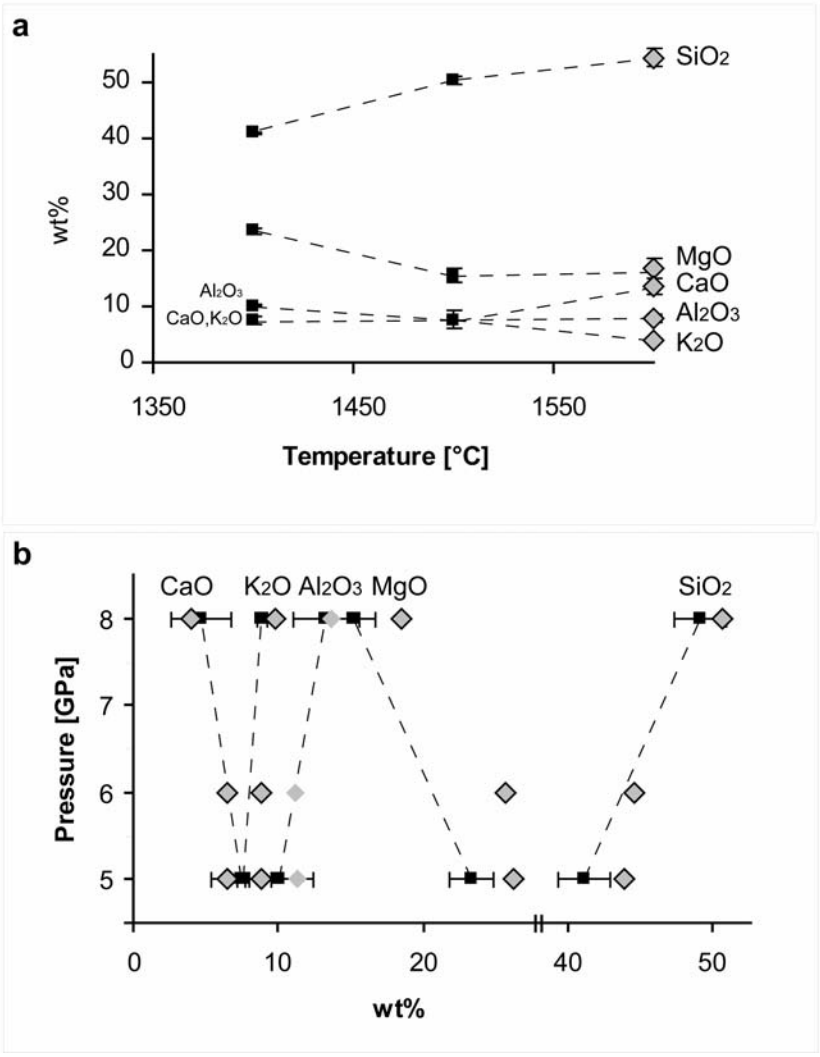

Figure 3-4 a) Compositional trend of the quench phase (q-phase, squares) and the glass (diamonds) with increasing temperature. b) Composition of the q-phase (squares) with increasing pressure. Tie lines not necessarily give a true trend but are a visual aid by connecting the same oxides. Diamonds give possible melt compositions assuming an abundance of ~30 % of melt with a 1:2 ratio of quench phlogopite (q-phl) to q-phase. Where no direct measurement of q-phl or q-phase was available, a comparable one was used from a different experiment. Error bars give the standard deviation. The q-phase and the glass were not normalized, the melt was normalized to 96.5 wt% assuming all volatiles being dissolved in the melt. See text for discussion.

3.4. Discussion

3.4.1. Phase relations

In both systems, the synthetic phlogopite in the starting material reacts to form primary phlogopite, garnet and a fluid at subsolidus conditions. A similar reaction was observed in previous studies at pressures >5 GPa (Sato et al. 1997), >6 GPa (Luth 1997) and at 4-8 GPa (Enggist et al. 2012).

In our experiments, diopside is involved in this reaction, as it is the only Ca-bearing phase that can contribute to the Ca content measured in garnets. But diopside is not used up and is present on both sides of the reaction. For simplicity, we assume that the synthetic phlogopite is stoichiometric and that the resulting primary phlogopite is enriched in Si and deficient in Al and Mg. Furthermore, we assume stoichiometric K and (OH), vacancies (□) to be in the octahedral site, all Al of the primary phlogopite in tetrahedral coordination, and $(Al, Si)^{IV}_{\Sigma=4}$. The garnet resulting from this breakdown is assumed to contain 0.4 Ca pfu, which is substituting for Mg, and we further assume that excess Mg and Si are dissolved in a fluid rather than used up by crystallizing olivine or enstatite, as seen in Enggist et al. (2012). The following simplified reaction (3.1) can be formulated:

$$2\ KMg_3AlSi_3O_{10}(OH)_2\ \text{(synthetic phlogopite)} + \frac{6}{20}\ CaMgSi_2O_6\ \text{(diopside)} =$$
$$KMg_{2.75}\square_{0.25}Al_{0.5}Si_{3.5}O_{10}(OH)_2\ \text{(Si-rich primary phlogopite)} +$$
$$\frac{15}{20}\ Ca_{0.4}Mg_{2.6}Al_2Si_3O_{12}\ \text{(Ca-bearing garnet)} +$$
$$(\frac{10}{20}\ K_2O + \frac{32}{20}\ MgO + \frac{17}{20}\ SiO_2 + H_2O)\ \text{(fluid)}\quad (3.1)$$

Reaction (3.1) illustrates the enrichment in Si of phlogopite observed in our experiments to higher pressures, and implies that the fluid present at subsolidus conditions mainly results from this breakdown reaction, with dehydroxylation of the mica playing a minor role. If this reaction takes place, ~0.7 wt% of fluid is produced from this breakdown. The presence of carbonate (and pyroxenes) can be ruled out to be the trigger for this breakdown reaction (3.1), as the same reaction was observed in pure phlogopite experiments (Enggist et al. 2012).

At pressures >6 GPa and subsolidus temperatures, the primary phlogopite starts to break down to potassic richterite, enstatite, Ca-bearing garnet and a fluid. Phlogopite coexists with potassic richterite at 7 GPa and is absent at 8 GPa. Kushiro and Erlank (1968) found potassic richterite to be stable at pressures <3 GPa. In the presence of garnet or spinel, however, the potassic richterite was reacting to produce phlogopite and pyroxene. Konzett et al. (1996) explored a mica-amphibole-rutile-ilmenite-diopside xenolith composition and found potassic richterite stable in absence of garnet at pressures <7 GPa. At 7 GPa potassic richterite did coexist with garnet in their study. Sudo and Tatsumi (1990) reported the breakdown of phlogopite to potassic richterite at 6 GPa and they formulated the following two reactions (3.2a, b) to explain such a breakdown:

$$2\ K_2Mg_6Al_2Si_6O_{20}(OH)_4\ \text{(phlogopite)} + 2\ CaMgSi_2O_6\ \text{(diopside)} =$$
$$K_2CaMg_5Si_8O_{22}(OH)_2\ \text{(potassic richterite)} +$$
$$CaMg_5Al_4Si_6O_{24}\ \text{(Ca-bearing garnet)} +$$
$$2\ Mg_2SiO_4\ \text{(olivine)} + (K_2O + 3\ H_2O)\ \text{(fluid)} \qquad (3.2a)$$

$2\ K_2Mg_6Al_2Si_6O_{20}(OH)_4$ (phlogopite) + $CaMgSi_2O_6$ (diopside) + $2\ MgSiO_3$ (enstatite) =

$K_2CaMg_5Si_8O_{22}(OH)_2$ (potassic richterite) +

$2\ Mg_3Al_2Si_3O_{12}$ (Ca-free garnet) +

$2\ Mg_2SiO_4$ (olivine) + ($K_2O + 3\ H_2O$) (fluid) (3.2b)

In our experiments, olivine was found below the solidus only in one experiment (ae-117). In other subsolidus charges it was either not present or was not abundant enough to be noticed. The Si-enrichment seen in phlogopite is less extreme at high pressures compared to Enggist et al. (2012). And, the texture of enstatite changes at these pressure conditions, which probably is associated with the breakdown of phlogopite to potassic richterite. The modal amount of orthopyroxene is not increasing by much, but the grain size of fewer crystals is larger, as illustrated in Figure 3-3. Probably, the Si of the fluid phase is buffered by the enstatite.

Furthermore, all the garnets produced in our systems contain Ca, and its modal abundance below the solidus increases from ~8 to ~10 modal% at high pressures. The following reaction (3.2c) can be formulated to describe our results the best, and which results in ~1 wt% of fluid:

$2\ K_2Mg_6Al_2Si_6O_{20}(OH)_4$ (phlogopite) + $2\ CaMgSi_2O_6$ (diopside) =

$K_2CaMg_5Si_8O_{22}(OH)_2$ (potassic richterite) +

$CaMg_5Al_4Si_6O_{24}$ (Ca-bearing garnet) +

$Mg_2Si_2O_6$ (enstatite) + ($K_2O + 2\ MgO + 3\ H_2O$) (fluid) (3.2c)

The solidi found in the present study coincide with the melting of the K-bearing phases, which is in agreement with previous studies. Luth (1997) found incongruent melting relations (3.3a) of phlogopite + diopside to diopside, olivine and melt at pressures of 3 and 5 GPa, and to diopside, olivine, garnet and melt at pressures of 7.5, 9 and 11 GPa. Sato et al. (1997) report a reaction (3.3b) phlogopite + enstatite to enstatite, olivine and melt at 4 GPa, and to enstatite, olivine, garnet and melt at pressures of 5 and 6 GPa, and to enstatite, garnet and melt at 8 GPa. Furthermore, for the simple phlogopite system they report the reaction (3.3c). Trønnes (2002) found phlogopite reacting to olivine, garnet and fluid at 7.5 and 10 GPa (3.3d). Enggist et al. (2012) located the melting reaction (3.3e) in the phlogopite and magnesite system (Fig. 3-5).

phlogopite + diopside = olivine + melt (3-5 GPa)
= olivine + garnet + melt (7.5-11 GPa) (3.3a)

phlogopite + enstatite = olivine + melt (4 GPa)
= olivine + garnet + melt (5-6 GPa)
= garnet + melt (8 GPa) (3.3b)

phlogopite = olivine + melt (4 GPa)
= olivine + garnet + melt (5-8 GPa) (3.3c)

phlogopite = olivine + garnet + fluid (7.5-10 GPa) (3.3d)

phlogopite + magnesite + fluid =
olivine + enstatite + garnet + melt (4-8 GPa) (3.3e)

In the present study, magnesite disappears at the solidus. Above the solidus, the amount of enstatite increases and olivine is present. Enstatite grains are large (≤200 µm) at pressures of 7 and 8 GPa, which probably is due to the release of MgO associated with the breakdown of the phlogopite to potassic richterite. The abundance of garnet does not increase by much with pressure, in contrast to the results of Enggist et al. (2012), who reported that in the Ca-free system, the pyrope mode increases from ~10 to ~30 modal% to higher pressures and temperatures.

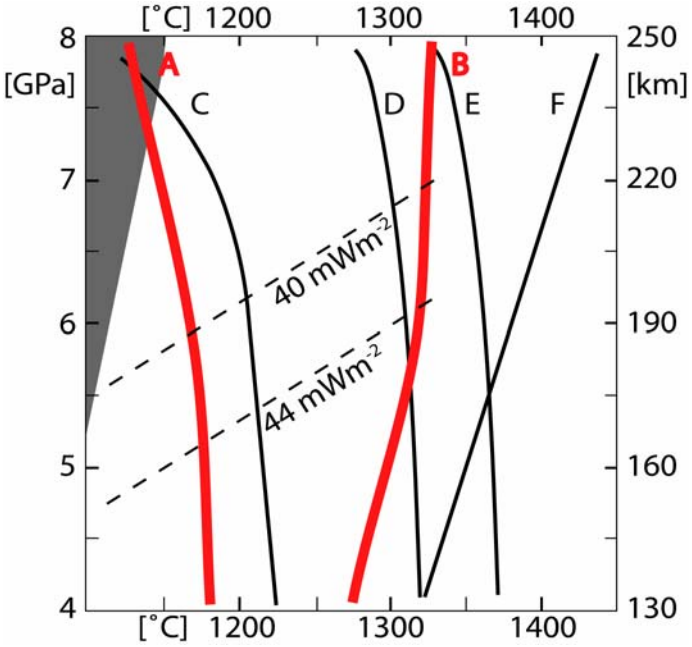

Figure 3-5 Compilation of phlogopite melting reactions with subcontinental geotherms (dashed) and with a Cascadia type adiabat (shaded region). See text for discussion. *A* phlogopite + magnesite + enstatite + diopside (this study), *B* phlogopite + enstatite + diopside (this study), *C* phlogopite + magnesite (Enggist et al. 2012), *D* phlogopite + enstatite (Sato et al. 1997), *E* natural phlogopite (Sato et al. 1997), synthetic phlogopite breakdown curve (Trønnes 2002), *F* phlogopite + diopside (Luth 1997)

Above 6 GPa, garnet grains only rarely grow bigger than 10 µm. The abundance of garnet at 4 GPa increases from ~8 below to ~15 modal% above the

solidus. From 5 GPa to higher pressures it increases to ~20 modal%. At 4 GPa and a temperature of 1600°C the modal amount of garnet has decreased to ~5 modal% indicating that the incorporation of Ca in garnet lowers its thermal stability. No garnet is found at 7 GPa and ~1500°C, nor at 8 GPa and 1600°C. Thus garnet cannot be a liquidus phase.

As in reaction (3.3a) diopside is involved in the present melting reaction, and as the case in (3.3e) the fluid is taking part and enstatite and olivine are produced above the solidus in the present study. All the magnesite is used up at the solidus. Considering our results, the following melting reactions (3.3f, g) can be formulated with the K-bearing phase being primary phlogopite at pressures of 4-6 GPa, primary phlogopite and potassic richterite at 7 GPa, and potassic richterite at 8 GPa:

K-bearing phase + magnesite + diopside + fluid =
olivine + enstatite + garnet + melt (3.3f)

K-bearing phase + diopside + fluid =
olivine + enstatite + garnet + melt (3.3g)

As for the quench phase, SiO_2 increases to higher temperatures (Figure 3-4a), which is similar to trends in the melt compositions reported by Foley et al. (2009), and similar to the quench phlogopite compositions reported in Enggist et al. (2012) and in the present study. Ca stays the same and Mg decreases from 23.4 to 15.5 wt% at 1400 and 1500°C, respectively. The glass is higher in CaO because all the Ca-bearing phases have melted out and only olivine coexists with melt at

this temperature. Figure 3-4b illustrates the evolution of the quench phase and a possible melt composition with increasing pressure. SiO_2 and K_2O contents of the quench phase are higher at 8 GPa, whereas MgO and CaO contents are lower. These trends, however, reflect not only pressure but also may reflect temperature effects as the run conditions at 5 and 8 GPa are ~100°C and ~50°C above the solidus, respectively. The possible melt composition follows the same general trends but is higher in MgO and SiO_2.

Canil and Scarfe (1990; simplified synthetic peridotite) and Luth (1997; phlogopite + diopside) report enrichment of MgO in melt at higher pressures. The present study does not cover the same pressure range, and MgO decreases at pressures from 5 to 8 GPa but is generally higher than reported in Luth (1997). Melts found by Canil and Scarfe (1990), Luth (1997) and in this study are Mg-, Si-rich and Ca-poor, and resemble kimberlitic melts (e.g. Becker and Le Roex 2006). Dalton and Presnall (1998) found their near-solidus melts to be carbonatitic. Gudfinnsson and Presnall (2005) report a gradual change from carbonatitic to kimberlitic melt compositions at higher melt fractions and pressures from 6-10 GPa. In the present study the analysis of low melt fractions was not possible and often there was a hydrous quench solution escaping the capsules upon breach. The melt composition estimated in this study is of higher melt fractions already (~30%). We expect lower melt fractions to be of carbonatitic character, as the carbonate is melting out first at the solidus.

Brey et al. (2008) and Foley et al. (2009) argue that kimberlitic melts probably are not primary melts derived form single-stage partial melting. Most

likely, the generation of kimberlites involves multi-stage processes. Potassic and hydrous phases and carbonates clearly play an important role in these processes.

3.4.2. Implications for subduction environments, subcontinental lithospheric mantle and diamond formation

Assuming that phlogopite and carbonate form above a subducting slab (see discussion in Enggist et al. 2012), alkali- and CO_2-rich melts can originate at a depth of ~240 km at pressures of ~7.5 GPa, where the temperatures at the slab surface reach 1150°C. Considering recent mantle temperatures, only a very hot, Cascadia-type subduction geometry could result in such high temperatures on the slab surface (shaded region in Fig. 3-5).

In the subcontinental lithospheric mantle, a 40-mWm^{-2} geotherm intersects the solidus found in this study at a depth of ~190 km (Figs. 3-5, 3-6). In case of a 44-mWm^{-2} lithospheric mantle geotherm, the carbonated phase assemblage, including a coexisting fluid, is stable to a depth of ~170 km, which is ~10 km shallower in depth than found in the simple system discussed in Enggist et al. (2012). At these depths, a hydrous, K- and CO_2- bearing melt rising from below will react with olivine, enstatite and form phlogopite, magnesite, diopside, garnet and stabilize a fluid in the diamond stability field. This fluid will percolate upwards and is a viable metasomatic agent at this and shallower depths (see discussion in Enggist et al. 2012).

Xenoliths described by Erlank et al. (1987) record two main events involving phlogopite: In a first event, the mantle peridotite is enriched modally with primary phlogopite, and potentially other phases. In a second infiltration

event, this primary assemblage is overprinted with secondary phlogopite. Our experimental results complement their petrographic observations. Their primary phlogopite is equivalent to our primary phlogopite, and their secondary phlogopite can be taken as a second generation of our primary phlogopite. This leads to the following multi-step scenario, where hydrous potassium-bearing and ± carbonated melts infiltrate the subcontinental lithospheric mantle and react with garnet peridotite to produce phlogopite, ± magnesite, diopside and a fluid. The fluid then percolates upwards, possibly carrying minor potassium among other solutes (see "Phase relations" section). With increasing metasomatism, as discussed in Erlank et al. (1987), potassic richterite occurs interstitially in the xenoliths, implying a late crystallization. Later melting of these low temperature assemblages could give rise to potassic magmas (cf. review by Foley 2008).

In addition, the magnesite-bearing assemblage and the fluid phase present may play an important role in the formation of diamonds in the mantle. Low fO_2 values in a subcratonic keel (e.g. Ballhaus 1993; Wood et al. 1996; McCammon and Kopylova 2004; Creighton et al. 2009), could reduce carbonate to diamond, following the reaction enstatite + magnesite = olivine + diamond (Eggler et al. 1980). Furthermore, diamonds could grow from the reduction of the CO_2 to diamond + O_2 (Luth 1993) from a CO_2-bearing, hydrous fluid (e.g. Thomassot et al. 2009; Stachel and Harris 2009; Smart et al. 2011).

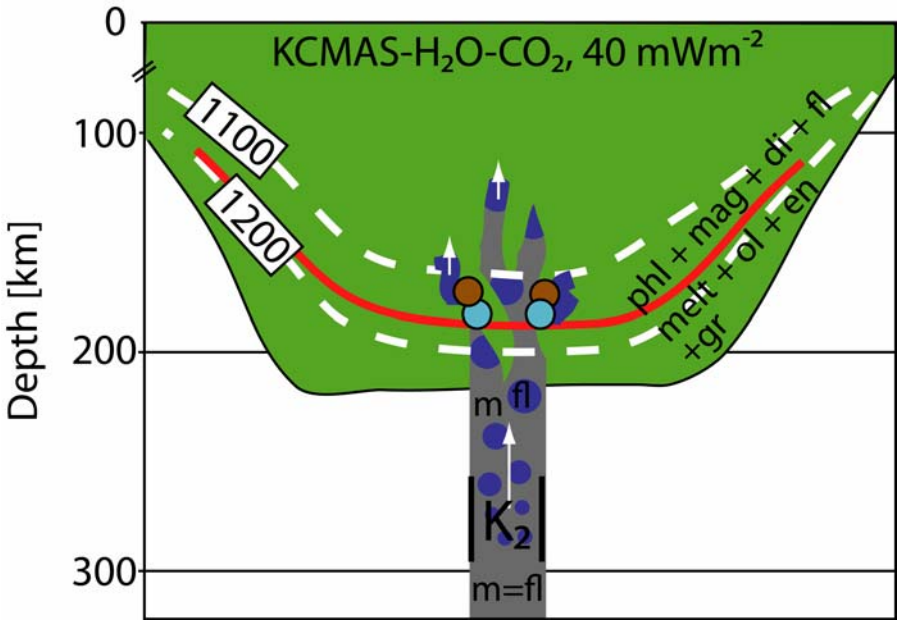

Figure 3-6 Subcontinental keel is intruded by a K-OH-CO_2-bearing magma. The ascending magma passes K_2 at a pressure >8 GPa, from where the magma, depending on the volatile content, could exsolve a fluid, which accelerates magma ascent. Within the subcontinental mantle the melt can react with en, ol, gr and crystallize phl, mag and di that will coexist with a hydrous fluid at a depth of ~190 km in a cool continental mantle (40 mWm^{-2}). See text for details. *di* diopside, *en* enstatite, *fl* fluid, *gr* garnet, K_2 second critical end-point, *mag* magnesite, *m* melt, *ol* olivine, *phl* phlogopite

3.4.3. Second critical end-point and implications for magma ascent

A controversial subject concerns the second critical end-point in CO_2-H_2O-bearing peridotite. Mibe et al. (2009) located it at a pressure of 3.5 GPa, whereas Keshav and Gudfinnsson (2009) did not find it at a pressure of 7 GPa. Wyllie and Ryabchikov (2000) arbitrarily placed the second critical end-point for carbonated lherzolite at a depth of 250 km. In our experiments the fluid and the melt remain two distinct phases to a pressure of 8 GPa, and the solidus extends to greater depths.

Two experiments in KCMAS-H_2O-CO_2 (ae-144, 153) yielded surprising results. Apparently, temperatures on the samples were not close to the solidus

(1100-1200°C) but in-between solidus and liquidus. Probably the elevated temperatures were caused by a shorting of the thermocouple wires, and the exact temperature on the sample is unknown. Two-pyroxene thermometry for ae-153 suggests a temperature of ~1500°C, and comparing ae-144 with other experiments indicates that the temperature probably was around ~1600°C. Sample ae-144 and ae-153 contain, besides melt that quenched to glass, olivine and olivine, diopside, enstatite, respectively. Furthermore, spherical voids in the glass indicate the presence of a fluid phase (Fig. 3-3e-f).

The starting mix used in the present study contains 1.4 and 2.1 wt% of H_2O and CO_2, respectively. Given the small amount of volatiles in the system, it would be surprising if the fluid would not be dissolved in the melt. Probably, the voids are caused by a fluid (mainly CO_2) that was exsolved from the melt during quenching of the experiment. The solidus, however, clearly extends to a pressure greater than 8 GPa and experiments are needed to further constrain it.

Depending on volatile content, a rising CO_2-H_2O-bearing magma, such as kimberlite, could exsolve a fluid once it passes the second critical end-point (>8 GPa, >250 km) (Fig. 3-6). This fluid exsolution would accelerate the melt's ascent rate and affect its way of propagation (e.g. Wilson and Head 2007).

3.4.4. Stability of phlogopite

Adding pyroxenes to an end-member system reduces the stability of phlogopite by ~50°C (this study). End-member and simple (Ca-free) systems all show a change in slope of solidi or breakdown curves from positive to negative

below and above ~5 GPa, respectively (Sato et al. 1997, Trønnes 2002; Enggist et al. 2012). Adding Ca to the system in the form of diopside will change this behavior by crystallizing potassic richterite, and the solidus remains positive to higher pressures (Luth 1997; this study). The amphibole seems to stabilize water in solid phases to higher pressures and temperatures.

Ti and F are known to stabilize phlogopite or amphibole to higher temperatures (Kushiro et al. 1967; Forbes and Flower 1974; Foley 1991; Konzett 1997; Melzer and Foley 2000), and Fe and Na will reduce the temperature stability (Konzett and Ulmer 1999). Furthermore, chlorine may be present in some parts of the upper mantle (e.g. Perfit et al. 1980; Philippot 1993; Wirth et al. 2009) and recently has been shown to have a great effect on solidus temperatures by reducing the a_{H2O} of a fluid phase. In the absence of OH-bearing phases, this causes a considerable shift of wet solidi to higher temperatures (Chu et al. 2011). Hydrous phases are strongly affected by such a reduction of a_{H2O} in the coexisting fluid (Aranovich and Newton 1998). The reduction of a_{H2O} can be interpreted similarly to the removal of H_2O from the system, which then shifts the reaction to the melt side, extracting OH from the solid into the melt phase, thereby triggering the breakdown of water-bearing phases, and lowering the solidus temperatures. Systematic experimentation in simple phlogopite systems containing Na, Fe, Ti, F, Cl and CO_2 at upper mantle conditions are needed to understand phlogopite stability.

As summarized in Figure 3-5, in carbonate-free harzburgitic systems, phlogopite is stable to temperatures of 1300-1250°C at 4-8 GPa, respectively. In

carbonate-free lherzolitic systems, phlogopite is stable to temperatures of 1250°C at 4-5.5 GPa, to 1300°C at 6 GPa, and coexists with potassic richterite to 1300°C at 7 GPa. Potassic richterite is stable to 1300°C at 8 GPa (Luth 1997; Sato et al. 1997; this study). Adding CO_2 to a lherzolitic system depresses the stability of the K-bearing phase by 100-200°C at 4 and 8 GPa, respectively. Phlogopite is stable to temperatures of 1150°C at 4-6 GPa, coexists with potassic richterite to temperatures of 1100°C at 7 GPa, and potassic richterite is stable to temperatures of 1100°C at 8 GPa (this study).

3.5. Conclusions

Phlogopite, enstatite, diopside, garnet and a fluid are stable to 1250°C at 4, 5 and 5.5 GPa, and to 1300°C at 6 GPa. Phlogopite, potassic richterite, enstatite, diopside, garnet and a fluid coexist to 1300°C and 7 GPa. At 8 GPa the stable assemblage to 1300°C is potassic richterite, enstatite, diopside, garnet and a fluid.

Phlogopite, enstatite, diopside, garnet with magnesite and a fluid are stable to 1150°C at 4, 5 and 6 GPa. Phlogopite, potassic richterite, enstatite, diopside, garnet with magnesite and a fluid coexist to 1100°C and 7 GPa. At 8 GPa the stable assemblage to 1100°C is potassic richterite, enstatite, diopside, garnet, magnesite and a fluid.

Compared to the carbonate-free system, the carbonated solidus temperatures are lowered by 100 to 200°C at 4 and 8 GPa, respectively. Phlogopite and potassic richterite melt over ~100°C. Above the solidus, olivine, enstatite, diopside and garnet coexist with melt.

In a very hot subduction zone, the K-bearing phase in the presence of carbonate will melt at a depth of ~240 km. In a subcontinental lithospheric mantle phlogopite remains stable with magnesite and a coexisting fluid to a depth of ~170-190 km with a 44- and 40-mWm^{-2} geotherm, respectively. The second critical end-point in the carbonated-peridotite-model system (KCMAS-H_2O-CO_2) is at a pressure >8 GPa.

References

Aranovich LY, Newton RC (1998) Reversed determination of the reaction: phlogopite + quartz = enstatite + potassium feldspar + H_2O in the ranges 750-875°C and 2-12 kbar at low H_2O activity with concentrated KCl solutions. Am Mineral 83:193-204.

Armstrong JT (1988) Quantitative analysis of silicate and oxide materials: comparison of Monte Carlo, ZAF, and phi(rho Z) procedures, In: Newbury DE (ed) Microbeam Analysis, pp 239-246.

Ballhaus C (1993) Redox states of lithospheric and asthenospheric upper mantle. Contrib Mineral Petrol 114:331-348.

Becker M, Le Roex AP (2006) Geochemistry of South African on- and offcraton, group I and group II kimberlites: Petrogenesis and source region evolution. J Petrol 47:673-703.

Brey GP, Bulatov VK, Girnis AV, Lahaye Y (2008) Experimental melting of carbonated peridotite at 6-10GPa. J Petrol 49:797-821.

Brey GP, Köhler T, Nickel KG (1990) Geothermobarometry in four-phase lherzolites I. Experimental results from 10 to 60 kb. J Petrol 31:1313-1352.

Canil D, Scarfe CM (1990) Phase relations in peridotite + CO_2 systems to 12 GPa: Implications for the origin of kimberlite and carbonate stability in the Earth's upper mantle. J Geophys Res 95:15,805-15,816.

Chu L, Enggist A, and Luth RW (2011) Effect of KCl on melting in the Mg_2SiO_4-$MgSiO_3$-H_2O system at 5 GPa. Contrib Mineral Petrol. doi:10.1007/s00410-011-0612-9

Creighton S, Stachel T, Matveev S, Höfer H, McCammon C, Luth RW (2009) Oxidation of the Kaapvaal lithospheric mantle driven by metasomatism. Contrib Mineral Petrol 157:491-504.

Dalton JA, Presnall DC (1998) Carbonatitic melts along the solidus of model lherzolite in the system CaO-MgO-Al_2O_3-SiO_2-CO_2 from 3 to 7 GPa. Contrib Mineral Petrol 131:123-135.

Dasgupta R, Hirschmann MM (2010) The deep carbon cycle and melting in Earth's interior. Earth Planet Sci Letters 298:1-13.

Eggler DH, Baker DR, Wendtland RF (1980) f_{O2} of the assemblage graphite-enstatite-forsterite-magnesite: experiment and application to mantle f_{O2} and diamond formation. Geol Soc Am Abstr Prog 12:420p.

Enggist A, Chu L, Luth RW (2012) Phase relations of phlogopite with magnesite from 4 to 8 GPa. Contrib Mineral Petrol 163:467-481. doi:10.1007/s00410-011-0681-9

Foley, SF (1991) High-pressure stability of the fluor- and hydroxy end-members of pargasite and K-richterite. Geochim Cosmochim Acta 55:2689-2694.

Foley SF (2008) Rejuvenation and erosion of the cratonic lithosphere. Nature Geosci 1:503-510.

Foley SF, Yaxley GM, Rosenthal A, Buhre S, Kiseeva ES, Rapp RP, Jacob DE (2009) The composition of near-solidus melts of peridotite in the presence of CO_2 and H_2O between 40 and 60 kbar. Lithos 112(S1):274-283.

Forbes, W C, Flower MFJ (1974) Phase relations of titan-phlogopite, $2Mg_4TiAl_2Si_6O_{20}(OH)_4$: a refractory phase in the upper mantle? Earth Planet Sci Letters 22:60-66.

Frost DJ (2006) The Stability of Hydrous Mantle Phases. In: Keppler, H., and Smyth, J.R. (eds) Water in nominally anhydrous minerals. Mineral Soc Am 62:243-271.

Gudfinnsson DH, Presnall DC (2005) Continuous gradations among primary carbonatitic, kimberlitic, melilititic, basaltic, picritic, and komatiitic melts in equilibrium with garnet lherzolite at 3–8 GPa. J Petrol 46:1645-1659.

Keshav S, Gudfinnsson G (2009) Eos Trans AGU 90(52) Fall Meet Suppl, Abstract MR31C-05.

Keshav S, Gudfinnsson G (2010) Experimentally dictated stability of carbonated oceanic crust to moderately great depths in the Earth: Results from the solidus determination in the system CaO-MgO-Al_2O_3-SiO_2-CO_2. J Geophys Res 115:20pp.

Konzett J (1997) Phase relations and chemistry of Ti-rich K-richterite-bearing mantle assemblages: An experimental study to 8.0 GPa in a Ti-KNCMASH system. Contrib Mineral Petrol 128:385-404.

Konzett J, Fei Y (2000) Transport and storage of potassium in the Earth's upper mantle and transition zone: An experimental study to 23 GPa in simplified and natural bulk compositions. J Petrol 41(4):583-603.

Konzett J, Sweeney RJ, Thompson AB, Ulmer P (1997) Potassium amphibole Stability in the upper mantle: An experimental study in a peralkaline KNCMASH system to 8·5 GPa. J Petrol 38:537-568.

Konzett J, Ulmer P (1999) The stability of hydrous potassic phases in lherzolitic mantle - an experimental study to 9.5 GPa in simplified and natural bulk compositions. J Petrol 40(4):629-652.

Kushiro I, Erlank AJ (1968) Stability of potassic richterite. Carnegie Inst. Wash. Year Book 68, 231-233.

Kushiro I, Syono Y, Akimoto S (1967) Stability of phlogopite at high pressures and possible presence of phlogopite in the earth's upper mantle. Earth Planet. Sci. Letters 3:197-203.

Luth RW (1993) Diamonds, eclogites, and the oxidation State of the Earth's mantle. Science 261:66-68.

Luth RW (1997) Experimental study of the system phlogopite-diopside from 3.5 to 17 GPa. Am

Mineral 82:1198-1209.

Luth RW (2004) Mantle volatiles-distribution and consequences. In: Holland HD, Turekian KK (eds) Treatise on Geochemistry. Elsevier, pp 319-361.

Luth RW (2006) Experimental study of the $CaMgSi_2O_6$-CO_2 system at 3-8 GPa. Contrib Mineral Petrol 151:141-157.

McCammon C, Kopylova MG (2004) A redox profile of the Slave mantle and oxygen fugacity control in the cratonic mantle. Contrib Mineral Petrol 148:55-68.

Melzer S, Foley SF (2000) Phase relations and fractionation sequences in potassic magma series modelled in the system $CaMgSi_2O_6$-$KAlSiO_4$-Mg_2SiO_4-SiO_2-F_2O_{-1} at 1 bar to 18 kbar. Contrib Mineral Petrol 138:186-197.

Mibe K, Kawamoto T, Ono S (2009) Effect of CO_2 on the second critical end-point in the system peridotite-H_2O-CO_2, Eos Trans AGU 90(52) Fall Meet Suppl, Abstract MR31C-04.

Modreski PJ, Boettcher, AL (1972) The stability of phlogopite + enstatite at high pressures: a model for micas in the interior of the earth. Am J Sci 272:852-869.

Modreski PJ, Boettcher, AL (1973) Modreski, P.J., and Boettcher, A.L., 1973, Phase relationships of phlogopite in the system K_2O-MgO-CaO-Al_2O_3-SiO_2-H_2O to 35 kilobars: A better model for micas in the interior of the earth: Am J Sci 273:385-414.

Perfit MR, Gust DA, Bence AE, Arculus RJ, Tylor SR (1980) Chemical characteristics of island-arc basalts: Implications for mantle sources. Chem Geol 30:227-256.

Philippot P (1993) Fluid-melt-rock interaction in mafic eclogites and coesite-bearing metasediments: Constraints on volatile recycling during subduction. Chem Geol 108:93-112.

Sato K, Katsura T, Ito E (1997) Phase relations of natural phlogopite with and without enstatite up to 8 GPa: Implication for mantle metasomatism. Earth Planet Sci Lett 146:511-526.

Smart KA, Chacko T, Stachel T, Muehlenbachs K, Stern RA, Heaman LM (2011) Diamond growth from oxidized carbon sources beneath the Northern Slave Craton, Canada: A $\delta^{13}C$–N study of eclogite-hosted diamonds from the Jericho kimberlite. Geochim Cosmochim Acta 75:6027-6047.

Stachel T, Harris JW (2009) Formation of diamond in the Earth's mantle. J Phys Condens Matter 21(364206):10p.

Sudo A, Tatsumi Y (1990) Phlogopite and K-amphibole in the upper mantle: Implication for magma genesis in subduction zones. Geophys Res Lett 17(1):29-32.

Thomassot E, Cartigny P, Harris JW, Lorand JP, Rollion-Bard C, Chaussidon M (2009) Metasomatic diamond growth: A multi-isotope study (^{13}C, ^{15}N, ^{33}S, ^{34}S) of sulphide inclusions and their host diamonds from Jwaneng (Botswana). Earth Planet Sci Lett 282:79-90.

Trønnes RG (2002) Stability range and decomposition of potassic richterite and phlogopite end members at 5-15 GPa. Mineral Petrol 74:129-148.

Walter MJ, Thibault Y, Wei K, Luth RW (1995) Characterizing experimental pressure and temperature conditions in multianvil apparatus. Can J Phys 73:273-286.

Wendlandt RF, Eggler DH (1980) The origins of potassic magmas: 2. stability of phlogopite in

natural spinel lherzolite and in the system $KAlSiO_4$-MgO-SiO_2-H_2O-CO_2 at high pressures and high temperatures. Am J Sci 280:421-458.

Wilson L, Head JW (2007) An integrated model of kimberlite ascent and eruption. Nature 447:53-57.

Wirth R, Kaminsky F, Matsyuk S, Schreiber A (2009) Unusual micro- and nano-inclusions in diamonds from the Juina Area, Brazil. Earth Planet Sci Lett 286:292-303.

Wyllie PJ, Ryabchikov ID (2000) Volatile components, magmas, and critical fluids in upwelling mantle. J Petrol 41:1195-1206.

Yang H, Konzett J, Prewitt CT, Fei Y (1999) Single-crystal structure refinement of synthetic ^{M4}K-substituted potassic richterite, $K(KCa)Mg_5Si_8O_{22}(OH)_2$. Am Mineral 84:681-684.

Chapter 4: Conclusions

4.1. Phlogopite stability

Hydrous potassic phases in the Earth's upper mantle, such as phlogopite or potassic richterite, can coexist with carbonates and a fluid phase to considerable depth in a subcontinental lithospheric mantle (chapters 2 and 3).

In carbonate-free harzburgitic systems, phlogopite is stable to temperatures of 1300-1250°C at 4-8 GPa, respectively (Sato et al. 1997). In carbonate-free lherzolitic systems, phlogopite is stable to temperatures of 1250°C at 4-5.5 GPa, to 1300°C at 6 GPa, and coexists with potassic richterite to 1300°C at 7 GPa. Potassic richterite is stable to 1300°C at 8 GPa (Sudo and Tatsumi 1990; Luth 1997; chapter 3).

In a carbonated lherzolitic system, the stability of the K-bearing phase is lowered by 100-200°C at 4 and 8 GPa, respectively (chapter 3). Phlogopite is stable to temperatures of 1150°C at 4-6 GPa, and coexists with potassic richterite to temperatures of 1100°C at 7 GPa. Potassic richterite is stable to temperatures of 1100°C at 8 GPa (chapter 3).

4.2. Coexisting fluids

Phlogopite and magnesite can coexist with a fluid at subsolidus conditions at pressures of 4-7 GPa (chapters 2 and 3), the same holds for potassic richterite and magnesite at pressures ≥7 GPa (chapter 3). The hydrous fluid in equilibrium with phlogopite can carry K_2O, SiO_2 and MgO as solute and gets richer in SiO_2 to

higher pressures, which leads to Si-enrichment in the associated phlogopite in the enstatite-free experiments (chapter 2). Enstatite possibly buffers this effect as reported in chapter 3, and the fluid would carry K_2O and MgO as solute.

4.3. Melts

In the carbonated systems investigated in this study, KMAS-H_2O-CO_2 (chapter 2) and KCMAS-H_2O-CO_2 (chapter 3), the disappearance of the carbonate also indicated the melting of the potassic phases, and the first occurrence of melt.

Textural investigation of the experimental results revealed that a hydrous, potassic, silicate melt can quench to (quench) phlogopite and a hydrous solution (chapter 2), or to quench phlogopite, a quench phase and a hydrous solution at low melt fractions (chapter 3), or to glass and a fluid at high melt fractions (chapter 3). It was not possible to measure the hydrous quench solution in my series of experiments.

The compositions of the quench phlogopite in the simple system (chapter 2) reflect the melt composition. Two main compositional trends were found: 1) extreme Si-enrichment to higher pressures, and 2), associated with 1), extreme depletion of Al with increasing pressures. Those trends were observed from 4-8 GPa but were enhanced at pressures ≥5 GPa. Furthermore, this observation may be linked to the increase of the garnet modal abundance to higher pressures and temperatures (chapter 2).

In the pyroxene-bearing experiments the above-mentioned compositional trends were not as extreme and possibly buffered by the enstatite. Possible melt

compositions, derived by combining the quench phlogopite and quench phase measurements, were, in a broad sense, similar to group II kimberlitic magmas with respect to K_2O, SiO_2, high MgO and low CaO contents (chapter 3).

4.4. Implications for metasomatism

Hydrous, potassic and CO_2-bearing melts infiltrating the subcontinental lithospheric mantle from below will take part in reactions at depths of 170-200 km with garnet, enstatite and olivine, crystallizing phlogopite, magnesite, diopside and stabilizing a K-bearing fluid, which can percolate further upwards (chapters 2 and 3). These K-rich patches or veins can melt in a subsequent heating event and give rise to K-rich melts (cf. review by Foley 2008).

In a very hot subduction zone, K- and CO_2-rich magmas would originate above a subducting slab at a depth of ~240 km. The rising melt could react with the cooler mantle underneath the continent and crystallize phlogopite, magnesite and diopside and a fluid, which could be transported back into the mantle wedge (chapters 2 and 3).

4.5. Future research

Considering the present study and previous experimental investigations (cf. review by Frost 2006), the phlogopite stability now is well constrained in simple experimental systems (KCMASH). Attention should be paid to the effect of Na, Fe, Ti, F, Cl, and combinations of them, on phlogopite stability at upper mantle conditions. The work about carbonate in the presence of hydrous potassic

phases still is at its beginning and will require the investigation of varying fO_2 as well. A recent study by Konzett et al. (2011) contains chlorine in the system, which seems to destabilize the phlogopite.

References

Foley SF (2008) Rejuvenation and erosion of the cratonic lithosphere. Nature Geosci 1:503-510.

Frost DJ (2006) The stability of hydrous mantle phases. In: Keppler, H., and Smyth, J.R. (eds) Water in nominally anhydrous minerals. Mineral Soc Am 62:243-271.

Konzett J, Rhede D, Frost DJ (2011) The high PT stability of apatite and Cl partitioning between apatite and hydrous potassic phases in peridotite: An experimental study to 19 GPa with implications for the transport of P, Cl and K in the upper mantle. Contrib Mineral Petrol. doi:10.1007/s00410-011-0672

Luth RW (1997) Experimental study of the system phlogopite-diopside from 3.5 to 17 GPa. Am Mineral 82:1198-1209.

Sato K, Katsura T, Ito E (1997) Phase relations of natural phlogopite with and without enstatite up to 8 GPa: implication for mantle metasomatism. Earth Planet Sci Lett 146:511-526.

Sudo A, Tatsumi Y (1990) Phlogopite and K-amphibole in the upper mantle: Implication for magma genesis in subduction zones. Geophys Res Lett 17(1):29-32.

Appendix A: mineral data KMAS-H_2O-CO_2[1]

Phase	**phl**									
P [GPa]	**4**									
T [°C]	**1150**									
ae-...	**05**									
wt%										
SiO_2	42.4	42.3	42.0	41.8	42.1	42.2	42.1	41.8	42.2	41.7
Al_2O_3	15.7	15.3	15.3	14.9	15.5	15.0	15.5	16.0	15.3	15.3
MgO	25.9	26.3	26.2	26.3	26.8	26.8	26.1	25.5	26.3	26.6
CaO	n/a	n/a	n/a	n/a	n/a	n/a	n/a	n/a	n/a	n/a
K_2O	11.0	11.3	11.2	11.4	11.3	11.3	11.3	11.0	11.4	11.4
Total	95.0	95.2	94.6	94.4	95.7	95.3	95.0	94.4	95.2	94.9

Phase				**phl**						
P [GPa]				**5.5**						
T [°C]				**1150**						
ae-...				**22**						
wt%										
SiO_2	42.4	42.0	42.1	41.6	41.8	41.6	43.7	42.7	43.6	43.4
Al_2O_3	15.6	15.5	15.2	14.9	15.0	17.8	15.9	15.0	15.6	15.2
MgO	26.0	25.5	26.1	27.8	26.6	24.1	25.2	25.6	25.7	26.4
CaO	n/a	n/a	n/a	n/a	n/a	n/a	n/a	n/a	n/a	n/a
K_2O	11.3	11.2	11.4	11.2	11.4	11.0	11.2	11.3	11.2	11.4
Total	95.3	94.2	94.8	95.6	94.8	94.5	95.9	94.5	96.1	96.4

Phase			**phl**							
P [GPa]			**6**							
T [°C]			**1150**							
ae-...			**15**							
wt%										
SiO_2	42.0	43.0	43.9	43.4	42.6	43.4	43.8	43.3	43.5	43.2
Al_2O_3	15.2	15.7	12.2	12.1	11.7	12.2	12.6	12.1	11.8	11.7
MgO	26.5	25.8	27.5	28.5	27.4	27.2	27.3	27.5	27.8	27.6
CaO	n/a	n/a	n/a	n/a	n/a	n/a	n/a	n/a	n/a	n/a
K_2O	11.4	11.3	11.2	11.1	11.4	11.2	11.0	11.1	11.1	11.2
Total	95.1	95.8	94.9	95.0	93.0	94.0	94.7	94.1	94.2	93.6

Phase					**phl**					
P [GPa]					**7**					
T [°C]					**1150**					
ae-...					**94**					
wt%										
SiO_2	43.4	43.8	42.8	43.7	44.6	44.9	44.6	44.0	43.3	42.3
Al_2O_3	11.7	11.6	11.8	11.4	11.9	12.3	12.3	11.9	11.7	11.4
MgO	28.3	28.7	28.7	27.8	29.1	28.2	28.4	28.8	28.6	29.9
CaO	n/a	n/a	n/a	n/a	n/a	n/a	n/a	n/a	n/a	n/a
K_2O	11.6	11.7	11.6	11.7	10.9	10.9	11.0	10.9	10.9	11.0
Total	95.0	95.8	94.8	94.6	96.6	96.3	96.3	95.6	94.4	94.5

[1] Data presented here was used in Chapter 2 and is published as Enggist A, Chu L, Luth RW (2011) Phase relations of phlogopite with magnesite from 4 to 8 GPa, *Contributions to Mineralogy and Petrology* 163:467-481. doi: 10.1007/s00410-011-0681-9

Phase	**phl**						**phl**			
P [GPa]	**7**						**8**			
T [°C]	**1150**						**1150**			
ae-...	**94**						**97**			
wt%										
SiO_2	42.0	44.2	43.4	43.6	43.5	44.3	45.4	45.9	45.7	44.6
Al_2O_3	11.4	11.7	11.7	11.7	11.7	11.8	10.8	12.4	12.5	11.9
MgO	30.1	29.0	28.2	28.4	28.6	27.4	27.5	27.8	28.0	29.1
CaO	n/a	n/a	n/a	n/a	n/a	n/a	n/a	n/a	n/a	n/a
K_2O	11.0	10.6	11.0	10.8	10.5	10.8	11.0	10.5	11.1	10.9
Total	94.4	95.4	94.2	94.5	94.3	94.3	94.7	96.5	97.3	96.6

Phase										
P [GPa]										
T [°C]										
ae-...										
wt%										
SiO_2	46.0	44.9	44.6	44.0	43.3	44.2	43.4	43.6	43.5	44.3
Al_2O_3	12.4	12.3	12.3	11.9	11.7	11.7	11.7	11.7	11.7	11.8
MgO	27.9	28.2	28.4	28.8	28.6	29.0	28.2	28.4	28.6	27.4
CaO	n/a	n/a	n/a	n/a	n/a	n/a	n/a	n/a	n/a	n/a
K_2O	11.0	10.9	11.0	10.9	10.9	10.6	11.0	10.8	10.5	10.8
Total	97.3	96.3	96.3	95.6	94.4	95.4	94.2	94.5	94.3	94.3

Phase	**phl**									
P [GPa]	**5**									
T [°C]	**1200**									
ae-...	**60**									
wt%										
SiO_2	41.6	41.5	41.1	42.0	42.4	40.8	41.0	41.8	40.9	40.2
Al_2O_3	16.1	15.7	16.3	15.8	15.3	15.3	14.4	15.9	14.7	14.3
MgO	26.5	26.3	26.7	27.2	26.6	27.2	27.8	25.8	27.4	28.7
CaO	n/a	n/a	n/a	n/a	n/a	n/a	n/a	n/a	n/a	n/a
K_2O	10.9	10.8	11.2	10.7	10.8	11.0	10.9	10.7	11.2	11.1
Total	95.2	94.3	95.3	95.8	95.1	94.2	94.1	94.2	94.2	94.6

Phase			**phl**							
P [GPa]			**4**							
T [°C]			**1250**							
ae-...			**07**							
wt%										
SiO_2	41.1	40.7	42.0	41.2	41.0	41.6	41.8	41.5	41.7	42.0
Al_2O_3	14.8	14.7	14.3	14.8	14.6	15.1	14.5	14.4	14.9	14.6
MgO	27.6	27.5	26.2	26.7	26.7	26.5	26.2	26.1	26.0	25.9
CaO	n/a	n/a	n/a	n/a	n/a	n/a	n/a	n/a	n/a	n/a
K_2O	11.1	11.1	11.4	11.6	11.4	11.5	11.6	11.5	11.4	11.3
Total	94.6	94.0	94.0	94.2	93.8	94.7	94.0	93.6	94.0	93.7

Phase	**phl**			**phl**						
P [GPa]	**4**			**5**						
T [°C]	**1250**			**1250**						
ae-...	**07**			**19**						
wt%										
SiO_2	41.6	41.0	41.1	44.0	42.4	42.2	42.0	43.2	43.6	43.5
Al_2O_3	14.5	15.1	14.9	13.3	12.7	12.6	12.6	13.0	12.9	13.0
MgO	26.3	26.3	26.6	27.6	27.4	27.9	27.9	27.5	26.8	27.6
CaO	n/a	n/a	n/a	n/a	n/a	n/a	n/a	n/a	n/a	n/a
K_2O	11.4	11.2	11.5	11.0	11.1	10.9	11.0	11.0	11.0	10.9
Total	93.8	93.6	94.1	95.9	93.5	93.5	93.5	94.6	94.3	94.9

Phase					**phl**					
P [GPa]					**6**					
T [°C]					**1250**					
ae-...					**20**					
wt%										
SiO_2	43.4	42.1	43.5	44.1	44.0	43.5	43.5	43.1	43.1	43.6
Al_2O_3	12.8	12.6	13.0	13.2	12.1	12.0	11.9	12.1	12.0	12.0
MgO	26.4	27.1	27.9	27.6	27.6	27.6	28.1	28.0	27.8	28.3
CaO	n/a	n/a	n/a	n/a	n/a	n/a	n/a	n/a	n/a	n/a
K_2O	10.7	11.2	11.0	11.0	10.8	11.0	11.2	11.1	11.0	11.2
Total	93.4	93.0	95.4	95.9	94.5	94.0	94.7	94.3	93.9	95.1

Phase										**phl**
P [GPa]										**6**
T [°C]										**1350**
ae-...										**24**
wt%										
SiO_2	43.8	43.7	43.4	43.6	44.0	42.2	43.8	43.8	44.7	52.9
Al_2O_3	11.7	11.8	11.7	11.7	12.6	12.6	11.7	11.7	11.9	4.5
MgO	27.0	27.5	27.4	27.3	27.7	29.1	28.3	28.8	26.7	26.5
CaO	n/a	n/a	n/a	n/a	n/a	n/a	n/a	n/a	n/a	n/a
K_2O	11.1	11.1	11.1	10.9	10.6	11.2	10.7	11.0	11.0	11.4
Total	93.6	94.1	93.4	93.5	95.0	95.0	94.6	95.3	94.3	95.3

Phase				**phl**						
P [GPa]				**7**						
T [°C]				**1350**						
ae-...				**58**						
wt%										
SiO_2	51.4	49.4	53.3	51.5	50.9	53.0	53.0	52.0	51.4	48.0
Al_2O_3	4.4	7.1	4.3	5.6	5.2	5.2	4.8	5.7	5.0	6.0
MgO	27.2	27.1	26.9	27.1	26.5	27.2	27.8	27.0	26.3	28.0
CaO	n/a	n/a	n/a	n/a	n/a	n/a	n/a	n/a	n/a	n/a
K_2O	11.5	11.3	10.8	9.8	11.3	9.5	10.1	9.7	11.2	11.4
Total	94.5	94.8	95.4	94.1	93.9	95.0	95.7	94.4	93.9	93.4

Phase	**phl**					**phl**				
P [GPa]	**7**					**5**				
T [°C]	**1350**					**1400**				
ae-...	**58**					**39**				
wt%										
SiO_2	51.5	49.2	49.8	49.4	48.8	51.7	49.9	46.7	49.1	49.9
Al_2O_3	5.9	6.1	5.3	5.3	5.1	9.3	9.2	10.2	8.8	8.2
MgO	27.2	27.7	27.1	28.6	27.9	22.2	23.2	28.5	25.9	25.7
CaO	n/a	n/a	n/a	n/a	n/a	n/a	n/a	n/a	n/a	n/a
K_2O	11.0	11.1	11.0	10.7	10.9	10.0	10.0	10.9	10.8	10.7
Total	95.6	94.1	93.1	94.0	92.7	93.3	92.4	96.3	94.6	94.5

Phase					**phl**					
P [GPa]					**4**					
T [°C]					**1450**					
ae-...					**23**					
wt%										
SiO_2	46.9	48.5	46.0	51.7	40.8	41.1	40.2	40.6	40.1	40.6
Al_2O_3	9.1	9.1	9.1	9.3	14.8	15.3	15.1	15.1	14.7	15.1
MgO	26.2	24.9	27.0	22.2	25.3	26.8	26.5	26.3	27.1	26.3
CaO	n/a	n/a	n/a	n/a	n/a	n/a	n/a	n/a	n/a	n/a
K_2O	11.0	11.0	10.9	10.0	11.5	11.4	11.8	11.6	11.6	11.7
Total	93.3	93.5	93.0	93.3	92.3	94.7	93.6	93.6	93.6	93.7

Phase						**phl**				
P [GPa]						**6**				
T [°C]						**1450**				
ae-...						**25**				
wt%										
SiO_2	40.1	42.2	42.7	49.8	49.3	53.1	48.7	48.8	49.6	46.5
Al_2O_3	15.3	15.7	15.6	4.5	7.2	5.8	6.3	5.6	7.6	8.5
MgO	27.4	26.1	26.3	30.6	28.4	25.6	27.6	30.6	27.2	28.4
CaO	n/a	n/a	n/a	n/a	n/a	n/a	n/a	n/a	n/a	n/a
K_2O	11.8	11.9	11.6	10.6	10.8	10.3	10.7	10.3	10.8	10.5
Total	94.7	95.9	96.2	95.5	95.7	94.7	93.3	95.3	95.2	93.9

Phase		**phl**								**phl**
P [GPa]		**4**								**4**
T [°C]		**1500**								**1550**
ae-...		**35**								**26**
wt%										
SiO_2	46.9	41.5	41.5	42.2	41.0	42.6	42.4	42.7	44.5	43.3
Al_2O_3	8.0	17.7	16.2	16.0	17.3	16.1	16.3	16.9	16.5	15.5
MgO	27.7	24.1	26.1	25.2	25.0	27.2	25.2	25.7	24.5	25.2
CaO	n/a	n/a	n/a	n/a	n/a	n/a	n/a	n/a	n/a	n/a
K_2O	11.3	10.9	11.1	11.2	11.1	10.5	11.0	11.1	10.9	11.3
Total	93.9	94.1	95.0	94.6	94.4	96.4	94.9	96.3	96.4	95.3

Phase	**phl**							**phl**		
P [GPa]	**4**							**5**		
T [°C]	**1550**							**1550**		
ae-...	**26**							**36**		
wt%										
SiO_2	44.2	41.8	42.2	42.0	42.2	43.2	42.7	42.6	42.7	43.3
Al_2O_3	14.8	14.8	15.1	15.3	13.2	16.7	15.4	13.6	12.8	14.1
MgO	24.7	26.5	26.8	24.7	26.9	22.9	25.8	27.2	26.4	26.2
CaO	n/a	n/a	n/a	n/a	n/a	n/a	n/a	n/a	n/a	n/a
K_2O	11.4	11.5	11.5	11.3	11.4	10.9	11.0	10.8	11.1	10.9
Total	95.1	94.7	95.5	93.3	93.8	93.7	94.9	94.2	93.0	94.5

Phase							**phl**			
P [GPa]							**6**			
T [°C]							**1550**			
ae-...							**38**			
wt%										
SiO_2	46.8	46.3	46.1	44.2	45.4	43.8	52.1	49.1	48.4	47.5
Al_2O_3	13.3	14.0	13.0	12.9	13.0	13.0	5.3	6.9	5.9	7.4
MgO	25.0	24.0	25.8	25.5	24.2	25.6	25.1	27.0	28.1	28.4
CaO	n/a	n/a	n/a	n/a	n/a	n/a	n/a	n/a	n/a	n/a
K_2O	8.6	10.1	10.7	10.8	10.7	11.0	10.7	10.8	11.0	10.9
Total	93.7	94.5	95.5	93.4	93.3	93.4	93.1	93.7	93.4	94.1

Phase					**mag**					
P [GPa]					**4**					
T [°C]					**1150**					
ae-...					**05**					
wt%										
SiO_2	53.0	48.6	48.0	48.4	0.1	0.1	0.1	0.1	0.0	0.1
Al_2O_3	6.8	6.2	8.6	8.7	0.0	0.1	0.1	0.0	0.0	0.0
MgO	23.7	27.8	25.7	25.8	41.1	40.4	40.5	37.2	40.5	40.4
CaO	n/a	n/a	n/a	n/a	n/a	n/a	n/a	n/a	n/a	n/a
K_2O	10.4	10.7	10.9	11.1	0.0	0.0	0.1	0.0	0.0	0.0
Total	93.9	93.3	93.2	94.0	41.2	40.6	40.7	37.4	40.6	40.6

Phase				**mag**						
P [GPa]				**5**						
T [°C]				**1200**						
ae-...				**60**						
wt%										
SiO_2	0.1	0.1	0.4	0.1	0.1	0.1	0.1	0.1	0.1	0.2
Al_2O_3	0.0	0.1	0.2	0.0	0.0	0.0	0.0	0.0	0.0	0.0
MgO	39.0	37.5	37.6	39.0	38.2	39.1	38.9	37.4	37.8	38.6
CaO	n/a	n/a	n/a	n/a	n/a	n/a	n/a	n/a	n/a	n/a
K_2O	0.1	0.0	0.2	0.1	0.1	0.3	0.1	0.0	0.1	0.2
Total	39.2	37.8	38.3	39.2	38.5	39.6	39.1	37.5	38.1	39.1

Phase	**mag**			**mag**						
P [GPa]	**5**			**6**						
T [°C]	**1200**			**1150**						
ae-...	**60**			**15**						
wt%										
SiO_2	0.1	0.1	0.1	0.1	0.0	0.5	0.0	0.0	0.1	0.1
Al_2O_3	0.0	0.0	0.0	0.0	0.0	0.1	0.0	0.0	0.0	0.1
MgO	40.0	38.9	38.7	40.6	40.9	42.6	40.7	41.9	42.0	39.5
CaO	n/a	n/a	n/a	n/a	n/a	n/a	n/a	n/a	n/a	n/a
K_2O	0.1	0.3	0.1	0.1	0.1	0.3	0.2	0.1	0.2	0.2
Total	40.2	39.3	38.9	40.8	41.1	43.5	41.0	42.0	42.3	39.9

Phase		**mag**							**mag**	
P [GPa]		**7**							**8**	
T [°C]		**1150**							**1150**	
ae-...		**94**							**97**	
wt%										
SiO_2	0.2	0.2	0.3	0.2	0.2	0.2	0.3	0.3	0.1	0.1
Al_2O_3	0.0	0.1	0.1	0.0	0.0	0.0	0.1	0.1	0.0	0.0
MgO	43.2	42.7	45.9	43.7	42.4	41.2	43.2	43.0	45.3	45.5
CaO	n/a	n/a	n/a	n/a	n/a	n/a	n/a	n/a	n/a	n/a
K_2O	0.1	0.0	0.0	0.0	0.0	0.0	0.0	0.0	0.6	0.3
Total	43.4	42.9	46.3	44.0	42.7	41.5	43.5	43.4	46.1	45.9

Phase			**py**							**py**
P [GPa]			**4**							**4**
T [°C]			**1150**							**1250**
ae-...			**05**							**07**
wt%										
SiO_2	0.1	0.1	44.1	44.7	44.7	43.5	45.6	45.2	44.2	44.5
Al_2O_3	0.0	0.0	25.3	25.6	25.9	25.2	26.0	26.1	25.3	25.4
MgO	43.8	44.9	29.6	29.5	29.8	30.3	28.8	29.3	28.8	29.2
CaO	n/a	n/a	n/a	n/a	n/a	n/a	n/a	n/a	n/a	n/a
K_2O	0.4	0.6	0.0	0.0	0.0	0.0	0.0	0.0	0.0	0.1
Total	44.3	45.6	99.0	99.8	100.4	99.0	100.4	100.6	98.4	99.3

Phase										
P [GPa]										
T [°C]										
ae-...										
wt%										
SiO_2	44.2	44.5	44.9	44.4	44.6	44.1	44.1	44.7	44.4	44.6
Al_2O_3	25.4	25.7	25.3	25.5	25.4	25.5	25.2	25.7	25.2	25.4
MgO	28.9	29.1	29.9	29.6	29.2	29.5	29.4	29.3	29.2	29.5
CaO	n/a	n/a	n/a	n/a	n/a	n/a	n/a	n/a	n/a	n/a
K_2O	0.1	0.1	0.1	0.1	0.2	0.2	0.2	0.2	0.2	0.1
Total	98.7	99.4	100.2	99.6	99.4	99.2	98.8	99.8	98.9	99.7

Phase	**py**									
P [GPa]	**4**									
T [°C]	**1250**									
ae-...	**07**									
wt%										
SiO_2	44.6	44.5	44.7	44.6	44.3	44.3	44.5	44.4	44.3	44.3
Al_2O_3	25.5	25.5	25.5	25.2	25.9	25.4	25.3	25.3	25.4	25.4
MgO	29.2	28.9	28.8	28.7	29.4	29.4	29.0	29.2	29.3	28.7
CaO	n/a	n/a	n/a	n/a	n/a	n/a	n/a	n/a	n/a	n/a
K_2O	0.1	0.2	0.3	0.3	0.2	0.1	0.1	0.2	0.2	0.2
Total	99.5	99.0	99.2	98.8	99.8	99.2	99.0	99.1	99.2	98.6

Phase							**py**			
P [GPa]							**4**			
T [°C]							**1500**			
ae-...							**35**			
wt%										
SiO_2	43.9	44.2	44.2	44.1	44.2	44.5	45.4	45.2	45.0	45.6
Al_2O_3	25.1	25.3	25.4	25.1	25.5	25.4	24.9	25.1	24.8	23.3
MgO	29.7	29.1	29.5	29.8	29.6	29.2	30.0	30.0	29.9	30.2
CaO	n/a	n/a	n/a	n/a	n/a	n/a	n/a	n/a	n/a	n/a
K_2O	0.1	0.1	0.1	0.1	0.2	0.2	0.0	0.0	0.3	0.0
Total	98.7	98.7	99.2	99.1	99.5	99.2	100.3	100.3	100.0	99.2

Phase								**py**		
P [GPa]								**5**		
T [°C]								**1200**		
ae-...								**60**		
wt%										
SiO_2	44.8	45.0	46.6	46.0	43.4	46.0	44.9	43.1	43.0	43.6
Al_2O_3	25.0	25.3	25.5	25.7	26.4	25.3	24.5	25.1	24.5	26.1
MgO	30.2	30.7	28.2	28.5	30.1	28.5	30.1	30.3	30.6	29.7
CaO	n/a	n/a	n/a	n/a	n/a	n/a	n/a	n/a	n/a	n/a
K_2O	0.0	0.0	0.0	0.0	0.1	0.0	0.0	0.1	0.2	0.2
Total	100.0	101.0	100.3	100.2	100.1	99.8	99.6	98.6	98.3	99.5

Phase								**py**		
P [GPa]								**5**		
T [°C]								**1250**		
ae-...								**19**		
wt%										
SiO_2	44.7	44.9	43.8	44.4	42.4	43.2	42.7	44.7	44.9	44.1
Al_2O_3	26.2	26.1	25.5	26.9	26.0	25.6	27.1	24.3	25.2	24.0
MgO	29.4	28.9	29.4	29.1	30.8	31.7	30.4	29.1	29.5	30.0
CaO	n/a	n/a	n/a	n/a	n/a	n/a	n/a	n/a	n/a	n/a
K_2O	0.1	0.1	0.1	0.1	0.1	0.3	0.0	0.0	0.0	0.0
Total	100.4	100.0	98.8	100.5	99.3	100.8	100.2	98.2	99.6	98.1

Phase	**py**					**py**				
P [GPa]	**5**					**5**				
T [°C]	**1250**					**1400**				
ae-...	**19**					**39**				
wt%										
SiO_2	44.6	44.8	45.0	46.0	45.6	45.2	45.6	46.3	45.3	45.9
Al_2O_3	24.6	25.5	25.4	24.9	24.6	24.9	24.8	25.5	24.5	24.9
MgO	29.9	28.3	28.3	27.4	29.0	30.2	28.9	27.9	30.5	30.0
CaO	n/a	n/a	n/a	n/a	n/a	n/a	n/a	n/a	n/a	n/a
K_2O	0.1	0.0	0.1	0.0	0.0	0.0	0.0	0.0	0.0	0.0
Total	99.2	98.7	98.7	98.4	99.1	100.3	99.2	99.8	100.3	100.8

Phase						**py**				
P [GPa]						**5**				
T [°C]						**1550**				
ae-...						**36**				
wt%										
SiO_2	45.5	46.7	46.2	45.4	46.1	44.9	45.3	44.2	45.3	45.6
Al_2O_3	24.8	24.1	24.4	23.6	23.7	23.8	23.7	24.7	24.2	23.9
MgO	29.1	30.0	29.9	30.1	29.6	30.2	29.4	29.5	29.2	29.3
CaO	n/a	n/a	n/a	n/a	n/a	n/a	n/a	n/a	n/a	n/a
K_2O	0.0	0.0	0.0	0.0	0.0	0.0	0.0	0.0	0.0	0.0
Total	99.4	100.8	100.5	99.1	99.4	98.9	98.4	98.4	98.7	98.7

Phase							**py**			
P [GPa]							**6**			
T [°C]							**1250**			
ae-...							**20**			
wt%										
SiO_2	46.1	45.2	44.6	45.5	44.8	46.2	46.6	46.2	45.8	45.1
Al_2O_3	24.9	24.7	24.9	25.2	24.6	24.9	24.7	24.2	23.6	24.8
MgO	29.1	29.0	29.5	29.5	29.5	29.1	27.8	29.6	28.6	29.5
CaO	n/a	n/a	n/a	n/a	n/a	n/a	n/a	n/a	n/a	n/a
K_2O	0.0	0.0	0.0	0.0	0.0	0.0	0.0	0.0	0.0	0.0
Total	100.1	99.0	98.9	100.2	98.9	100.1	99.1	100.0	98.1	99.4

Phase			**py**							
P [GPa]			**6**							
T [°C]			**1450**							
ae-...			**25**							
wt%										
SiO_2	46.0	46.3	45.9	45.3	44.6	45.4	44.8	45.3	44.8	45.7
Al_2O_3	23.5	23.6	24.4	24.5	23.7	23.7	24.3	24.3	24.5	23.9
MgO	29.3	29.0	29.6	30.0	30.7	30.6	30.8	30.4	30.5	29.9
CaO	n/a	n/a	n/a	n/a	n/a	n/a	n/a	n/a	n/a	n/a
K_2O	0.0	0.0	0.0	0.0	0.0	0.0	0.0	0.0	0.0	0.0
Total	98.8	98.8	99.9	99.8	99.0	99.8	99.9	100.1	99.8	99.5

Phase	**py**									
P [GPa]	**6**									
T [°C]	**1450**									
ae-...	**25**									
wt%										
SiO_2	44.9	45.9	44.9	45.3	44.4	45.0	44.1	43.8	44.5	43.7
Al_2O_3	24.2	23.3	23.4	23.6	25.3	25.8	25.9	25.0	25.1	24.1
MgO	29.7	30.3	31.0	30.6	29.8	29.5	30.4	31.8	30.3	31.7
CaO	n/a	n/a	n/a	n/a	n/a	n/a	n/a	n/a	n/a	n/a
K_2O	0.3	0.0	0.0	0.0	0.0	0.0	0.0	0.2	0.0	0.0
Total	99.1	99.5	99.4	99.5	99.5	100.3	100.4	100.7	99.9	99.5
Phase	**py**				**py**					
P [GPa]	**7**				**7**					
T [°C]	**1150**				**1350**					
ae-...	**94**				**58**					
wt%										
SiO_2	43.9	43.5	42.8	44.3	43.9	42.9	44.0	44.1	43.6	43.9
Al_2O_3	24.9	24.7	23.9	25.0	25.1	24.9	24.4	25.3	25.2	25.2
MgO	32.0	31.7	31.8	30.4	30.3	30.6	32.1	30.6	30.1	29.8
CaO	n/a	n/a	n/a	n/a	n/a	n/a	n/a	n/a	n/a	n/a
K_2O	0.1	0.1	0.1	0.2	0.5	0.4	0.5	0.2	0.4	0.1
Total	100.9	100.0	98.7	100.0	99.7	98.7	101.1	100.1	99.4	98.9
Phase					**py**					
P [GPa]					**8**					
T [°C]					**1150**					
ae-...					**97**					
wt%										
SiO_2	43.5	43.2	44.6	44.0	47.1	46.3				
Al_2O_3	25.1	24.1	23.9	24.5	25.5	24.6				
MgO	30.3	32.4	29.6	30.4	28.2	27.3				
CaO	n/a	n/a	n/a	n/a	n/a	n/a				
K_2O	0.3	0.1	0.5	0.5	0.3	0.3				
Total	99.2	99.9	98.6	99.3	101.2	98.6				

Appendix B: mineral data KCMAS-H_2O±CO_2[1]

Phase	**phl**							**phl**		
P [GPa]	**4**							**5**		
T [°C]	**1250**							**1250**		
ae-...	**157**							**147**		
wt%										
SiO_2	43.0	43.4	43.6	43.7	42.5	43.3	43.2	40.3	41.7	39.9
Al_2O_3	14.1	13.8	14.1	14.1	13.2	13.1	13.6	12.4	12.8	11.9
MgO	27.0	25.7	26.0	26.1	24.9	26.3	25.4	28.1	27.3	29.4
CaO	0.1	0.1	0.1	0.1	0.0	0.1	0.1	0.3	0.1	0.3
K_2O	11.3	11.2	11.4	11.4	11.7	10.7	11.1	10.8	11.3	11.3
Total	95.5	94.1	95.1	95.3	92.4	93.5	93.3	91.8	93.2	92.8

Phase		**phl**		**phl**						
P [GPa]		**7**		**6**						
T [°C]		**1300**		**1350**						
ae-...		**152**		**33**						
wt%										
SiO_2	40.7	44.2	47.1	42.1	44.2	43.8	44.0	43.7	43.3	43.5
Al_2O_3	12.2	11.4	13.3	11.5	12.1	11.7	11.9	11.8	11.7	11.7
MgO	27.4	26.5	25.6	28.2	26.2	26.7	27.0	26.8	27.9	27.0
CaO	0.7	0.8	0.5	0.2	0.1	0.1	0.1	0.1	0.0	0.0
K_2O	10.4	9.9	10.1	11.2	10.9	10.9	11.0	11.2	11.0	11.0
Total	91.3	92.8	96.6	93.2	93.5	93.2	93.9	93.5	93.9	93.1

Phase										**phl**
P [GPa]										**5**
T [°C]										**1400**
ae-...										**32**
wt%										
SiO_2	43.7	44.2	44.8	44.4	43.3	44.5	44.1	44.0	44.3	41.6
Al_2O_3	11.8	11.9	12.0	12.0	11.6	12.6	12.0	12.2	12.0	12.7
MgO	27.2	26.9	26.0	26.4	27.7	25.5	28.2	26.9	27.2	28.1
CaO	0.0	0.1	0.0	0.0	0.0	0.1	0.0	0.1	0.0	0.0
K_2O	10.7	11.0	11.1	10.8	11.0	11.2	10.7	10.6	10.6	10.8
Total	93.4	93.9	93.9	93.6	93.6	93.8	95.0	93.7	94.1	93.2

Phase										
P [GPa]										
T [°C]										
ae-...										
wt%										
SiO_2	39.2	40.6	41.5	40.0	40.9	39.1	39.3	40.4	40.4	39.6
Al_2O_3	12.4	13.0	13.3	12.6	13.0	12.7	12.4	12.7	12.7	12.4
MgO	29.4	28.0	28.5	27.1	28.5	29.7	29.4	28.5	29.0	29.0
CaO	0.1	0.1	0.0	0.2	0.1	0.1	0.1	0.0	0.0	0.1
K_2O	10.7	11.1	10.8	10.9	11.0	10.4	10.9	10.8	10.8	10.9
Total	91.7	92.8	94.0	90.8	93.5	92.1	92.1	92.5	93.0	92.0

[1] Data presented here was used in Chapter 3 and submitted for publication in *Contributions to Mineralogy and Petrology*.

Phase	**phl**	**phl**								
P [GPa]	**5**	**6**								
T [°C]	**1400**	**1400**								
ae-...	**32**	**30**								
wt%										
SiO_2	38.7	43.9	43.2	43.6	43.6	44.5	44.0	44.1	44.6	43.4
Al_2O_3	13.0	11.9	11.8	11.7	11.7	12.8	13.0	13.1	12.2	11.4
MgO	29.1	26.3	27.2	27.3	27.9	27.0	27.5	28.0	26.8	25.9
CaO	0.4	0.3	0.4	0.3	0.5	0.3	0.4	0.4	0.7	0.7
K_2O	10.0	10.8	10.6	10.8	9.9	10.9	11.0	10.6	9.6	10.7
Total	91.2	93.2	93.2	93.6	93.6	95.5	95.8	96.2	93.8	92.1

Phase		**phl**								
P [GPa]		**5**								
T [°C]		**1450**								
ae-...		**65**								
wt%										
SiO_2	44.1	43.9	41.4	43.7	42.7	43.0	44.1	42.4	41.9	42.9
Al_2O_3	11.6	13.3	12.6	13.3	12.8	13.1	13.4	13.1	12.9	13.0
MgO	26.6	27.1	27.8	27.0	27.1	27.1	27.3	28.3	27.1	26.9
CaO	0.7	0.0	0.1	0.1	0.1	0.1	0.1	0.0	0.1	0.2
K_2O	10.0	11.5	11.4	11.1	11.3	11.5	11.1	11.3	11.3	11.3
Total	93.1	95.8	93.2	95.1	94.0	94.8	96.0	95.1	93.2	94.2

Phase	**phl**				**phl**					
P [GPa]	**5**				**7**					
T [°C]	**1500**				**1100**					
ae-...	**50**				**155**					
wt%										
SiO_2	50.7	48.5	49.7	50.6	45.0	45.5	43.5	44.3	43.4	42.6
Al_2O_3	12.5	12.2	12.3	12.4	10.8	11.0	11.2	11.5	10.8	10.9
MgO	21.4	23.5	23.5	23.2	27.2	27.5	26.8	27.4	26.7	26.5
CaO	0.7	0.3	0.3	0.3	0.2	0.2	0.1	0.1	0.3	0.3
K_2O	7.7	9.4	7.9	6.5	10.1	9.5	10.7	10.6	10.3	10.4
Total	93.0	93.9	93.8	93.0	93.3	93.6	92.2	93.9	91.5	90.6

Phase			**phl**							
P [GPa]			**4**							
T [°C]			**1150**							
ae-...			**151**							
wt%										
SiO_2	42.8	44.2	44.1	44.1	43.2	44.3	44.9	45.5	42.2	43.6
Al_2O_3	10.5	10.6	13.4	12.9	12.6	13.6	13.4	14.0	13.0	13.3
MgO	27.7	26.9	27.2	26.1	25.8	27.6	27.0	26.1	27.1	27.3
CaO	0.1	0.5	0.1	0.7	0.7	0.1	0.1	0.1	0.2	0.2
K_2O	10.3	9.8	10.8	10.5	10.4	10.9	10.6	10.9	10.9	10.7
Total	91.5	92.0	95.6	94.2	92.7	96.4	96.1	96.6	93.4	95.1

Phase	**phl**		**phl**							
P [GPa]	**4**		**6**							
T [°C]	**1150**		**1150**							
ae-...	**151**		**149**							
wt%										
SiO_2	45.7	45.9	45.3	43.4	44.5	44.9	42.6	44.5	43.6	43.7
Al_2O_3	13.7	13.8	12.5	11.7	11.3	11.1	11.8	11.4	11.1	11.1
MgO	25.4	25.7	25.0	26.5	26.7	27.3	27.0	26.2	25.9	26.4
CaO	0.0	0.1	0.1	0.2	0.4	0.4	0.2	0.1	0.1	0.2
K_2O	11.0	11.0	10.0	10.7	10.1	10.3	10.8	9.5	10.8	10.2
Total	95.8	96.4	92.9	92.3	92.9	94.0	92.3	91.7	91.5	91.4

Phase							**phl**			
P [GPa]							**5**			
T [°C]							**1200**			
ae-...							**110**			
wt%										
SiO_2	43.6	44.1	44.0	44.9	45.8	45.3	44.7	45.0	43.4	42.2
Al_2O_3	11.2	11.4	11.5	11.5	11.9	11.4	12.5	12.9	12.6	13.8
MgO	26.7	26.6	25.5	26.0	26.7	26.0	26.2	25.4	26.4	26.9
CaO	0.1	0.1	0.1	0.1	0.1	0.4	0.1	0.0	0.0	0.1
K_2O	10.7	10.2	11.0	10.5	8.5	8.7	9.9	10.1	10.4	9.5
Total	92.3	92.4	92.1	93.0	93.0	91.8	93.4	93.4	92.8	92.5

Phase										**phl**
P [GPa]										**5**
T [°C]										**1300**
ae-...										**59**
wt%										
SiO_2	42.2	43.7	43.6	43.2	42.7	42.3	42.6	42.7	44.1	42.6
Al_2O_3	13.0	11.8	11.9	12.5	12.7	11.7	11.7	11.9	13.6	14.3
MgO	25.5	25.5	25.5	26.9	25.5	27.0	26.6	26.0	26.6	27.2
CaO	0.5	0.1	0.1	0.1	0.1	0.1	0.0	0.1	0.9	0.2
K_2O	9.9	10.2	10.2	10.6	10.6	10.3	10.1	10.2	9.2	11.0
Total	91.1	91.4	91.2	93.3	91.4	91.2	91.0	90.7	94.4	95.2

Phase				**phl**						
P [GPa]				**5**						
T [°C]				**1400**						
ae-...				**52**						
wt%										
SiO_2	41.3	38.2	41.1	46.4	46.4	44.6	46.5	44.8	44.5	45.1
Al_2O_3	10.8	14.3	12.3	10.0	11.1	9.8	9.6	10.9	11.0	10.9
MgO	28.8	29.9	27.4	26.7	26.4	27.0	27.9	28.0	28.6	27.1
CaO	0.2	0.3	0.3	0.4	0.2	0.8	0.5	0.1	0.2	0.1
K_2O	10.3	10.0	10.1	10.9	11.1	10.4	10.1	10.9	10.4	11.1
Total	91.4	92.7	91.1	94.4	95.2	92.6	94.6	94.6	94.6	94.2

Phase	**phl**			**phl**				**phl**		
P [GPa]	**5**			**4**				**4**		
T [°C]	**1400**			**1500**				**1600**		
ae-...	**52**			**55**				**70**		
wt%										
SiO_2	43.7	45.1	46.5	40.9	43.3	42.8	42.7	44.0	43.1	42.4
Al_2O_3	10.2	11.7	10.1	11.6	9.7	9.5	9.7	15.0	14.6	15.3
MgO	27.4	27.1	26.4	25.9	28.7	28.4	28.2	22.8	25.3	23.3
CaO	0.6	0.2	0.1	0.5	0.5	0.6	0.6	0.5	0.9	0.5
K_2O	10.3	10.5	10.9	11.6	11.1	10.1	9.3	10.5	10.9	10.5
Total	92.3	94.6	94.0	90.6	93.2	91.5	90.4	92.7	94.9	91.9

Phase			**mag**							
P [GPa]			**7**							
T [°C]			**1100**							
ae-...			**155**							
wt%										
SiO_2	43.0	43.2	0.1	0.2	0.5	0.1	0.1	0.1	0.1	0.0
Al_2O_3	15.8	15.7	0.1	0.0	0.0	0.0	0.0	0.0	0.0	0.0
MgO	25.6	25.6	47.5	46.7	46.5	47.5	46.9	46.7	46.1	46.6
CaO	0.3	0.3	0.3	0.3	0.6	0.5	0.5	0.6	0.5	0.5
K_2O	11.3	11.0	0.0	0.0	0.0	0.0	0.0	0.0	0.0	0.0
Total	95.9	95.8	48.0	47.2	47.7	48.2	47.6	47.4	46.6	47.1

Phase								**mag**		
P [GPa]								**8**		
T [°C]								**1100**		
ae-...								**156**		
wt%										
SiO_2	0.1	0.1	0.1	0.1	0.1	0.1	0.1	0.1	0.1	0.5
Al_2O_3	0.0	0.0	0.0	0.1	0.0	0.0	0.0	0.1	0.1	0.3
MgO	46.7	46.4	46.4	47.4	46.1	47.5	47.5	48.2	48.1	46.7
CaO	0.4	0.1	0.1	0.5	0.5	0.5	0.5	0.3	0.4	0.4
K_2O	0.0	0.0	0.0	0.0	0.0	0.0	0.0	0.0	0.0	0.0
Total	47.3	46.6	46.6	48.1	46.7	48.1	48.1	48.7	48.7	48.0

Phase								**mag**		
P [GPa]								**4**		
T [°C]								**1150**		
ae-...								**151**		
wt%										
SiO_2	0.1	0.1	0.1	0.1	0.1	0.2	0.6	0.1	0.1	0.2
Al_2O_3	0.0	0.1	0.0	0.1	0.0	0.1	0.0	0.1	0.2	0.1
MgO	48.5	48.6	48.2	48.5	48.0	46.7	47.2	45.4	45.3	44.7
CaO	0.3	0.5	0.3	0.5	0.3	0.5	0.4	1.9	1.9	2.0
K_2O	0.0	0.0	0.0	0.0	0.0	0.0	0.0	0.0	0.1	0.0
Total	48.9	49.3	48.6	49.1	48.5	47.5	48.3	47.4	47.7	47.0

Phase	**mag**									
P [GPa]	**4**									
T [°C]	**1150**									
ae-...	**151**									
wt%										
SiO_2	0.1	0.2	0.2	0.3	0.2	1.1	0.3	0.2	0.1	0.1
Al_2O_3	0.0	0.0	0.0	0.1	0.0	0.2	0.0	0.0	0.0	0.0
MgO	44.0	44.3	43.3	45.3	45.6	43.3	45.3	43.7	43.9	43.6
CaO	1.8	1.9	2.0	1.8	1.9	1.9	1.9	1.8	1.9	1.9
K_2O	0.0	0.0	0.1	0.1	0.0	0.2	0.0	0.1	0.1	0.0
Total	45.9	46.4	45.6	47.5	47.7	46.6	47.4	45.8	45.9	45.6

Phase		**mag**							**mag**	
P [GPa]		**5**							**6**	
T [°C]		**1150**							**1150**	
ae-...		**159**							**149**	
wt%										
SiO_2	0.4	0.1	0.1	0.2	0.3	0.1	0.1	0.4	0.3	0.1
Al_2O_3	0.0	0.1	0.1	0.1	0.1	0.1	0.0	0.1	0.1	0.1
MgO	43.9	47.5	48.9	46.9	47.3	48.5	46.9	46.2	45.3	47.4
CaO	1.8	1.1	0.9	0.8	1.3	1.3	1.3	1.3	1.0	1.0
K_2O	0.0	0.0	0.0	0.0	0.0	0.0	0.0	0.0	0.1	0.1
Total	46.1	48.8	50.0	48.1	49.0	50.0	48.3	48.1	46.7	48.5

Phase										
P [GPa]										
T [°C]										
ae-...										
wt%										
SiO_2	0.2	0.2	0.1	0.5	0.4	0.3	0.2	0.3	0.2	0.2
Al_2O_3	0.0	0.0	0.0	0.0	0.0	0.0	0.0	0.0	0.0	0.1
MgO	47.4	47.4	46.7	47.1	46.7	47.3	45.8	47.7	47.1	47.4
CaO	1.1	1.0	0.2	0.8	1.0	0.2	0.9	0.6	1.0	0.7
K_2O	0.0	0.0	0.0	0.0	0.0	0.0	0.0	0.0	0.0	0.1
Total	48.7	48.6	47.0	48.5	48.1	47.9	47.3	48.6	48.4	48.6

Phase	**gr**	**gr**								
P [GPa]	**5**	**8**								
T [°C]	**1250**	**1300**								
ae-...	**147**	**117**								
wt%										
SiO_2	43.0	45.4	45.6	44.5	44.9	45.4	45.7	45.7	45.0	45.4
Al_2O_3	26.7	23.2	24.3	22.5	23.6	23.9	23.8	24.0	23.6	23.9
MgO	24.7	27.1	25.3	26.9	27.0	25.4	25.6	25.8	26.9	26.3
CaO	4.8	5.1	4.6	4.9	4.6	4.1	4.1	4.1	4.3	4.2
K_2O	0.1	0.1	0.0	0.0	0.1	0.0	0.0	0.0	0.1	0.0
Total	99.3	100.8	99.8	98.9	100.1	98.8	99.3	99.7	99.9	99.9

Phase	**gr**	**gr**					**gr**			
P [GPa]	**8**	**4**					**6**			
T [°C]	**1300**	**1350**					**1350**			
ae-...	**117**	**140**					**33**			
wt%										
SiO_2	45.9	45.2	43.9	44.8	43.6	44.5	43.4	45.3	43.6	44.2
Al_2O_3	24.3	25.8	25.7	25.9	25.5	24.0	24.3	25.2	25.8	24.4
MgO	25.2	24.7	24.1	23.4	24.8	26.4	26.0	25.0	24.3	25.9
CaO	4.0	4.7	4.8	4.7	4.8	5.2	4.8	4.9	5.7	5.0
K_2O	0.1	0.6	0.1	0.4	0.1	0.2	0.3	0.4	0.5	0.4
Total	99.5	100.9	98.6	99.1	98.8	100.2	98.8	100.7	100.0	99.9

Phase							**gr**			
P [GPa]							**6**			
T [°C]							**1400**			
ae-...							**30**			
wt%										
SiO_2	44.2	46.2	44.3	44.1	45.1	44.5	44.8	44.4	44.5	45.1
Al_2O_3	24.4	23.8	24.8	24.3	24.7	24.4	24.5	23.6	23.2	23.9
MgO	25.8	25.1	25.3	25.1	24.3	25.4	26.1	25.5	26.6	24.5
CaO	5.2	5.8	6.0	5.0	5.2	5.2	4.5	5.3	5.7	5.4
K_2O	0.4	0.4	0.2	0.2	0.3	0.1	0.2	0.4	0.2	0.2
Total	99.9	101.2	100.6	98.8	99.6	99.6	100.1	99.1	100.2	99.1

Phase								**gr**		
P [GPa]								**7**		
T [°C]								**1400**		
ae-...								**111**		
wt%										
SiO_2	45.2	44.6	45.2	44.9	44.9	44.0	44.4	44.6	44.0	45.0
Al_2O_3	24.4	24.2	23.4	24.4	24.5	23.6	24.5	24.4	23.6	23.6
MgO	26.1	26.3	26.6	25.8	25.1	26.2	25.4	27.6	27.1	27.3
CaO	5.2	4.6	5.3	5.3	5.7	5.6	6.1	4.3	4.3	4.7
K_2O	0.1	0.1	0.2	0.1	0.1	0.1	0.2	0.0	0.0	0.0
Total	100.9	99.7	100.5	100.4	100.3	99.5	100.5	100.9	98.9	100.6

Phase										
P [GPa]										
T [°C]										
ae-...										
wt%										
SiO_2	45.1	44.4	44.3	44.0	44.4	44.0	44.3	44.2	43.9	44.2
Al_2O_3	24.2	23.8	23.6	23.6	23.6	23.8	23.6	23.7	23.6	23.3
MgO	27.6	27.2	27.7	27.5	28.0	27.7	27.8	27.7	27.6	27.2
CaO	4.4	4.5	4.2	4.2	4.2	4.1	4.2	4.2	3.9	4.8
K_2O	0.0	0.0	0.0	0.0	0.0	0.0	0.0	0.0	0.0	0.0
Total	101.3	99.7	99.7	99.4	100.2	99.6	100.0	99.7	99.0	99.5

Phase	**gr**	**gr**								
P [GPa]	**7**	**8**								
T [°C]	**1400**	**1400**								
ae-...	**111**	**120**								
wt%										
SiO_2	44.2	45.5	45.6	44.8	44.7	45.2	44.7	44.7	46.2	46.2
Al_2O_3	23.2	24.0	23.6	22.6	22.5	23.2	23.7	23.8	24.2	23.5
MgO	27.2	27.5	27.9	26.9	27.2	27.5	27.6	27.2	24.9	26.6
CaO	4.5	4.0	4.0	5.3	5.1	3.9	4.0	4.1	3.9	4.5
K_2O	0.1	0.2	0.3	0.4	0.3	0.3	0.1	0.2	0.3	0.2
Total	99.1	101.2	101.5	99.9	99.8	100.1	100.1	99.9	99.5	101.0

Phase		**gr**								
P [GPa]		**5**								
T [°C]		**1450**								
ae-...		**65**								
wt%										
SiO_2	44.7	44.7	43.5	43.2	44.6	43.1	43.2	43.7	43.3	43.7
Al_2O_3	22.6	24.2	23.4	24.6	24.8	23.7	24.0	23.9	24.2	24.2
MgO	28.2	25.3	26.2	26.3	26.0	27.1	27.9	27.4	26.9	26.5
CaO	3.9	4.9	5.4	5.1	5.1	5.0	5.7	4.6	5.5	5.3
K_2O	0.4	0.7	0.1	0.1	0.0	0.0	0.1	0.0	0.1	0.1
Total	99.7	99.8	98.5	99.4	100.5	98.9	100.8	99.7	99.9	99.7

Phase			**gr**							
P [GPa]			**5**							
T [°C]			**1500**							
ae-...			**50**							
wt%										
SiO_2	43.6	43.2	45.5	43.3	43.8	43.1	43.7	43.2	43.5	43.4
Al_2O_3	24.0	24.2	21.2	23.9	24.8	24.2	24.3	24.5	24.0	24.2
MgO	26.9	27.0	24.8	26.4	25.9	26.5	25.7	26.0	25.7	26.4
CaO	5.3	4.7	6.4	4.9	4.8	5.1	5.3	5.0	5.5	4.8
K_2O	0.1	0.0	0.8	0.3	0.2	0.0	0.0	0.1	0.1	0.0
Total	99.9	99.1	98.6	98.9	99.4	98.9	99.0	98.8	98.8	98.8

Phase								**gr**		
P [GPa]								**7**		
T [°C]								**1500**		
ae-...								**131**		
wt%										
SiO_2	45.2	44.7	43.7	43.9	44.0	43.8	44.2	44.7	45.2	45.5
Al_2O_3	24.4	23.6	23.8	24.8	24.1	24.0	23.7	23.0	22.7	22.6
MgO	25.7	25.9	26.1	26.2	26.6	26.1	25.4	26.5	27.3	26.0
CaO	4.7	5.4	5.5	4.8	5.3	4.8	5.7	4.1	5.8	4.7
K_2O	0.2	0.1	0.0	0.1	0.1	0.0	0.1	1.0	0.3	0.3
Total	100.2	99.6	99.1	99.8	100.1	98.7	99.1	99.3	101.2	99.1

Phase	**gr**	**gr**		**gr**				**gr**		
P [GPa]	**7**	**7**		**8**				**4**		
T [°C]	**1500**	**1100**		**1100**				**1150**		
ae-...	**131**	**155**		**156**				**151**		
wt%										
SiO_2	45.2	46.0	46.5	43.8	43.9	43.2	43.4	45.6	43.7	44.2
Al_2O_3	23.1	24.1	24.3	23.8	23.9	22.8	23.1	23.3	25.6	25.3
MgO	26.5	23.9	24.2	28.1	28.0	27.6	27.9	27.2	26.6	26.6
CaO	4.1	3.7	3.7	4.8	4.9	4.1	4.4	4.2	5.4	5.6
K_2O	0.3	1.3	1.2	0.5	0.4	0.8	0.7	0.0	0.1	0.1
Total	99.2	99.0	99.9	101.0	101.1	98.6	99.5	100.3	101.4	101.7

Phase									**gr**	
P [GPa]									**6**	
T [°C]									**1150**	
ae-...									**149**	
wt%										
SiO_2	43.4	43.8	43.5	43.9	44.3	44.1	43.4	43.1	44.5	44.7
Al_2O_3	24.4	24.5	24.3	24.9	24.7	24.8	24.6	25.0	23.9	23.3
MgO	25.4	25.5	25.4	25.4	25.7	25.8	26.2	26.2	26.0	26.6
CaO	5.5	5.7	5.7	5.7	5.7	5.7	5.4	6.1	4.6	6.6
K_2O	0.0	0.0	0.0	0.0	0.0	0.0	0.0	0.0	0.1	0.0
Total	98.7	99.5	98.9	99.9	100.5	100.5	99.6	100.4	99.1	101.1

Phase		**gr**								**gr**
P [GPa]		**7**								**4**
T [°C]		**1150**								**1200**
ae-...		**148**								**143**
wt%										
SiO_2	45.0	44.5	43.2	43.6	43.3	44.3	43.7	43.1	44.5	42.9
Al_2O_3	24.5	24.3	22.3	22.4	22.2	24.0	23.8	23.4	23.7	25.8
MgO	26.7	27.1	28.5	28.1	28.0	27.6	26.4	27.4	27.8	27.1
CaO	5.1	4.4	4.8	5.1	5.1	5.0	5.0	4.7	5.3	5.1
K_2O	0.1	0.1	0.5	0.9	0.9	0.3	0.2	0.3	0.2	0.1
Total	101.3	100.4	99.2	100.1	99.4	101.1	99.1	98.9	101.5	100.9

Phase					**gr**					
P [GPa]					**5**					
T [°C]					**1200**					
ae-...					**110**					
wt%										
SiO_2	42.8	42.3	43.1	44.2	44.3	45.5	44.6	44.7	43.8	45.0
Al_2O_3	25.3	25.2	25.8	24.5	24.4	25.1	24.2	24.0	24.2	25.3
MgO	25.2	25.1	25.2	25.8	25.5	24.7	25.7	24.9	25.8	26.3
CaO	6.1	6.5	6.3	6.6	5.1	4.9	5.1	5.6	4.6	4.3
K_2O	0.0	0.0	0.0	0.0	0.0	0.0	0.0	0.0	0.1	0.0
Total	99.3	99.0	100.4	101.1	99.3	100.3	99.6	99.2	98.6	100.8

Phase	**gr**			**gr**						
P [GPa]	**5**			**5**						
T [°C]	**1200**			**1300**						
ae-...	**110**			**59**						
wt%										
SiO_2	45.0	45.2	44.8	45.8	43.7	44.0	43.8	43.6	45.4	43.6
Al_2O_3	24.4	24.7	24.5	25.1	23.9	24.2	23.9	25.6	24.6	24.3
MgO	24.5	24.3	24.6	25.2	26.5	25.5	26.1	24.2	24.8	26.4
CaO	4.9	4.6	4.7	4.7	5.1	5.0	5.0	5.8	6.0	5.6
K_2O	0.2	0.0	0.0	0.1	0.1	0.1	0.0	0.1	0.1	0.0
Total	98.9	98.8	98.7	100.9	99.4	98.7	98.8	99.3	100.8	99.9

Phase				**gr**						
P [GPa]				**6**						
T [°C]				**1300**						
ae-...				**69**						
wt%										
SiO_2	43.4	44.1	44.0	45.6	44.8	44.7	46.0	45.9	45.3	43.8
Al_2O_3	24.5	24.9	25.0	23.5	22.6	23.8	23.0	22.3	22.1	23.4
MgO	26.1	25.9	26.2	25.2	26.9	27.4	26.5	27.5	26.9	26.1
CaO	6.0	5.5	5.5	5.3	5.1	5.5	5.6	5.2	6.5	5.7
K_2O	0.2	0.1	0.2	0.1	0.1	0.1	0.1	0.1	0.2	0.1
Total	100.2	100.6	100.8	99.7	99.6	101.5	101.1	100.9	101.0	99.0

Phase		**gr**				**gr**			**gr**	
P [GPa]		**7**				**8**			**5**	
T [°C]		**1300**				**1300**			**1400**	
ae-...		**145**				**71**			**52**	
wt%										
SiO_2	44.3	45.7	45.0	45.7	44.4	46.8	45.7	47.6	44.5	43.7
Al_2O_3	23.1	22.4	24.0	24.7	24.2	19.3	20.2	19.4	25.0	24.5
MgO	27.2	27.2	26.3	25.2	26.6	26.9	27.7	27.1	26.2	25.9
CaO	5.3	5.9	4.6	5.3	5.1	6.4	5.6	6.2	5.0	5.2
K_2O	0.1	0.1	0.4	0.1	0.1	0.4	0.5	0.7	0.0	0.2
Total	100.0	101.2	100.2	101.0	100.4	99.8	99.6	100.9	100.7	99.5

Phase										
P [GPa]										
T [°C]										
ae-...										
wt%										
SiO_2	45.4	45.5	44.3	44.1	44.8	45.5	44.8	44.2	44.2	44.0
Al_2O_3	24.7	24.5	24.1	24.1	24.5	22.2	23.8	24.2	24.1	23.7
MgO	26.2	25.6	25.7	25.9	26.5	26.9	27.0	25.9	25.1	26.1
CaO	4.7	4.7	5.7	5.8	5.4	5.4	5.5	5.8	5.9	5.9
K_2O	0.1	0.1	0.1	0.1	0.0	0.6	0.1	0.0	0.0	0.1
Total	101.0	100.4	99.8	99.9	101.3	100.6	101.1	100.2	99.3	99.7

Phase	**gr**				**gr**			**en**		
P [GPa]	**5**				**4**			**8**		
T [°C]	**1400**				**1500**			**1300**		
ae-...	**52**				**55**			**117**		
wt%										
SiO_2	44.8	45.2	44.5	44.7	43.5	44.4	44.5	60.9	59.9	59.9
Al_2O_3	24.3	24.6	24.3	24.2	22.5	24.9	24.4	0.5	0.6	0.3
MgO	26.0	26.3	25.3	25.4	27.5	26.7	25.9	37.6	37.8	38.2
CaO	5.7	5.1	4.9	4.9	5.5	4.8	5.1	1.4	1.0	0.8
K_2O	0.1	0.0	0.1	0.0	0.6	0.1	0.1	0.1	0.0	0.0
Total	100.9	101.2	99.1	99.2	99.5	100.7	100.0	100.4	99.3	99.4

Phase										**en**
P [GPa]										**4**
T [°C]										**1350**
ae-...										**140**
wt%										
SiO_2	60.4	58.9	59.7	59.5	59.1	59.1	60.7	61.0	59.5	58.5
Al_2O_3	1.2	1.1	0.4	1.0	0.5	0.9	0.3	0.4	0.4	1.2
MgO	38.2	38.1	38.4	38.6	39.8	39.5	37.8	38.8	38.2	37.1
CaO	1.1	1.0	0.8	1.3	0.6	0.8	0.5	0.7	0.8	1.5
K_2O	0.0	0.1	0.1	0.1	0.1	0.0	0.0	0.0	0.0	0.0
Total	100.8	99.2	99.4	100.3	100.2	100.3	99.3	100.8	98.9	98.1

Phase						**en**				
P [GPa]						**6**				
T [°C]						**1350**				
ae-...						**33**				
wt%										
SiO_2	58.2	59.1	60.5	59.5	60.2	57.6	58.4	58.7	58.4	59.1
Al_2O_3	1.4	1.1	1.4	1.1	1.0	0.6	0.6	1.3	0.9	0.7
MgO	37.2	39.4	37.5	37.6	37.1	39.4	39.1	36.7	37.9	39.5
CaO	1.3	1.3	1.5	1.3	1.1	0.9	0.9	1.6	1.0	0.8
K_2O	0.4	0.4	0.5	0.2	0.1	0.3	0.1	0.6	0.6	0.4
Total	98.5	101.2	101.3	99.6	99.5	98.7	99.1	99.0	98.8	100.4

Phase				**en**						
P [GPa]				**5**						
T [°C]				**1400**						
ae-...				**32**						
wt%										
SiO_2	59.7	58.2	59.5	58.2	60.1	58.7	58.5	58.6	59.0	59.6
Al_2O_3	1.0	0.7	0.6	1.3	1.3	0.8	1.1	1.0	1.1	1.1
MgO	36.5	39.0	37.0	37.4	37.3	38.4	37.7	37.9	37.4	37.6
CaO	1.0	1.2	1.4	1.3	1.4	0.8	1.5	1.4	1.5	1.4
K_2O	0.4	0.2	0.3	0.4	0.4	0.8	0.1	0.1	0.1	0.1
Total	98.6	99.3	98.8	98.6	100.6	99.5	98.8	98.9	99.1	99.7

Phase	**en**	**en**								
P [GPa]	**5**	**6**								
T [°C]	**1400**	**1400**								
ae-...	**32**	**30**								
wt%										
SiO_2	60.3	61.0	57.9	59.0	58.4	59.0	58.9	59.0	59.0	58.2
Al_2O_3	1.1	0.7	0.7	0.7	0.8	0.7	0.7	0.6	0.7	0.9
MgO	37.8	38.7	38.4	38.9	39.0	37.5	38.4	38.3	38.2	39.5
CaO	1.4	0.8	1.2	0.8	1.3	1.7	1.1	1.0	1.2	0.4
K_2O	0.1	0.1	0.1	0.1	0.3	0.2	0.2	0.1	0.1	0.1
Total	100.6	101.3	98.3	99.4	99.7	99.2	99.3	99.1	99.1	99.2

Phase	**en**									
P [GPa]	**7**									
T [°C]	**1400**									
ae-...	**111**									
wt%										
SiO_2	58.4	59.1	60.4	58.8	58.9	59.5	59.3	60.4	59.5	60.2
Al_2O_3	0.4	0.4	0.5	0.4	0.4	1.0	0.8	0.5	0.5	0.4
MgO	38.9	38.7	38.0	38.4	39.6	37.3	40.0	38.7	39.5	37.8
CaO	1.0	0.9	1.0	1.0	1.0	1.3	1.1	1.0	1.3	1.1
K_2O	0.0	0.0	0.0	0.0	0.1	0.2	0.1	0.0	0.1	0.0
Total	98.7	99.2	99.9	98.7	100.0	99.3	101.3	100.6	100.8	99.6

Phase						**en**				
P [GPa]						**8**				
T [°C]						**1400**				
ae-...						**120**				
wt%										
SiO_2	59.1	60.4	60.1	59.5	59.4	59.0	58.3	57.3	58.6	59.1
Al_2O_3	0.4	0.4	0.5	0.5	0.5	0.5	1.0	1.1	1.0	0.3
MgO	38.5	37.7	38.2	38.9	38.6	38.1	37.7	39.3	37.7	38.7
CaO	1.1	0.9	1.0	1.1	1.1	1.0	1.3	1.1	1.1	0.3
K_2O	0.0	0.0	0.0	0.0	0.0	0.3	0.4	0.4	0.7	0.2
Total	99.1	99.5	99.8	100.0	99.5	99.0	98.6	99.2	99.1	98.6

Phase						**en**				
P [GPa]						**5**				
T [°C]						**1450**				
ae-...						**65**				
wt%										
SiO_2	59.3	60.3	58.9	57.3	60.3	59.0	58.9	59.3	58.3	59.9
Al_2O_3	0.5	0.8	0.6	1.7	0.5	1.2	1.7	1.2	1.0	1.0
MgO	38.0	36.9	38.2	38.2	37.5	38.9	38.7	39.0	37.8	38.4
CaO	0.8	1.0	1.2	1.0	1.0	1.6	1.6	1.8	1.4	1.5
K_2O	0.2	0.4	0.3	0.4	0.5	0.1	0.3	0.0	0.2	0.1
Total	98.9	99.4	99.1	98.7	99.8	100.8	101.1	101.4	98.6	100.9

Phase	**en**						**en**			
P [GPa]	**5**						**5**			
T [°C]	**1450**						**1500**			
ae-...	**65**						**50**			
wt%										
SiO_2	59.2	58.1	59.5	58.6	58.1	59.1	58.5	58.7	58.8	58.3
Al_2O_3	1.1	1.1	1.0	1.0	1.5	1.1	1.5	1.4	1.4	1.5
MgO	36.9	38.9	38.1	39.0	38.5	38.4	38.1	37.6	37.6	38.7
CaO	1.6	1.5	1.4	1.6	1.7	1.5	1.9	1.7	1.7	1.8
K_2O	0.0	0.0	0.1	0.1	0.1	0.1	0.3	0.1	0.1	0.0
Total	98.7	99.6	100.1	100.3	99.8	100.1	100.3	99.5	99.7	100.3

Phase										**en**
P [GPa]										**7**
T [°C]										**1500**
ae-...										**131**
wt%										
SiO_2	57.7	58.7	58.2	57.5	57.6	57.9	58.3	58.8	57.3	59.3
Al_2O_3	1.4	1.5	1.5	1.5	1.4	1.4	1.4	1.4	1.5	1.6
MgO	38.5	38.8	37.2	37.5	37.4	38.2	37.8	37.4	38.5	37.0
CaO	1.8	1.9	1.9	1.9	1.7	1.6	1.7	1.8	1.9	1.3
K_2O	0.2	0.0	0.0	0.0	0.3	0.0	0.1	0.0	0.1	0.5
Total	99.7	100.9	98.8	98.4	98.4	99.1	99.3	99.5	99.3	99.8

Phase										
P [GPa]										
T [°C]										
ae-...										
wt%										
SiO_2	60.6	60.1	58.6	58.9	60.0	58.0	58.1	59.1	58.2	58.5
Al_2O_3	1.0	0.6	0.6	0.6	1.0	0.6	0.6	0.7	0.6	0.6
MgO	38.0	38.7	38.5	37.9	37.1	38.1	38.9	38.2	38.7	38.0
CaO	1.2	1.4	1.3	1.6	1.3	1.3	1.3	1.4	1.3	1.4
K_2O	0.3	0.2	0.2	0.2	0.7	0.3	0.6	0.2	0.2	0.2
Total	101.1	101.0	99.2	99.3	100.1	98.4	99.5	99.5	99.0	98.7

Phase							**en**			
P [GPa]							**7**			
T [°C]							**1100**			
ae-...							**155**			
wt%										
SiO_2	58.4	58.1	58.7	58.9	60.8	59.0	59.7	59.2	59.4	59.2
Al_2O_3	0.6	0.6	0.6	0.4	0.7	0.6	0.3	0.3	0.3	0.2
MgO	38.2	38.0	38.3	38.5	37.7	37.7	38.1	39.8	39.3	39.7
CaO	1.4	1.7	1.5	0.9	1.7	1.3	0.6	0.7	0.6	0.6
K_2O	0.5	0.2	0.2	0.2	0.3	0.2	0.0	0.0	0.0	0.0
Total	99.0	98.6	99.3	98.8	101.1	98.8	98.6	100.0	99.6	99.7

Phase	**en**			**en**						**en**
P [GPa]	**7**			**8**						**4**
T [°C]	**1100**			**1100**						**1150**
ae-...	**155**			**156**						**151**
wt%										
SiO_2	59.8	59.4	58.5	60.0	59.6	58.1	58.9	58.8	58.3	57.4
Al_2O_3	0.4	1.7	0.3	0.3	0.2	0.6	0.3	0.4	0.3	0.7
MgO	38.3	39.5	39.2	39.0	39.5	40.0	39.4	39.3	39.8	39.8
CaO	0.7	0.8	1.2	0.3	0.2	0.7	0.6	0.1	0.3	0.8
K_2O	0.0	0.0	0.0	0.0	0.0	0.0	0.0	0.0	0.0	0.2
Total	99.2	101.5	99.2	99.7	99.6	99.3	99.2	98.6	98.8	98.9

Phase										
P [GPa]										
T [°C]										
ae-...										
wt%										
SiO_2	57.5	57.5	58.7	58.3	57.9	58.0	59.4	59.2	59.1	58.6
Al_2O_3	0.7	0.6	0.6	0.6	0.7	0.7	0.6	0.6	0.6	0.6
MgO	40.2	39.9	39.7	39.3	40.0	39.3	39.3	40.3	38.9	38.8
CaO	0.7	0.6	0.7	0.7	0.6	0.6	0.7	0.7	0.6	0.6
K_2O	0.2	0.1	0.1	0.1	0.1	0.0	0.1	0.1	0.1	0.1
Total	99.3	98.8	99.8	98.9	99.2	98.6	100.2	100.8	99.3	98.8

Phase			**en**							
P [GPa]			**6**							
T [°C]			**1150**							
ae-...			**149**							
wt%										
SiO_2	58.6	58.8	58.9	60.0	59.5	58.8	60.2	58.8	59.2	59.0
Al_2O_3	0.6	0.7	0.3	0.5	0.5	0.3	0.3	0.3	0.4	0.3
MgO	40.6	39.1	40.2	38.3	37.9	39.6	39.0	39.3	39.9	38.9
CaO	0.7	0.7	0.7	0.7	0.6	0.6	0.7	0.6	0.7	0.7
K_2O	0.1	0.1	0.1	0.1	0.1	0.0	0.1	0.0	0.0	0.0
Total	100.5	99.3	100.2	99.6	98.6	99.3	100.2	99.0	100.2	99.0

Phase		**en**								
P [GPa]		**7**								
T [°C]		**1150**								
ae-...		**148**								
wt%										
SiO_2	59.9	58.7	59.1	59.8	59.7	59.1	60.4	59.0	58.9	59.1
Al_2O_3	0.3	0.3	0.4	0.3	0.3	0.3	0.4	0.6	0.7	0.3
MgO	40.2	38.4	38.3	38.7	38.8	39.2	38.5	38.7	38.3	38.4
CaO	0.6	0.8	0.7	0.7	0.8	0.6	0.7	0.7	0.8	0.8
K_2O	0.0	0.6	0.2	0.2	0.1	0.1	0.3	0.2	0.2	0.1
Total	101.0	98.8	98.8	99.6	99.8	99.3	100.1	99.1	98.8	98.8

Phase	**en**		**en**				**en**			
P [GPa]	**7**		**4**				**5**			
T [°C]	**1150**		**1200**				**1200**			
ae-...	**148**		**143**				**110**			
wt%										
SiO_2	59.6	58.7	58.2	58.4	59.1	59.4	59.7	59.2	60.2	59.6
Al_2O_3	0.3	0.6	0.8	0.8	0.8	0.8	0.5	0.5	0.5	0.5
MgO	38.8	38.5	38.9	40.3	39.8	40.0	38.6	38.3	38.5	39.1
CaO	0.7	0.7	0.9	1.2	1.0	0.9	0.6	0.7	0.6	0.6
K_2O	0.1	0.1	0.1	0.1	0.0	0.0	0.1	0.1	0.0	0.0
Total	99.5	98.6	98.9	100.7	100.7	101.1	99.5	98.7	99.7	99.8

Phase								**en**		
P [GPa]								**5**		
T [°C]								**1300**		
ae-...								**59**		
wt%										
SiO_2	59.0	59.3	58.4	58.6	58.8	59.3	59.9	60.1	60.0	59.0
Al_2O_3	0.6	0.5	0.6	0.5	0.5	0.6	0.5	1.1	1.0	1.1
MgO	39.2	38.6	38.9	39.7	39.6	39.7	38.4	37.5	37.2	38.1
CaO	0.6	0.6	0.6	0.6	0.7	0.7	0.7	1.3	1.6	1.6
K_2O	0.0	0.2	0.1	0.0	0.1	0.1	0.1	0.0	0.0	0.0
Total	99.4	99.2	98.7	99.4	99.7	100.3	99.6	100.1	99.8	99.9

Phase										
P [GPa]										
T [°C]										
ae-...										
wt%										
SiO_2	58.7	60.0	60.2	58.8	59.1	58.6	60.2	59.0	59.3	60.0
Al_2O_3	1.0	1.1	1.0	1.0	1.0	1.0	0.7	1.1	0.7	0.9
MgO	38.0	37.5	37.3	38.1	38.1	39.1	38.2	38.4	38.7	37.5
CaO	1.5	1.6	1.5	1.6	1.3	1.5	1.2	1.2	1.4	1.2
K_2O	0.1	0.1	0.1	0.0	0.0	0.1	0.0	0.0	0.0	0.0
Total	99.3	100.3	100.1	99.5	99.7	100.3	100.4	99.6	100.1	99.5

Phase								**en**		
P [GPa]								**6**		
T [°C]								**1300**		
ae-...								**69**		
wt%										
SiO_2	59.7	60.3	61.0	58.2	59.2	59.6	59.7	57.8	59.1	57.7
Al_2O_3	0.7	0.7	0.7	0.8	0.7	0.6	0.7	0.7	0.5	0.4
MgO	37.9	38.0	37.1	39.0	39.5	38.0	39.3	39.9	39.6	40.5
CaO	1.1	1.1	1.2	1.3	1.3	1.1	1.2	1.1	1.0	1.0
K_2O	0.0	0.0	0.0	0.0	0.0	0.0	0.0	0.0	0.0	0.0
Total	99.4	100.2	100.0	99.2	100.7	99.3	100.9	99.5	100.2	99.7

Phase	**en**				**en**				**en**	
P [GPa]	**6**				**7**				**8**	
T [°C]	**1300**				**1300**				**1300**	
ae-...	**69**				**145**				**71**	
wt%										
SiO_2	57.2	57.4	58.3	58.6	59.5	59.1	58.0	58.8	56.8	58.3
Al_2O_3	0.8	0.5	0.8	0.5	0.5	0.4	0.6	0.4	1.0	0.6
MgO	39.8	41.5	41.0	39.8	38.2	39.4	38.8	38.9	37.9	37.5
CaO	1.0	1.1	0.9	1.0	1.0	1.0	1.6	0.9	2.6	1.7
K_2O	0.4	0.0	0.0	0.0	0.1	0.0	0.0	0.0	0.2	0.5
Total	99.1	100.5	101.0	99.9	99.4	99.9	99.0	99.0	98.5	98.6

Phase			**en**							
P [GPa]			**5**							
T [°C]			**1400**							
ae-...			**52**							
wt%										
SiO_2	57.5	57.5	57.4	57.7	57.4	57.9	58.9	57.9	57.4	57.4
Al_2O_3	1.2	1.0	1.4	0.9	1.3	1.1	1.2	1.1	1.1	1.2
MgO	36.8	38.4	39.0	39.4	39.5	39.0	38.5	38.6	39.3	38.7
CaO	2.7	1.8	1.3	0.7	1.4	1.3	1.5	1.1	1.4	1.4
K_2O	0.5	0.4	0.0	0.0	0.4	0.0	0.1	0.1	0.0	0.0
Total	98.6	99.0	99.2	98.7	99.9	99.3	100.1	98.9	99.2	98.6

Phase						**en**				
P [GPa]						**4**				
T [°C]						**1500**				
ae-...						**55**				
wt%										
SiO_2	59.0	58.2	57.1	57.1	57.8	57.8	57.1	57.5	57.8	56.8
Al_2O_3	1.1	0.9	1.1	1.1	1.4	1.8	1.9	1.8	1.9	1.8
MgO	37.2	39.7	39.2	39.4	39.4	37.3	38.0	38.2	36.8	38.3
CaO	1.3	1.2	1.3	1.5	1.8	2.0	1.9	2.1	1.9	2.0
K_2O	0.0	0.0	0.0	0.0	0.0	0.1	0.0	0.5	0.3	0.1
Total	98.6	100.0	98.8	99.0	100.3	98.9	98.9	100.1	98.8	99.0

Phase	**en**									
P [GPa]	**4**									
T [°C]	**1600**									
ae-...	**70**									
wt%										
SiO_2	57.1	56.4	57.0	57.0	57.1	57.3	55.9	57.0	57.0	57.8
Al_2O_3	2.5	2.3	2.3	2.4	2.4	2.4	2.3	2.6	2.4	2.5
MgO	38.4	37.2	37.7	37.1	37.2	38.0	38.1	37.2	38.0	37.6
CaO	2.5	2.5	2.6	2.4	2.4	2.4	2.4	2.5	2.4	2.4
K_2O	0.3	0.2	0.1	0.3	0.1	0.1	0.3	0.3	0.2	0.3
Total	100.8	98.7	99.7	99.2	99.1	100.2	99.0	99.5	100.1	100.5

Phase	**en**				**di**					
P [GPa]	**4**				**8**					
T [°C]	**1600**				**1300**					
ae-...	**70**				**117**					
wt%										
SiO_2	57.7	56.7	56.9	58.1	56.6	55.5	56.0	55.5	55.9	56.1
Al_2O_3	2.4	2.3	2.5	2.4	1.0	0.8	0.9	0.9	0.9	1.0
MgO	36.9	37.2	38.6	38.1	20.7	21.9	20.5	20.4	20.7	20.5
CaO	2.5	2.5	2.4	2.4	21.8	20.4	21.8	21.3	21.4	21.9
K_2O	0.2	0.3	0.7	0.1	0.7	0.7	0.8	0.7	0.6	0.7
Total	99.7	99.0	101.1	101.0	100.8	99.3	99.9	98.7	99.5	100.1

Phase										**di**
P [GPa]										**4**
T [°C]										**1350**
ae-...										**140**
wt%										
SiO_2	56.1	56.8	56.3	55.9	55.9	56.2	56.0	55.5	55.5	55.6
Al_2O_3	1.0	0.9	0.9	0.9	1.0	0.9	0.8	1.0	0.8	1.5
MgO	19.6	21.2	21.3	20.8	21.5	21.0	22.1	21.0	20.8	20.1
CaO	22.2	21.3	20.5	20.6	20.8	21.0	21.1	21.0	21.1	20.4
K_2O	0.8	0.7	0.9	0.8	0.7	0.8	0.7	0.8	0.7	1.1
Total	99.6	100.9	99.9	99.0	100.0	99.9	100.6	99.2	98.9	98.7

Phase				**di**						
P [GPa]				**6**						
T [°C]				**1350**						
ae-...				**33**						
wt%										
SiO_2	55.3	55.7	56.3	54.5	53.6	56.0	54.0	55.1	55.4	56.2
Al_2O_3	1.5	1.4	1.5	0.6	0.8	0.9	0.7	0.7	0.9	1.0
MgO	21.0	21.0	23.7	21.7	22.1	21.2	22.6	21.0	21.2	19.8
CaO	20.5	20.4	18.0	20.9	21.4	21.2	21.0	22.3	21.5	21.0
K_2O	1.0	0.7	0.8	0.3	0.5	0.5	0.4	0.4	0.5	0.7
Total	99.4	99.2	100.3	98.0	98.4	99.8	98.8	99.5	99.4	98.6

Phase								**di**		
P [GPa]								**5**		
T [°C]								**1400**		
ae-...								**32**		
wt%										
SiO_2	55.5	56.6	55.3	52.6	54.2	56.3	54.8	54.9	54.0	54.5
Al_2O_3	1.4	0.9	0.9	4.3	0.9	0.9	1.3	1.2	1.4	1.3
MgO	21.1	20.5	20.9	21.8	20.3	20.4	20.8	22.9	21.9	21.8
CaO	20.5	20.9	22.1	20.1	22.0	22.0	21.5	20.5	20.7	20.6
K_2O	1.0	0.5	0.6	0.6	0.6	0.5	0.8	0.9	1.2	0.9
Total	99.6	99.4	99.8	99.4	98.1	100.1	99.2	100.3	99.2	99.1

Phase	**di**							**di**		
P [GPa]	**5**							**6**		
T [°C]	**1400**							**1400**		
ae-...	**32**							**30**		
wt%										
SiO_2	55.4	53.9	54.0	54.7	55.8	55.7	56.1	56.4	55.7	56.3
Al_2O_3	1.3	1.4	1.2	1.4	1.4	1.3	1.4	1.0	1.0	0.6
MgO	21.3	21.8	22.8	21.5	22.1	22.1	22.5	21.8	21.6	20.5
CaO	20.5	20.4	20.1	20.3	19.8	19.8	19.6	20.7	20.0	22.2
K_2O	1.3	1.4	1.2	1.3	0.5	0.7	0.6	0.6	0.5	0.3
Total	99.8	98.8	99.3	99.1	99.6	99.6	100.2	100.4	98.9	99.9
Phase										
P [GPa]										
T [°C]										
ae-...										
wt%										
SiO_2	56.0	54.7	54.9	55.8	55.6	55.9	55.2	55.5	56.3	54.9
Al_2O_3	0.9	0.7	1.1	0.9	1.3	0.9	4.0	1.2	1.0	1.7
MgO	20.9	21.3	20.7	21.0	21.8	21.2	18.3	21.0	19.7	21.2
CaO	21.3	21.9	21.8	21.7	21.9	21.9	22.6	20.9	21.1	21.5
K_2O	0.5	0.3	0.6	0.6	0.4	0.4	0.5	0.6	0.5	0.5
Total	99.5	98.9	99.1	100.0	101.1	100.4	100.5	99.2	98.7	99.8
Phase	**di**									
P [GPa]	**7**									
T [°C]	**1400**									
ae-...	**111**									
wt%										
SiO_2	55.2	55.3	55.6	55.3	55.6	55.9	54.3	54.9	55.2	55.9
Al_2O_3	1.5	2.1	1.4	1.3	1.7	1.5	1.5	1.4	1.9	1.4
MgO	21.6	21.7	20.4	21.3	20.2	21.0	21.0	22.0	22.3	21.6
CaO	20.2	20.2	20.8	21.2	20.4	20.7	20.2	20.0	20.6	20.2
K_2O	1.4	0.8	1.1	0.9	1.2	1.1	1.7	1.0	1.1	1.0
Total	99.9	100.1	99.4	99.9	99.2	100.2	98.7	99.3	101.1	100.0
Phase	**di**									
P [GPa]	**8**									
T [°C]	**1400**									
ae-...	**120**									
wt%										
SiO_2	55.5	54.4	55.7	55.5	55.8	54.2	55.9	55.5	56.5	55.5
Al_2O_3	1.4	1.2	1.4	1.4	1.4	1.3	1.2	1.3	1.4	1.3
MgO	21.3	22.8	21.2	22.3	21.4	22.6	22.5	21.2	22.2	21.9
CaO	19.5	19.7	19.3	19.0	19.8	19.1	18.4	19.0	19.7	18.7
K_2O	1.7	1.3	1.4	1.3	1.3	1.4	1.4	1.5	1.3	1.3
Total	99.4	99.4	99.1	99.4	99.7	98.7	99.3	98.5	101.0	98.6

Phase	**di**									
P [GPa]	**5**									
T [°C]	**1450**									
ae-...	**65**									
wt%										
SiO_2	55.0	55.4	54.9	56.4	54.3	56.7	55.3	55.4	54.9	57.0
Al_2O_3	1.3	1.4	1.3	1.4	1.2	1.4	1.9	1.4	1.5	1.3
MgO	21.3	21.3	22.2	23.7	23.8	21.1	22.5	23.3	22.8	21.7
CaO	19.7	20.0	19.7	18.2	19.1	19.0	17.6	19.1	18.9	19.1
K_2O	1.1	1.2	0.9	0.7	0.5	0.6	1.5	1.1	0.8	0.6
Total	98.4	99.4	99.1	100.5	98.9	98.7	98.7	100.2	98.9	99.7
Phase					**di**		**di**			
P [GPa]					**6**		**5**			
T [°C]					**1450**		**1500**			
ae-...					**146**		**50**			
wt%										
SiO_2	56.7	56.6	56.9	56.5	56.9	53.3	55.5	56.4	55.8	55.8
Al_2O_3	1.4	1.5	1.8	1.3	1.3	1.0	1.9	1.7	1.5	1.9
MgO	21.8	22.2	22.5	22.7	21.8	23.8	22.9	22.9	22.5	24.3
CaO	19.1	18.5	18.8	18.3	19.4	19.4	17.5	18.6	19.2	18.4
K_2O	0.6	0.8	0.6	0.5	1.2	1.4	1.0	0.7	0.5	0.5
Total	99.5	99.7	100.6	99.4	100.6	99.0	98.7	100.3	99.5	100.7
Phase										
P [GPa]										
T [°C]										
ae-...										
wt%										
SiO_2	55.3	54.5	55.1	54.6	54.7	54.9	55.0	55.1	56.1	54.8
Al_2O_3	1.5	1.7	1.5	1.5	1.6	1.4	1.5	1.6	1.5	1.5
MgO	23.2	24.3	24.7	24.5	24.1	23.6	23.4	23.0	23.6	24.1
CaO	19.3	17.9	17.7	18.5	18.3	18.5	18.2	18.5	18.3	18.2
K_2O	0.5	0.7	0.5	0.4	0.4	0.4	0.5	0.5	0.6	0.4
Total	99.7	99.0	99.5	99.4	99.1	98.9	98.6	98.5	100.1	99.1
Phase					**di**					
P [GPa]					**7**					
T [°C]					**1500**					
ae-...					**131**					
wt%										
SiO_2	55.8	55.5	55.2	56.5	54.7	57.0	56.8	56.1	55.1	56.8
Al_2O_3	1.6	1.5	1.4	1.6	1.8	1.5	1.3	1.4	1.6	1.7
MgO	22.9	23.1	23.3	23.2	23.5	23.3	21.9	21.9	22.2	21.1
CaO	18.1	18.6	18.4	17.9	17.0	16.4	19.9	19.6	18.2	18.4
K_2O	0.5	0.5	0.5	0.5	1.7	1.7	1.1	1.2	1.5	1.4
Total	98.9	99.2	98.8	99.7	98.7	99.8	100.9	100.2	98.5	99.4

Phase	**di**				**di**					
P [GPa]	**7**				**7**					
T [°C]	**1500**				**1100**					
ae-...	**131**				**155**					
wt%										
SiO_2	56.4	56.2	54.9	56.0	55.7	56.2	55.4	56.9	56.3	54.9
Al_2O_3	1.6	1.2	1.2	1.6	1.6	1.3	1.0	1.1	0.9	1.2
MgO	22.4	22.3	22.5	21.1	20.4	19.9	20.4	19.9	20.9	20.4
CaO	18.0	18.3	19.0	18.8	22.0	22.7	22.1	21.5	23.0	22.3
K_2O	1.4	1.5	1.2	1.6	1.2	0.9	0.6	0.9	0.5	0.7
Total	99.8	99.4	98.7	99.2	100.8	101.0	99.6	100.3	101.6	99.5

Phase			**di**			**di**				
P [GPa]			**8**			**4**				
T [°C]			**1100**			**1150**				
ae-...			**156**			**151**				
wt%										
SiO_2	55.5	55.0	55.2	55.0	55.2	53.4	53.3	54.4	53.7	52.5
Al_2O_3	0.9	1.0	0.9	0.7	1.1	1.5	1.5	1.4	0.8	0.8
MgO	19.6	19.5	21.2	19.2	20.5	23.0	22.9	22.5	21.5	23.0
CaO	23.1	22.8	21.4	22.9	22.2	21.7	21.5	22.2	23.2	23.0
K_2O	0.6	0.6	0.5	0.6	0.5	0.9	0.9	0.8	0.5	0.3
Total	99.7	98.9	99.1	98.4	99.6	100.5	100.2	101.3	99.8	99.5

Phase						**di**				
P [GPa]						**6**				
T [°C]						**1150**				
ae-...						**149**				
wt%										
SiO_2	54.1	54.0	53.0	53.3	54.7	55.1	55.3	56.1	55.6	55.9
Al_2O_3	0.7	0.7	0.7	0.7	0.8	0.7	0.7	1.1	0.6	0.6
MgO	22.7	22.9	22.6	22.7	21.1	21.1	22.2	20.4	22.0	20.3
CaO	23.5	23.3	22.7	22.6	22.7	21.9	21.2	22.5	21.6	22.2
K_2O	0.3	0.2	0.2	0.2	0.2	0.5	0.6	0.8	0.5	0.4
Total	101.2	101.2	99.2	99.5	99.5	99.3	100.0	100.9	100.3	99.4

Phase					**di**					
P [GPa]					**7**					
T [°C]					**1150**					
ae-...					**148**					
wt%										
SiO_2	56.0	53.5	54.3	55.0	56.4	57.1	55.3	55.3	55.4	55.2
Al_2O_3	0.6	0.8	0.8	0.7	0.7	0.7	0.7	0.9	0.7	0.7
MgO	20.2	22.1	22.8	22.5	21.8	21.1	20.5	23.0	23.2	21.5
CaO	22.5	22.6	22.2	21.5	21.6	21.6	22.0	19.7	19.7	22.1
K_2O	0.3	0.6	0.6	0.4	0.5	0.5	0.9	0.5	0.6	0.6
Total	99.6	99.7	100.8	100.0	100.9	101.0	99.4	99.4	99.6	100.0

Phase	**di**	**di**								
P [GPa]	**7**	**4**								
T [°C]	**1150**	**1200**								
ae-...	**148**	**143**								
wt%										
SiO_2	55.1	57.8	56.7	56.9	57.3	57.5	57.0	57.8	58.0	57.8
Al_2O_3	0.7	1.0	0.9	1.0	1.2	1.4	1.1	1.1	1.0	1.0
MgO	21.2	20.0	19.6	20.0	20.8	19.2	19.8	19.4	19.8	19.8
CaO	21.9	21.6	21.8	21.9	21.1	21.2	21.3	21.2	21.0	21.4
K_2O	0.5	0.3	0.3	0.3	0.4	0.4	0.3	0.4	0.3	0.3
Total	99.4	100.7	99.3	100.1	100.9	99.7	99.4	99.8	100.1	100.3

Phase										**di**
P [GPa]										**5**
T [°C]										**1200**
ae-...										**110**
wt%										
SiO_2	56.9	56.7	55.7	56.0	56.6	57.0	56.3	56.2	55.0	55.4
Al_2O_3	0.9	1.0	0.8	0.8	0.9	1.2	1.2	1.3	1.0	0.4
MgO	19.9	20.0	20.1	22.0	21.1	19.9	19.1	19.3	21.2	19.7
CaO	22.6	22.6	22.4	21.1	22.1	22.0	22.6	22.4	22.5	23.5
K_2O	0.3	0.3	0.2	0.3	0.3	0.4	0.4	0.4	0.3	0.1
Total	100.5	100.4	99.2	100.2	101.0	100.5	99.6	99.6	100.0	99.2

Phase							**di**			
P [GPa]							**5**			
T [°C]							**1300**			
ae-...							**59**			
wt%										
SiO_2	54.3	56.7	56.2	56.4	54.9	56.6	55.1	53.7	54.3	55.5
Al_2O_3	0.4	0.5	0.4	0.4	0.5	0.4	1.7	1.3	1.2	1.4
MgO	20.5	20.0	19.5	19.5	21.1	19.4	23.0	23.8	23.9	21.8
CaO	23.6	22.1	22.2	22.3	22.2	22.2	19.2	19.6	18.9	19.4
K_2O	0.1	0.2	0.1	0.2	0.1	0.1	0.7	0.8	0.5	0.6
Total	98.8	99.5	98.5	98.8	98.8	98.7	99.7	99.1	98.8	98.6

Phase							**di**			
P [GPa]							**6**			
T [°C]							**1300**			
ae-...							**69**			
wt%										
SiO_2	55.5	55.9	56.2	54.8	52.2	56.3	56.3	56.3	55.4	56.3
Al_2O_3	1.4	1.1	1.3	1.2	2.0	1.4	0.9	0.9	0.9	0.9
MgO	23.1	21.9	22.8	22.0	22.5	22.7	21.6	21.8	21.5	20.9
CaO	19.2	20.4	19.2	19.4	21.0	19.9	21.5	21.5	21.2	21.6
K_2O	0.6	0.5	0.6	0.6	0.4	0.4	0.6	0.6	0.7	0.6
Total	99.7	99.7	100.0	98.0	98.1	100.6	100.9	101.1	99.7	100.3

Phase	**di**									**di**
P [GPa]	**6**									**7**
T [°C]	**1300**									**1300**
ae-...	**69**									**145**
wt%										
SiO_2	56.4	54.8	57.8	55.4	55.8	55.6	56.4	55.5	55.3	55.9
Al_2O_3	1.0	0.8	1.0	0.9	0.8	0.8	0.8	0.9	0.8	1.4
MgO	21.3	21.1	20.2	21.1	22.6	22.9	20.9	21.5	22.0	20.0
CaO	21.4	21.2	21.3	21.5	20.1	21.0	20.9	21.0	20.4	21.2
K_2O	0.5	0.6	0.6	0.6	0.4	0.5	0.5	0.6	0.6	0.9
Total	100.5	98.5	100.8	99.4	99.6	100.8	99.5	99.4	99.0	99.3

Phase							**di**			
P [GPa]							**8**			
T [°C]							**1300**			
ae-...							**71**			
wt%										
SiO_2	55.2	56.1	55.9	57.0	57.7	55.9	56.1	55.6	57.2	55.4
Al_2O_3	1.1	1.3	1.7	1.4	1.3	1.7	0.9	0.9	1.2	1.3
MgO	22.1	20.7	19.2	20.6	19.3	21.8	22.4	22.3	20.9	22.2
CaO	21.0	21.6	21.6	20.6	21.7	19.9	19.5	19.3	19.7	19.7
K_2O	0.7	0.9	1.4	0.7	0.8	1.4	0.8	0.9	0.9	0.9
Total	100.1	100.6	99.7	100.2	100.9	100.7	99.8	99.0	99.9	99.5

Phase										
P [GPa]										
T [°C]										
ae-...										
wt%										
SiO_2	55.7	57.1	56.5	56.5	56.6	56.1	55.1	56.1	57.2	56.1
Al_2O_3	1.0	1.5	1.0	0.9	1.0	1.0	1.3	0.9	0.9	0.8
MgO	22.1	22.8	22.2	24.2	22.7	22.4	21.8	22.9	23.4	23.1
CaO	19.7	18.5	19.3	18.3	19.1	19.7	19.5	19.1	19.1	19.4
K_2O	1.0	0.9	0.8	0.9	0.8	1.0	1.1	1.0	0.8	1.0
Total	99.5	100.8	99.9	100.9	100.1	100.3	98.7	100.0	101.4	100.4

Phase	**di**									
P [GPa]	**5**									
T [°C]	**1400**									
ae-...	**52**									
wt%										
SiO_2	54.8	55.2	55.9	56.4	56.9	54.6	54.6	54.9	55.1	55.0
Al_2O_3	1.1	1.1	1.0	1.1	1.1	1.1	1.0	1.0	2.6	2.5
MgO	22.8	23.6	22.1	22.5	23.7	22.2	22.6	22.4	22.0	22.5
CaO	20.6	19.8	20.2	20.8	18.9	20.9	20.5	20.7	18.4	18.4
K_2O	0.2	0.2	0.2	0.2	0.2	0.3	0.2	0.2	0.4	0.4
Total	99.5	99.8	99.5	100.9	100.7	99.1	98.9	99.2	98.6	98.8

Phase	**di**		**di**	**di**						**kr**
P [GPa]	**5**		**4**	**4**						**8**
T [°C]	**1400**		**1500**	**1600**						**1300**
ae-...	**52**		**55**	**70**						**117**
wt%										
SiO_2	55.2	55.0	53.7	56.3	55.3	55.3	55.6	55.2	56.1	54.6
Al_2O_3	2.1	1.7	2.0	2.4	2.2	2.4	2.4	2.4	2.8	1.9
MgO	21.8	21.9	24.8	25.6	25.0	26.8	27.1	26.3	24.8	22.8
CaO	19.0	19.7	17.6	16.3	17.1	14.9	14.9	15.4	14.8	8.4
K_2O	0.6	0.5	0.6	0.4	0.4	0.4	0.3	0.3	0.5	9.0
Total	98.6	98.8	98.7	100.9	100.0	99.9	100.2	99.6	99.0	96.6
Phase										
P [GPa]										
T [°C]										
ae-...										
wt%										
SiO_2	55.1	53.9	55.1	54.7	54.5	54.7	54.7	53.3	54.1	53.3
Al_2O_3	2.0	1.9	1.9	1.7	1.9	2.2	2.0	1.9	1.8	2.1
MgO	22.9	24.2	22.3	22.7	22.6	23.3	23.1	21.9	23.0	22.0
CaO	8.0	8.0	8.6	7.5	8.0	7.7	7.5	8.2	8.5	7.5
K_2O	9.1	9.3	8.9	9.3	9.2	9.4	9.8	9.4	9.1	9.8
Total	97.1	97.2	96.7	95.8	96.1	97.3	97.1	94.7	96.5	94.6
Phase								**kr**		
P [GPa]								**7**		
T [°C]								**1400**		
ae-...								**139**		
wt%										
SiO_2	56.4	57.0	54.6	53.6	54.6	54.6	54.8	54.8	56.0	54.9
Al_2O_3	1.9	2.2	2.0	1.8	1.9	1.7	1.9	2.7	2.4	2.7
MgO	22.0	21.9	22.5	22.9	23.5	22.5	22.2	22.7	23.5	22.8
CaO	7.6	7.8	7.8	7.9	7.4	8.9	7.8	8.9	7.1	7.1
K_2O	9.7	9.9	9.7	9.5	9.7	8.8	9.3	9.0	10.4	10.1
Total	97.6	98.7	96.6	95.7	97.0	96.5	96.0	98.1	99.4	97.5
Phase										**kr**
P [GPa]										**7**
T [°C]										**1100**
ae-...										**155**
wt%										
SiO_2	54.6	57.0	53.8	54.7	57.4	54.3	55.6	55.5	56.1	53.7
Al_2O_3	2.2	3.0	3.7	3.1	3.3	2.2	2.4	2.5	2.4	1.4
MgO	24.4	19.1	23.1	21.5	19.6	23.8	22.9	23.5	23.0	23.1
CaO	7.2	7.2	7.0	7.0	7.0	7.1	7.1	7.1	7.2	7.5
K_2O	10.3	10.2	9.9	11.1	10.2	10.5	10.3	10.3	10.4	9.9
Total	98.7	96.5	97.5	97.3	97.5	97.7	98.3	98.9	99.2	95.6

Phase	**kr**									
P [GPa]	**7**									
T [°C]	**1100**									
ae-...	**155**									
wt%										
SiO_2	54.6	54.1	55.7	56.1	55.6	54.2	54.1	55.8	55.1	53.3
Al_2O_3	1.5	1.8	1.7	1.4	1.4	1.8	1.4	1.4	1.4	1.4
MgO	23.0	23.1	23.2	23.6	23.0	22.7	22.6	23.0	22.2	21.7
CaO	7.5	7.3	7.6	7.5	7.5	7.4	7.4	7.5	7.4	7.3
K_2O	9.7	9.7	9.0	10.0	9.8	9.7	9.8	9.4	9.8	9.8
Total	96.3	96.0	97.2	98.6	97.3	95.8	95.3	97.1	95.9	93.5
Phase		**kr**								
P [GPa]		**8**								
T [°C]		**1100**								
ae-...		**156**								
wt%										
SiO_2	54.3	54.8	55.2	53.9	54.0	54.7	53.7	54.6	54.3	54.5
Al_2O_3	1.4	1.2	1.1	1.4	1.4	1.3	1.3	1.3	1.3	1.3
MgO	22.1	23.0	22.6	23.4	23.3	22.9	23.6	23.8	23.1	23.0
CaO	7.5	7.7	7.5	7.5	7.8	7.4	7.3	7.5	7.6	7.6
K_2O	9.2	9.9	10.0	9.7	9.6	9.5	9.5	9.5	9.7	9.7
Total	94.5	96.6	96.4	95.9	96.1	95.8	95.4	96.7	96.0	96.1
Phase										
P [GPa]										
T [°C]										
ae-...										
wt%										
SiO_2	55.0	53.3	54.6	54.8	53.9	55.6	55.1			
Al_2O_3	1.4	1.4	1.3	1.3	1.2	1.1	1.1			
MgO	22.9	23.3	23.2	22.9	22.7	21.7	22.2			
CaO	7.6	7.7	7.8	7.8	7.7	7.6	7.4			
K_2O	9.2	9.4	9.8	9.8	9.8	9.7	9.7			
Total	96.1	95.1	96.7	96.4	95.2	95.7	95.5			